Supporting Information

Data Dependent Middle-Down nano-Liquid Chromatography-Electron Capture Dissociation Tandem Mass Spectrometry: An Application for the Analysis of Unfractionated Histones

Anastasia Kalli[¥], *Michael J. Sweredoski and Sonja Hess*[*]

Proteome Exploration Laboratory, Division of Biology, Beckman Institute, California Institute of Technology, Pasadena, CA 91125, USA

[¥] Current address: Department of Pathology and Laboratory Medicine, Children's Hospital Los Angeles, Los Angeles, CA 90027, USA

EXPERIMENTAL SECTION

Sample Preparation

Histones from calf thymus were obtained from Roche (Indianapolis, IN, USA). HeLa, Jurkat and MCF-7 cells were generously provided from Dr. Raymond J. Deshaies laboratory. Histones from HeLa, Jurkat and MCF-7 cells were acid extracted with 0.4 N H_2SO_4 and precipitated with 30% (v/v) trichloroacetic acid as previously described.[1] The histone pellet was dried, resuspended in water and protein concentration was determined by Bradford assay (Bio-Rad Laboratories, Hercules, CA, USA). For middle-down analysis, 10 µg of unfractionated histones were digested either with Glu-C (Roche) at an enzyme to protein ratio of 1:30 in 25 mM NH_4HCO_3 (pH = 7.8) at 25 °C, or, Asp-N at an enzyme to protein ratio of 1:25 in 50 mM NH_4HCO_3 (pH = 8.0) at 37 °C. Digestions were performed for 9 to 14 hours. All reactions were quenched with 0.5% formic acid. Digested samples were desalted with C_{18} Ziptips (Millipore, Billerica, MA). Unfractionated desalted peptides were lyophilized and stored at -20°C. Prior to LC-ECD-MS/MS analyses, digested histone peptides were resuspended in 0.2% formic acid.

Data Analysis

For peptide and protein identification an in-house developed search engine, ROCCIT, was used. ROCCIT is a next generation MS/MS database search engine that can increase the number of confident peptide identifications made at a fixed false discovery (FDR) rate by taking advantage of the following features. First, ROCCIT uses a novel peptide-spectrum match (PSM) scoring metric that is based on a commonly used performance metric in machine learning, the area under the ROC curve. This new scoring metric excels at differentiating true matches from false matches and is sensitive enough to help localize PTMs. Second, ROCCIT uses a high mass accuracy filter to identify matches unlikely to be correct based on precursor mass error alone. Thus ROCCIT achieves a high level of sensitivity while maintaining its specificity. Third, ROCCIT takes into account known modifications and cleavages when conducting the search by encoding modifications such as known phosphorylation sites in Uniprot. This allows for identifying modifications and cleavages that are common at a particular position on a particular protein but rare in general. Fourth, ROCCIT takes advantage of the MapReduce distributed computing framework to allow for massively parallel searches across many computers simultaneously. This allows for a greater number of variable modifications to be considered per peptide. One additional feature of ROCCIT that was particularly useful to this study was the display of search results in an easy to interpret web page. More specifically, each identified PSM included a link to the MS-Product function of ProteinProspector (http://prospector.ucsf.edu/prospector/cgi-bin/msform.cgi?form=msproduct) to allow visualization of each match and, therefore, alternate peptide hypotheses could be explored.

In addition to the variable modifications mentioned in the main manuscript, the data was also searched for phosphorylation on Ser, Thr and Tyr. However, no high scoring phosphorylated peptides were identified, with the exception of three phosphorylated peptides from H2A 2-C, H2A.1 and H1.1 from calf thymus (Supporting Information, Figures S30A and S31D). This is presumably due to the fact that no enrichment of phosphorylated peptides was performed in the samples. As phosphorylated peptides are of lower abundance, compared to other peptides present in the samples, and given that the instrument was operated in data-dependent acquisition mode, in which only the most abundant peptides are sequenced, is not very surprising that, in general,

phosphorylated peptides were not identified. We should note that the search engine, ROCCIT, used for peptide identification will take into consideration known modifications, which are already included in Uniprot, even if they are not specified in the search as variable modifications. The phosphorylated peptides identified for H2A 2-C, H2A.1 and H1.1 correspond to known phosphorylated sites included in Uniprot and as such they were also identified in the search, in which phosphorylation was not included as variable modification.

Positional isomers (peptides with the same amino acid sequence that are modified at different positions) were identified by manually examining and verifying the ECD spectra for which a single precursor ion mass was assigned to more than one modified peptides differing only at the position of the modification.

We note that for histone variants sharing the same N-terminal tail it is not feasible to determine, with neither the bottom-up nor the middle-down approach, if the identified PTMs are present in all variants or only in one specific histone variant. This information can only be revealed by the top-down approach.

RESULTS AND DISCUSSION

Optimization of middle-down nano-LC-ECD MS/MS

Figure S1 displays the results obtained from an *in silico* digest of bovine and human histones. Bovine and human histones sequences were obtained from UniProt (containing 55 and 105 sequences for bovine and human, respectively), and an *in silico* digest was performed with trypsin, Lys-C, Arg-C, Glu-C, and Asp-N to calculate the theoretical number of proteolytic peptides produced by each enzyme.

Figure S2 displays the theoretical number of derived proteolytic peptides as a function of the peptide mass for trypsin, Lys-C, Arg-C, Glu-C and Asp-N. As illustrated in this Figure, Glu-C and Asp-N generate the higher number of peptides in the desirable mass range for middle-down analysis of histones. We note that peptides having a mass of $\leq$ 3000 Da cannot be considered as middle-down size peptides; however, they are unavoidable following digestion with any of the enzymes examined. A good compromise is to select proteolytic enzymes like Glu-C and Asp-N, which produce fewer peptide of this size (Figure S2, inset).

Figures S3 to S9 show representative examples of the effect of electron energy and irradiation time on the ECD outcome as a function of the peptide charge state.

For several peptides more than one charge state was selected for fragmentation. As the data was collected in data-acquisition mode the number of charge states selected for fragmentation per peptide was highly dependent on the number of charge states detected per peptide, on the abundance of each charge state and also on the abundance of other peptides present in the MS spectrum. Under the same ECD conditions (same electron energy and irradiation time), no major differences were observed between different charge states. Representative examples of ECD

spectra of peptides fragmented in two different charge states are shown in Figures S10 to S17.Although some product ions are unique for each charge state, the total number of product ions and the peptide sequence coverage obtained is very similar or identical between different charge states. This is mainly due to the fact that the vast majority of peptides subjected to ECD was highly charged and therefore fragment efficiently in ECD. This is in accordance with previously published data[2] in which it was shown that peptides with m/z < 950 fragment efficiently in ECD and that high peptide sequence coverage is obtained in ECD of highly charged precursor ions.

It is worth pointing out that data from histone H3 is fairly low. This is a result of the unspecific cleavages we observed for Glu-C. When a search was performed without enzyme specificity, we have identified several modified peptides from i.e. H3.2 as illustrated in some representatives examples in Figure S18. These observations are in agreement with those of Gupta et al. who examine proteases specificity, including Glu-C, and reported unspecific cleavage sites.[3] Since in our identifications we consider only peptides resulting from specific enzymatic cleavages and given that for H3 we mainly observed unspecific Glu-C cleavages the data from H3 was low.

FIGURES AND TABLES

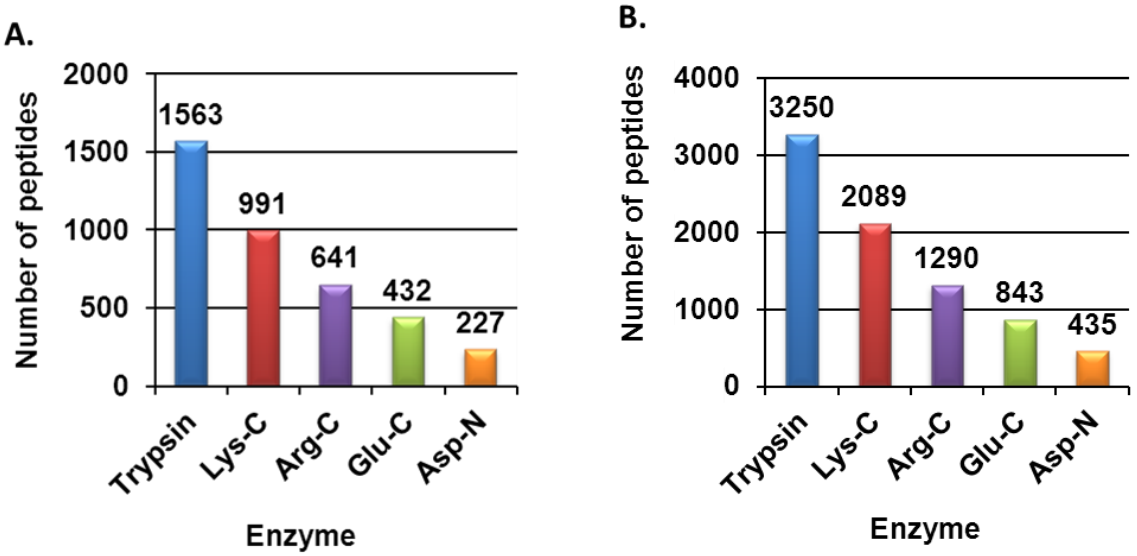

Figure S1. Number of peptides produced by *in silico* digests of bovine (A) and human (B) histones for different proteolytic enzymes assuming zero missed cleavages. Data was constructed from bovine and humans histone sequences obtained from UniProt (containing 55 sequences for bovine and 105 sequences for human).

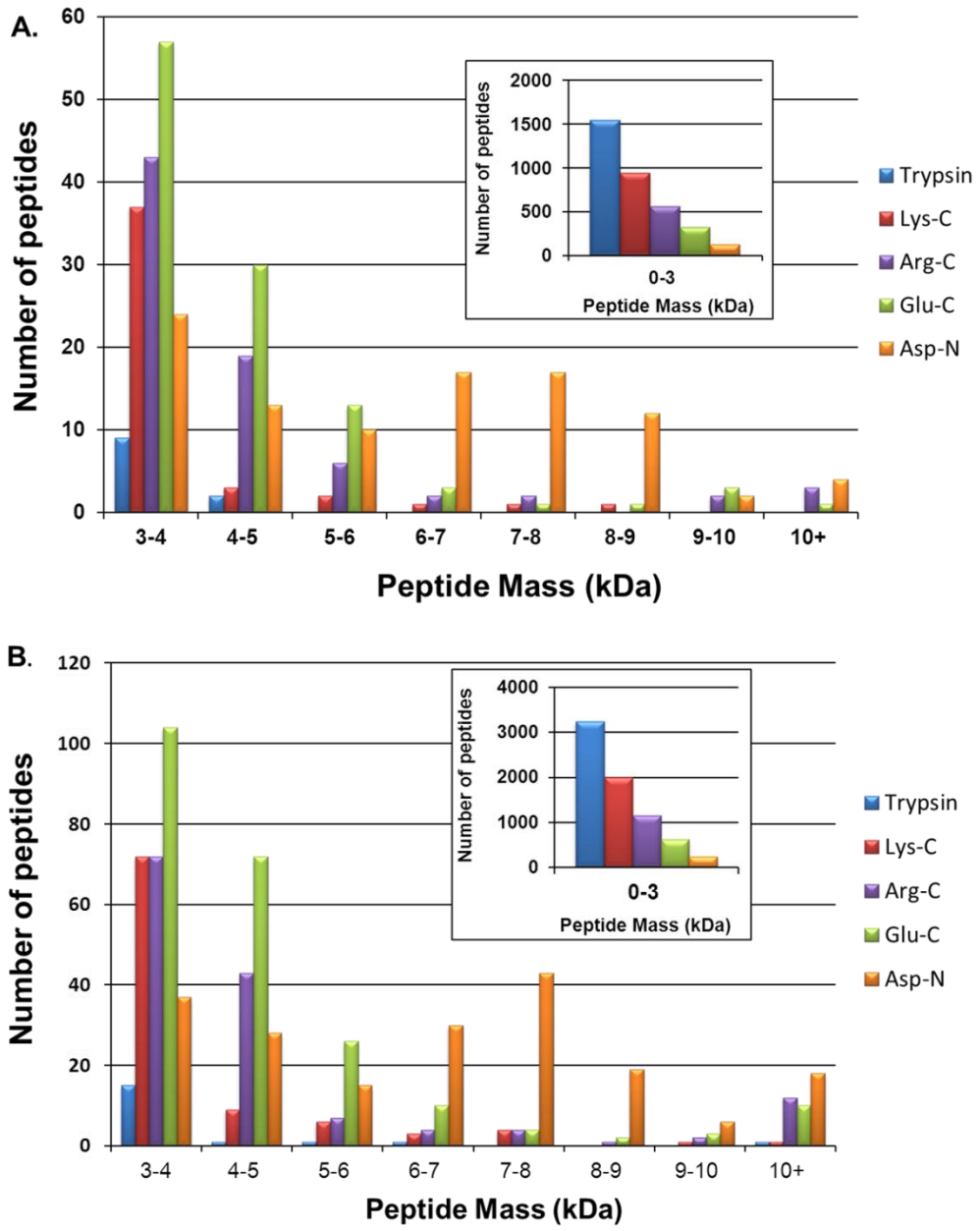

Figure S2. Number of peptides as a function of peptide mass produced by *in silico* digestions of bovine (A) and human (B) histones with different proteolytic enzymes assuming zero missed cleavages. Data was constructed from bovine and humans histone sequences obtained from UniProt (containing 55 sequences for bovine and 105 sequences for human).

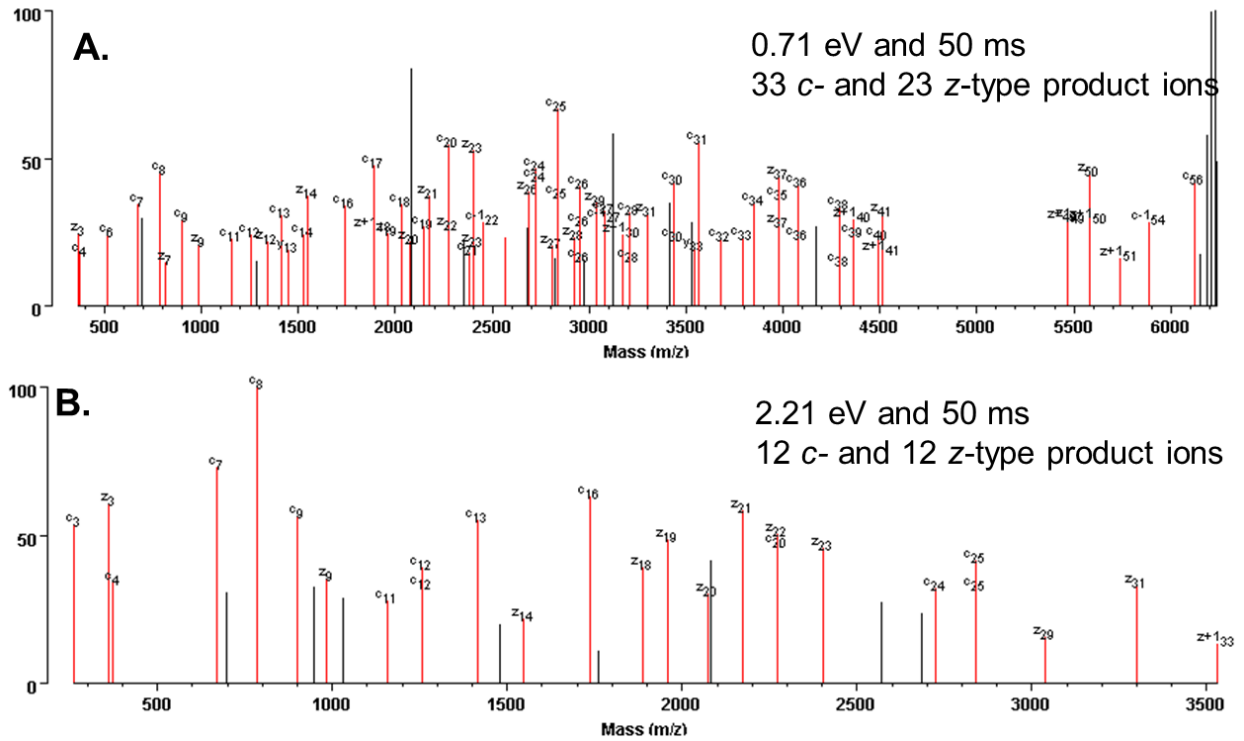

Figure S3. ECD spectra acquired at different electron energies for the $[M + 9H]^{9+}$ precursor ions of the peptide 65-120 (6.3 KDa) from histone H2A 2-C (and/or H2A 1-H, H2A 1-D). The peptide was successfully identified at both electron energies, however, a significantly higher number of *c*- and *z*-type product ions was observed at lower electron energy (A). The peptide was derived from a Glu-C digest of histones extracted from Jurkat cells. Deconvoluted spectra are displayed using Protein Prospector (http://prospector.ucsf.edu/prospector/cgi-bin/msform.cgi?form=msproduct).

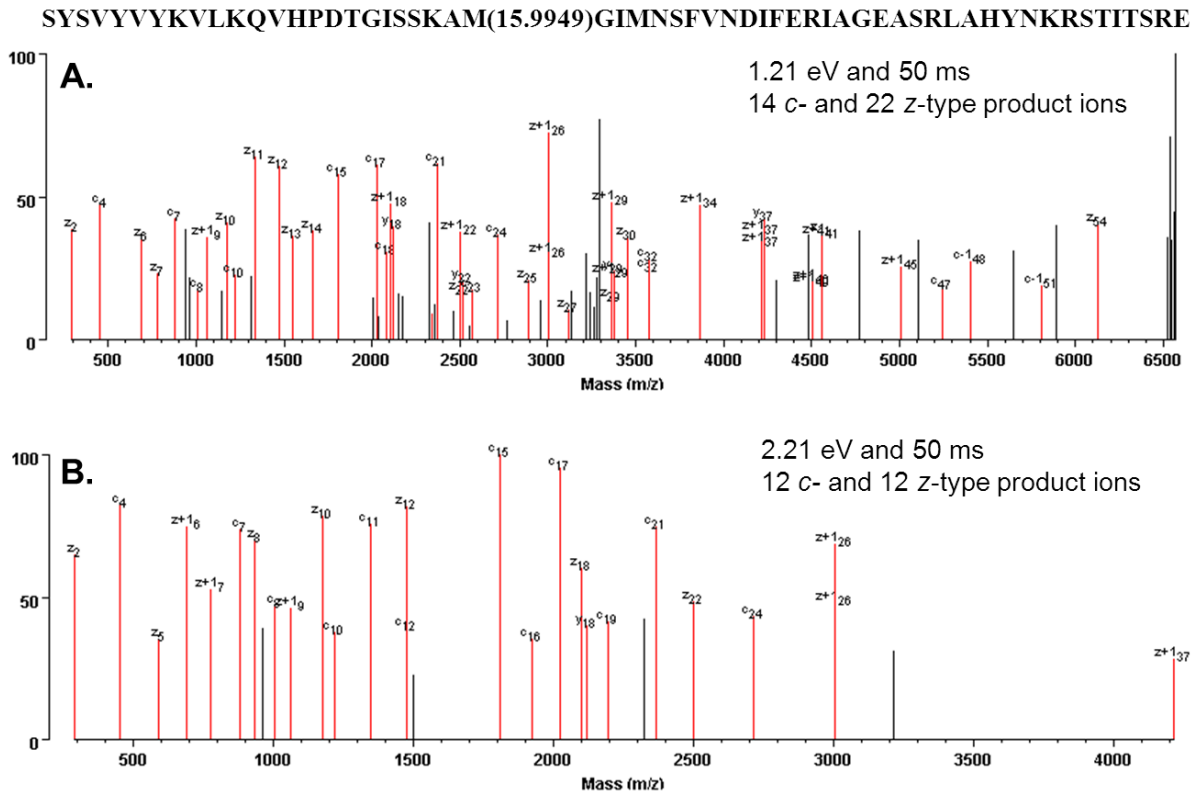

Figure S4. ECD spectra acquired at different electron energies for the $[M + 7H]^{7+}$ precursor ions of the peptide 35-92 (6.6 KDa) from histone H2B 1-K (and/or H2B 2-7, H2B 1-H, H2B 1-C/E/F/G/I). A higher number of *c*- and *z*-type product ions was observed at the lower electron energy setting (A) resulting in a higher peptide score and a more confident identification. The peptide was derived from a Glu-C digest of histones extracted from Jurkat cells. Deconvoluted spectra are displayed using Protein Prospector (http://prospector.ucsf.edu/prospector/cgi-bin/msform.cgi?form=msproduct).

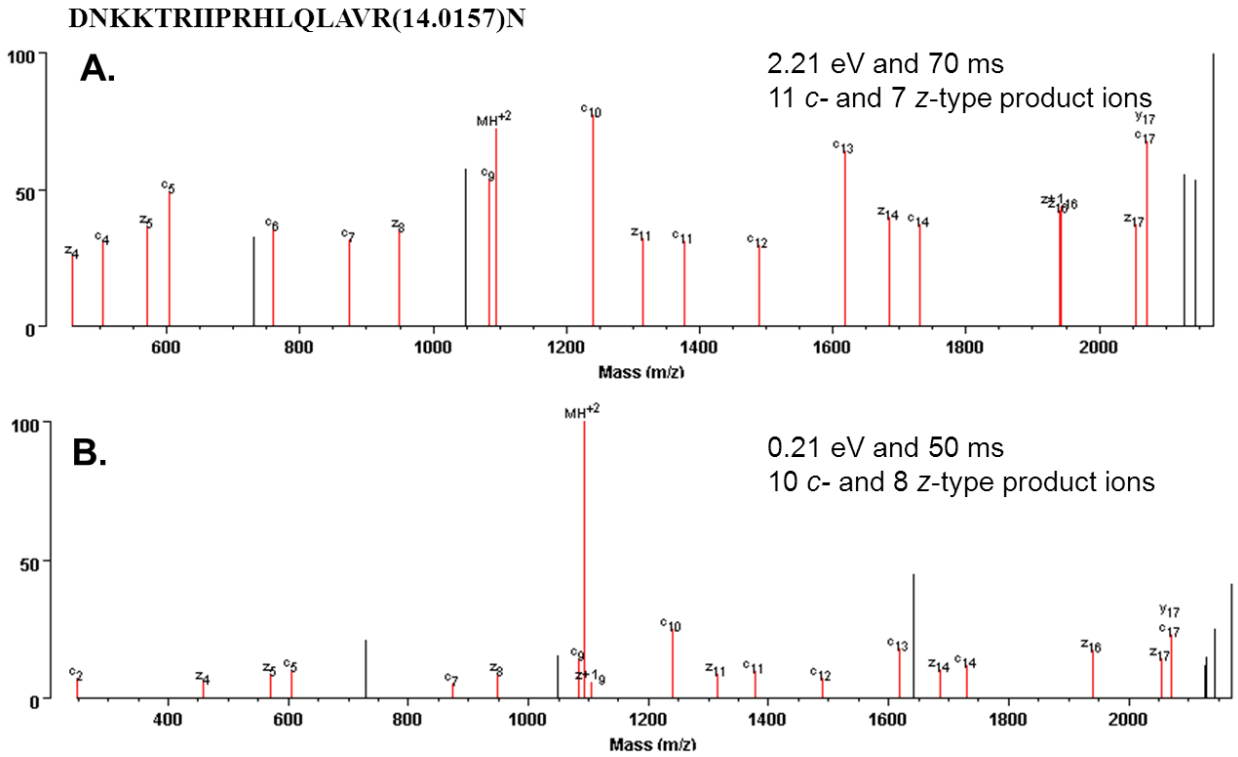

Figure S5. ECD spectra acquired at different electron energies for the $[M + 4H]^{4+}$ precursor ions of the peptide 72-89 (2.3 KDa) from histone H2A 2-B. An almost identical number of *c*- and *z*-type product ions was observed at both experimental conditions, but the intensity of the product ions was significantly improved at higher electron energies (A) resulting in a more confident peptide identification. The peptide was derived from Asp-N digestion of histones extracted from HeLa cells. Deconvoluted spectra are displayed using Protein Prospector (http://prospector.ucsf.edu/prospector/cgi-bin/msform.cgi?form=msproduct).

DIFERIAGEASRLAHYNKRSTITSREIQTAVRLLLPGELAKHAVSEGTKAVTKYTSSK

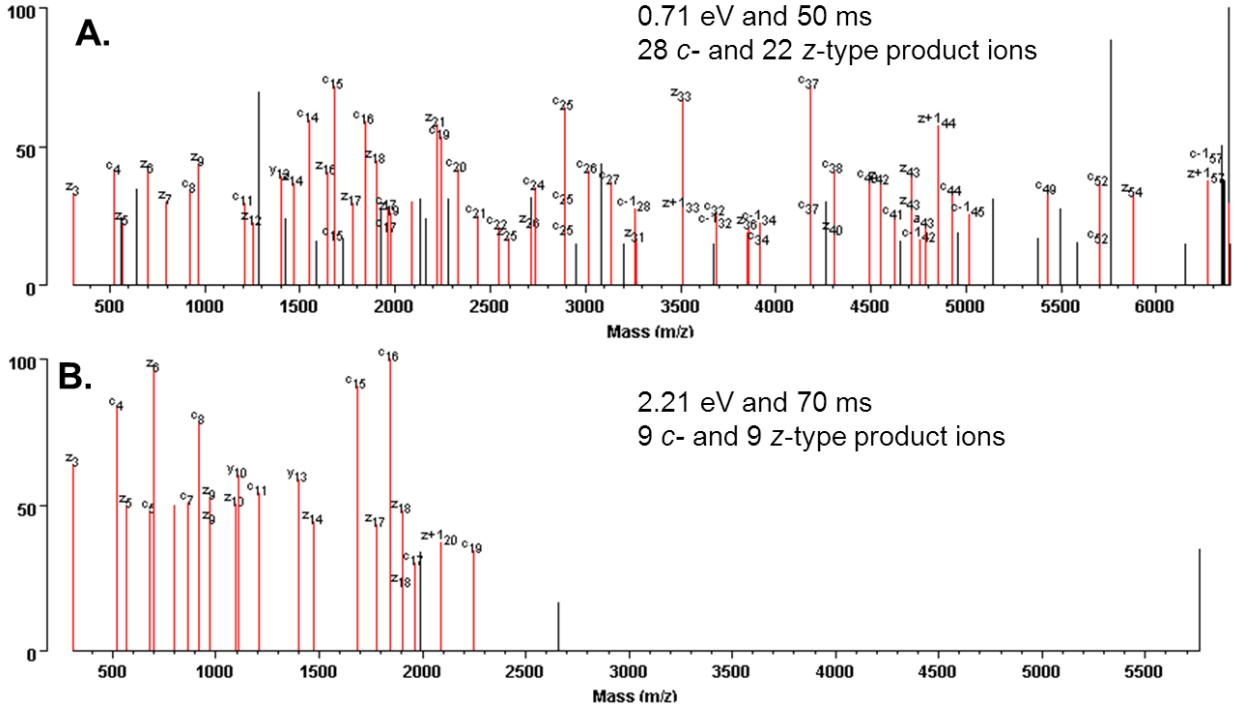

Figure S6. ECD spectra acquired at different electron energies for the $[M + 10H]^{10+}$ precursor ions of the peptide 69-125 (6.4 KDa) from histone H2B 2-E (and/or H2B 1-O, H2B 1-H, H2B 1-D, H2B 2-F, H2B 1-C/E/F/G/I). The peptide sequence coverage obtained was highly dependent on the ECD settings (electron energy and irradiation time) employed, with the lower electron energy and lower irradiation time (A) resulting in 32 more *c*- and *z*-type product ions. The peptide was derived from an Asp-N digestion of histones extracted from HeLa cells. Deconvoluted spectra are displayed using Protein Prospector (http://prospector.ucsf.edu/prospector/cgi-bin/msform.cgi?form=msproduct).

S(42.0106)GRGKQGGKARAKAKSRSSRAGLQFPVGRVHRLLRK(14.0157)GNYAE

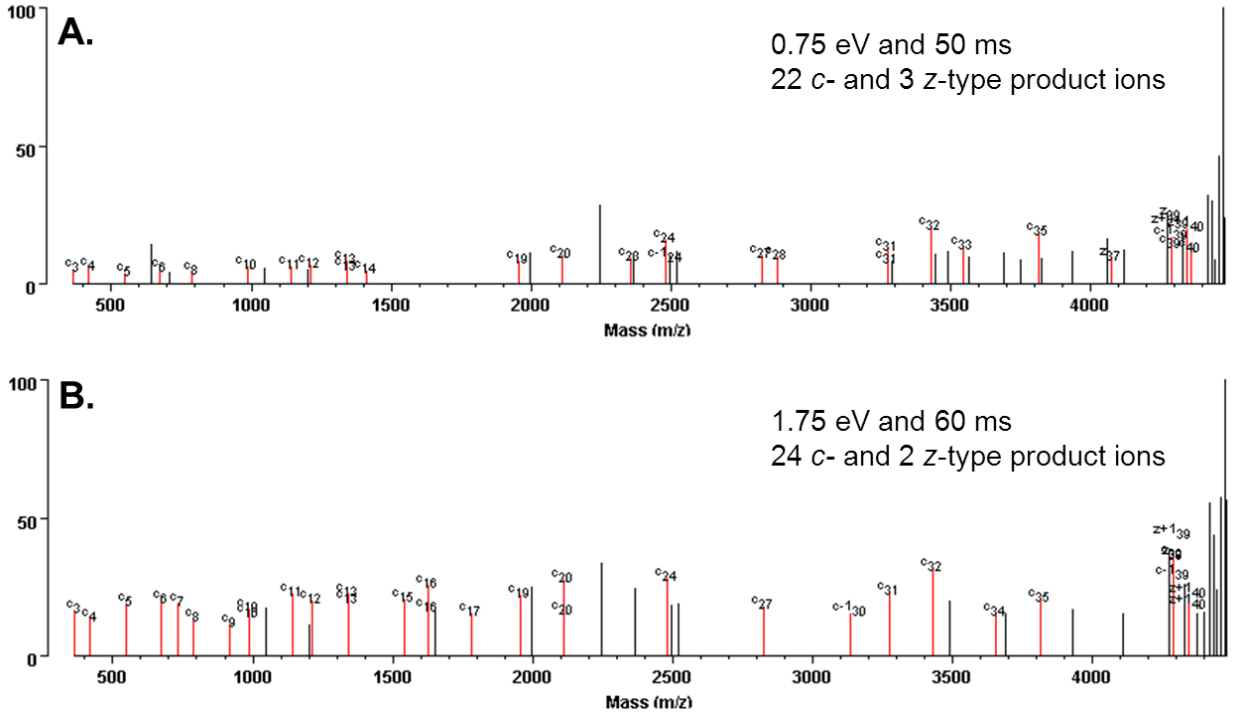

Figure S7. ECD spectra acquired at different electron energies for the $[M + 8H]^{8+}$ precursor ions of the peptide 1-41 (4.5 KDa) from histone H2A 1-C (and/or H2A 2-C, H2A 2-B). Although an almost identical number of *c*- and *z*-type product ions was observed with both settings, a higher score was obtained for spectrum (B) due to the higher product ion intensity. The peptide was derived from a Glu-C digest of histones extracted from MCF-7 cells. Deconvoluted spectra are displayed using Protein Prospector (http://prospector.ucsf.edu/prospector/cgi-bin/msform.cgi?form=msproduct).

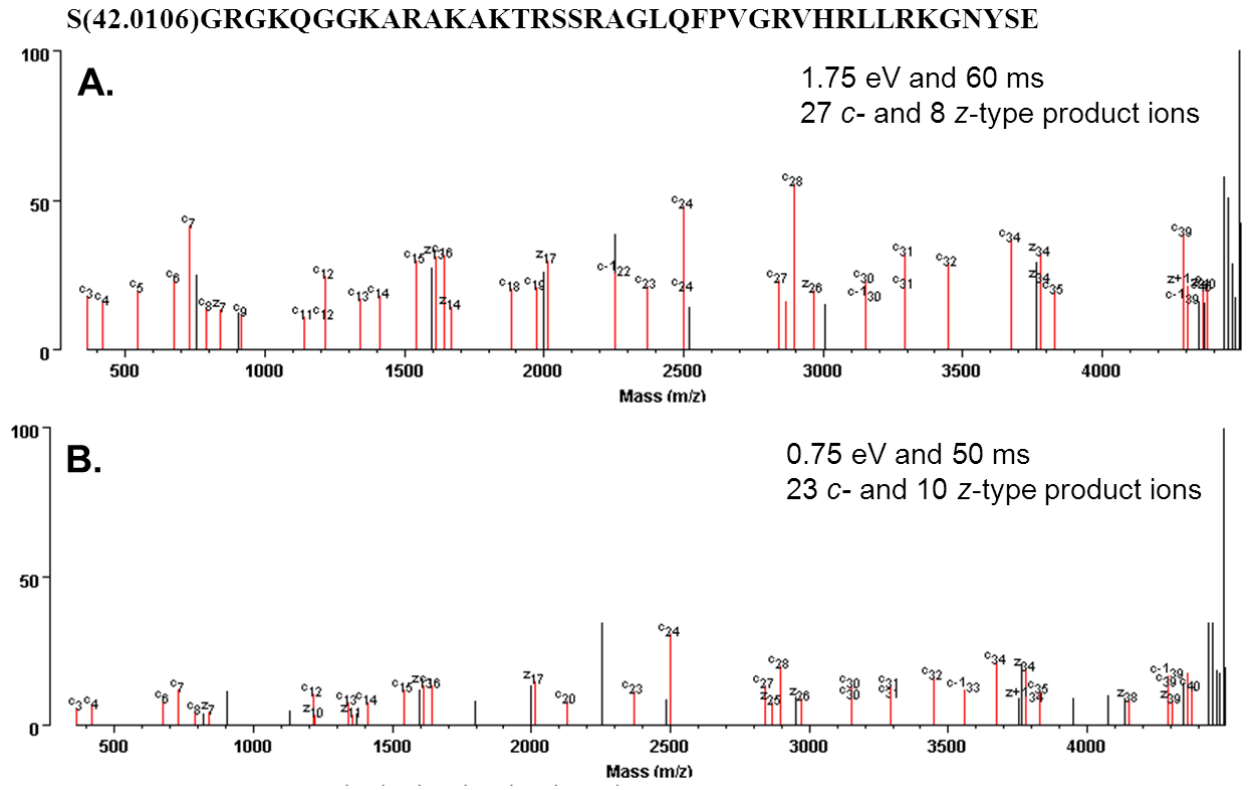

Figure S8. ECD spectra acquired at different electron energies for the $[M + 6H]^{6+}$ precursor ions of the peptide 1-41(4.5 KDa) from histone H2A 1-D (and/or H2A 1-B/E). A higher quality ECD spectrum was obtained with the experimental settings shown in (A), resulting in higher score and more confident peptide identification. The peptide was derived from a Glu-C digest of histones extracted from MCF-7 cells. Deconvoluted spectra are displayed using Protein Prospector (http://prospector.ucsf.edu/prospector/cgi-bin/msform.cgi?form=msproduct).

S(42.0106)ETAPAAPAAAPPAEKTPVKKKAAKKPAGARRKASGPPVSELITKAVAASKERSG VSLAALKKALAAAGY

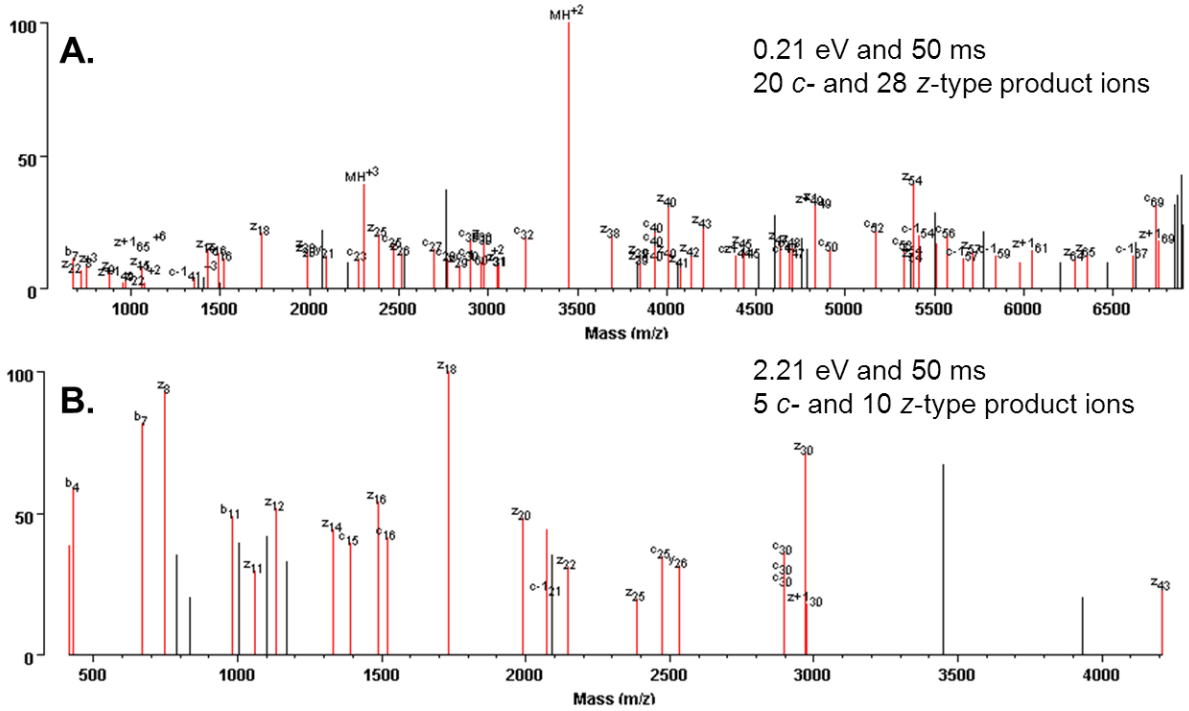

Figure S9. ECD spectra acquired at different electron energies for the $[M + 10H]^{10+}$ precursor ions of the peptide 1-69 (6.9 KDa) from histone H1.1. A noticeably higher number of *c*- and *z*-type product ions was observed at the lower electron energy setting (A), resulting in higher peptide sequence coverage. The peptide was derived from an Asp-N digestion of histones from calf thymus. Deconvoluted spectra are displayed using Protein Prospector (http://prospector.ucsf.edu/prospector/cgi-bin/msform.cgi?form=msproduct).

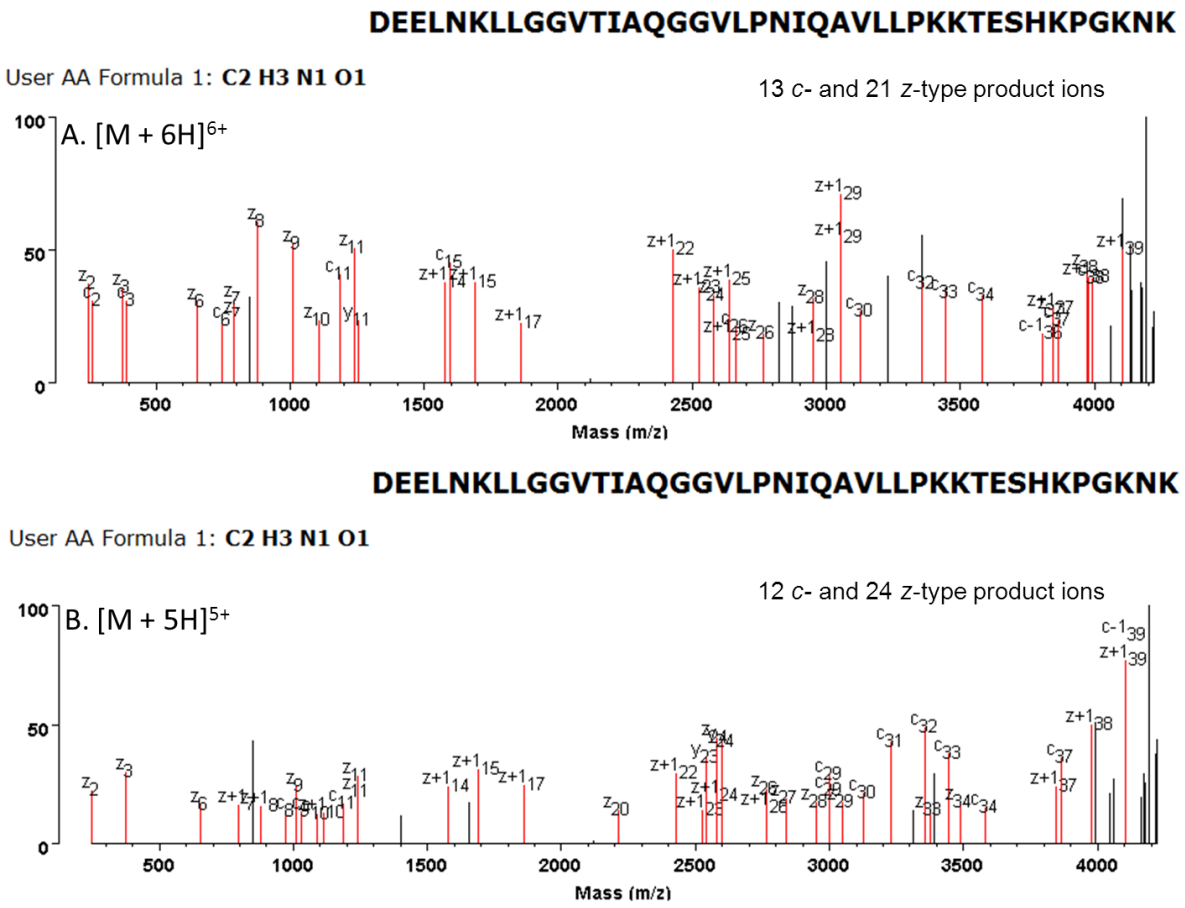

Figure S10. ECD spectra of the $[M + 6H]^{6+}$ (A) and $[M + 5H]^{5+}$ (B) precursor ions of the peptide 90-130 from histone H2A 2-B.Very similar ECD fragmentation was observed between the two charge states. For the ECD experiments the electron energy was set at 1.21 eV and the irradiation time at 50 ms. The peptide was derived from an Asp-N digestion of histones from Jurkat cells. Deconvoluted spectra are displayed using Protein Prospector (http://prospector.ucsf.edu/prospector/cgi-bin/msform.cgi?form=msproduct).

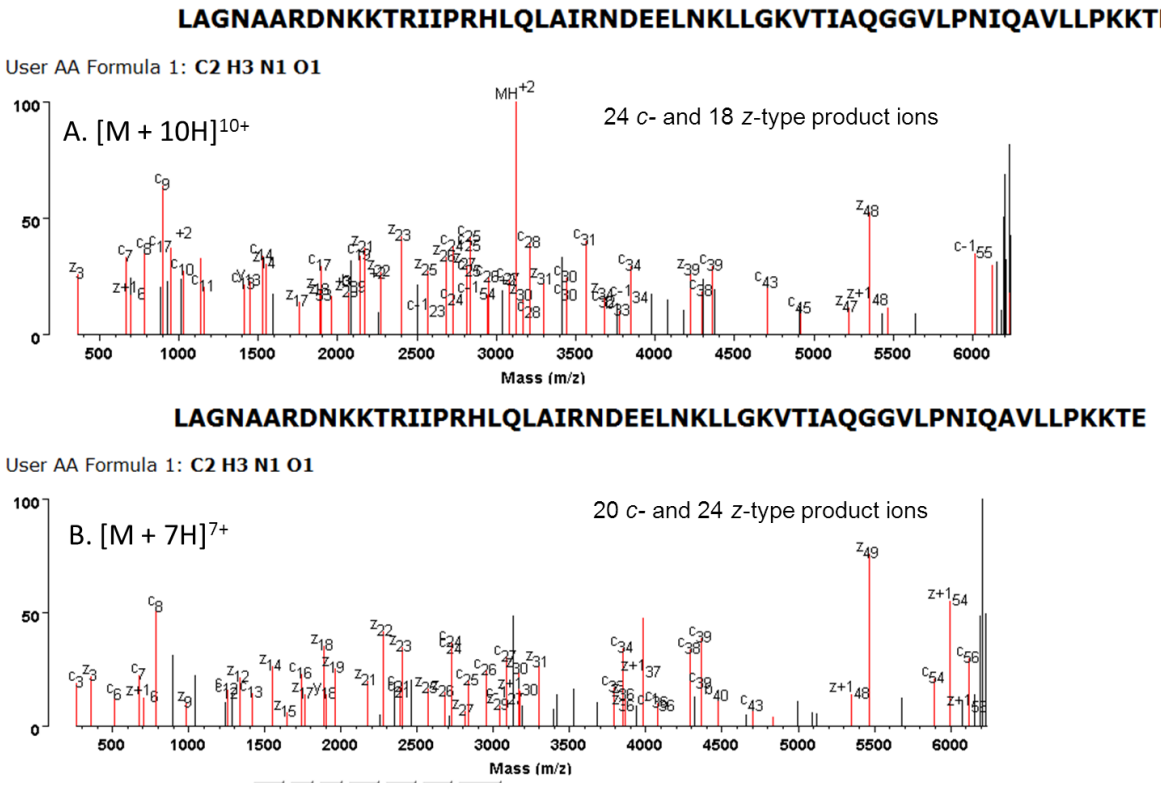

Figure S11. ECD spectra of the $[M + 10H]^{10+}$ (A) and $[M + 7H]^{7+}$ (B) precursor ions of the peptide 65-121 from histone H2A 2-C (and/or H2A 1-H, H2A 1-D). ECD of the $[M + 10H]^{10+}$ and $[M + 7H]^{7+}$ precursor ions resulted in the formation of 42 and 44 product ions, respectively. For the ECD experiments the electron energy was set at 0.71 eV and the irradiation time at 50 ms. The peptide was derived from a Glu-C digest of histones from Jurkat cells. Deconvoluted spectra are displayed using Protein Prospector (http://prospector.ucsf.edu/prospector/cgi-bin/msform.cgi?form=msproduct).

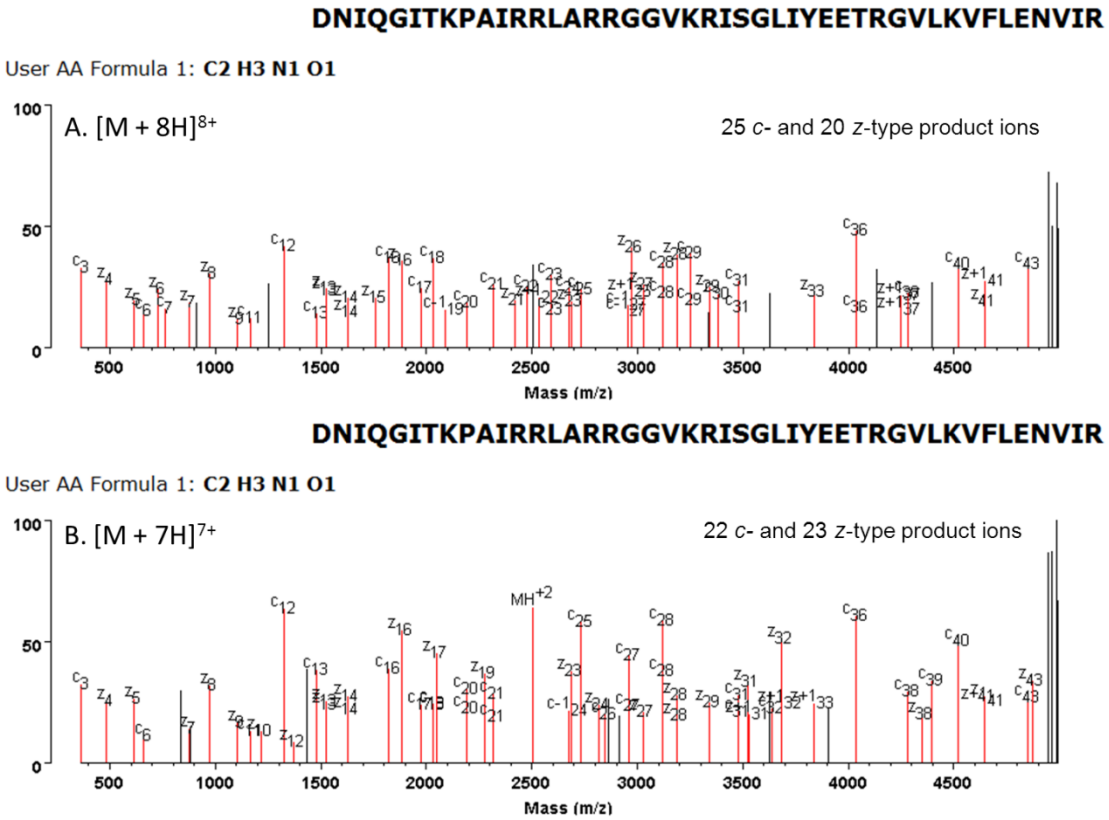

Figure S12. ECD spectra of the $[M + 8H]^{8+}$ (A) and $[M + 7H]^{7+}$ (B) precursor ions of the peptide 24-67 from histone H4. Similar ECD spectra were obtained and the total number of product ions is identical for both charge states. For the ECD experiments the electron energy was set at 0.71 eV and the irradiation time at 50 ms. The peptide was derived from an Asp-N digestion of histones from Jurkat cells. Deconvoluted spectra are displayed using Protein Prospector (http://prospector.ucsf.edu/prospector/cgi-bin/msform.cgi?form=msproduct).

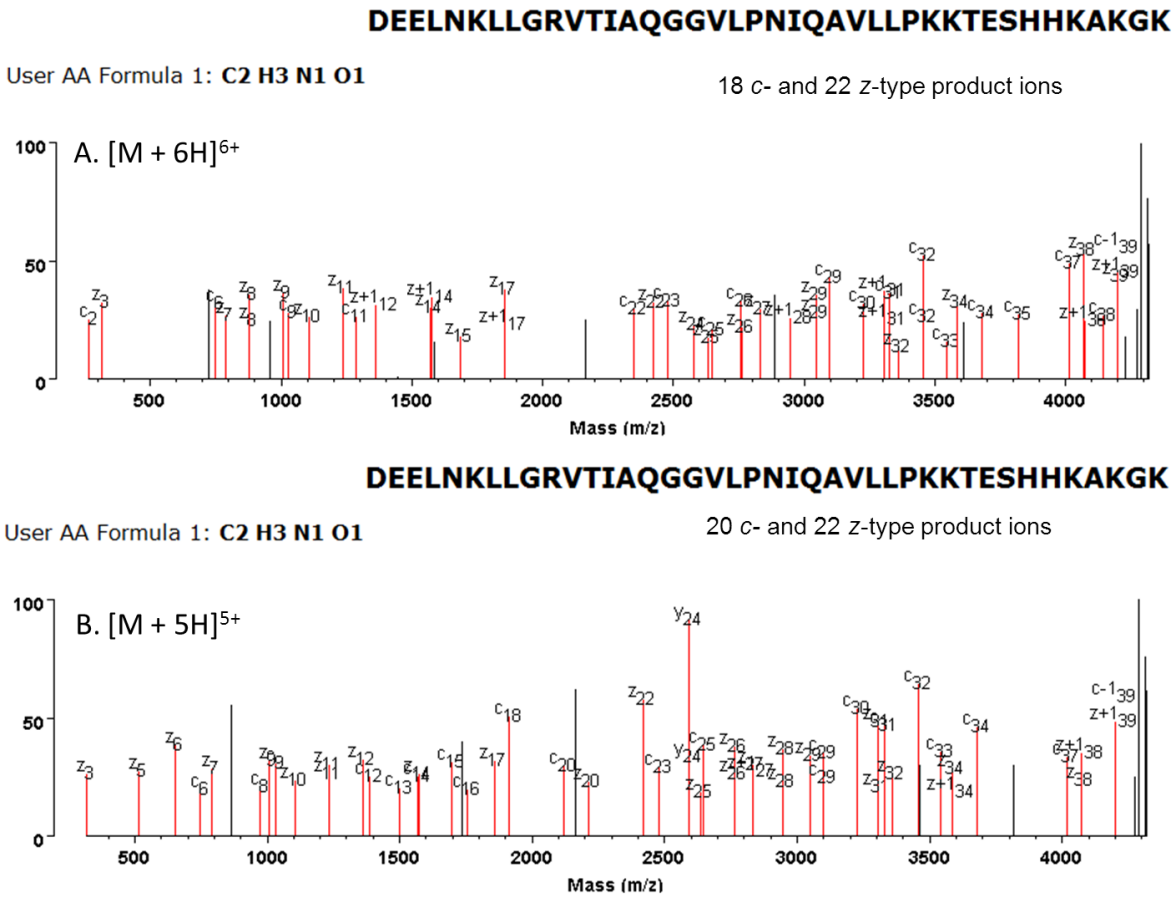

Figure S13. ECD spectra of the $[M + 6H]^{6+}$ (A) and $[M + 5H]^{5+}$ (B) precursor ions of the peptide 90-130 from histone H2A 1-B/E (and/or H2A.3). Some product ions were unique for each charge state but the ECD peptide sequence coverage was very similar between the two charge states. For the ECD experiments the electron energy was set at 0.71 eV and the irradiation time at 50 ms. The peptide was derived from an Asp-N digestion of histones from Jurkat cells. Deconvoluted spectra are displayed using Protein Prospector (http://prospector.ucsf.edu/prospector/cgi-bin/msform.cgi?form=msproduct).

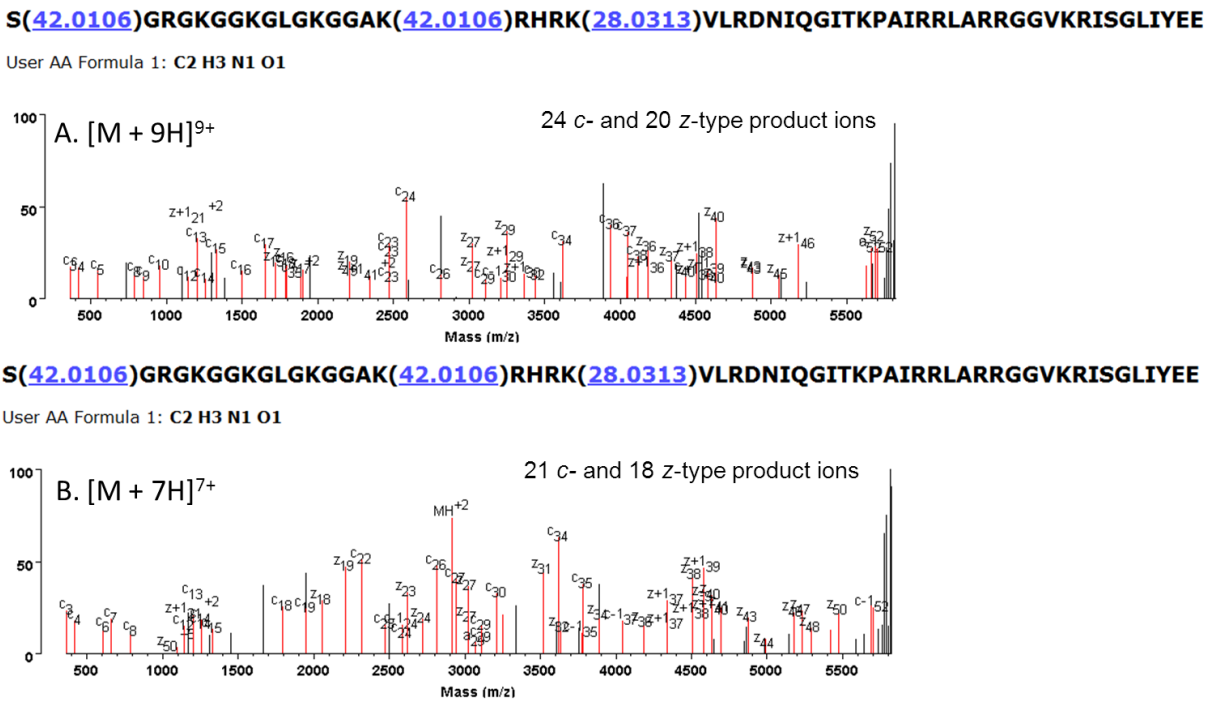

Figure S14. ECD spectra of the $[M + 9H]^{9+}$ (A) and $[M + 7H]^{7+}$ (B) precursor ions of the peptide 1-53 from histone H4. Four more product ions were detected for the $[M + 9H]^{9+}$ precursor ions, but, overall extensive ECD fragmentation is obtained from both charge states. For the ECD experiments the electron energy was set at 0.21 eV and the irradiation time at 50 ms. The peptide was derived from a Glu-C digestion of histones from Jurkat cells. Deconvoluted spectra are displayed using Protein Prospector (http://prospector.ucsf.edu/prospector/cgi-bin/msform.cgi?form=msproduct).

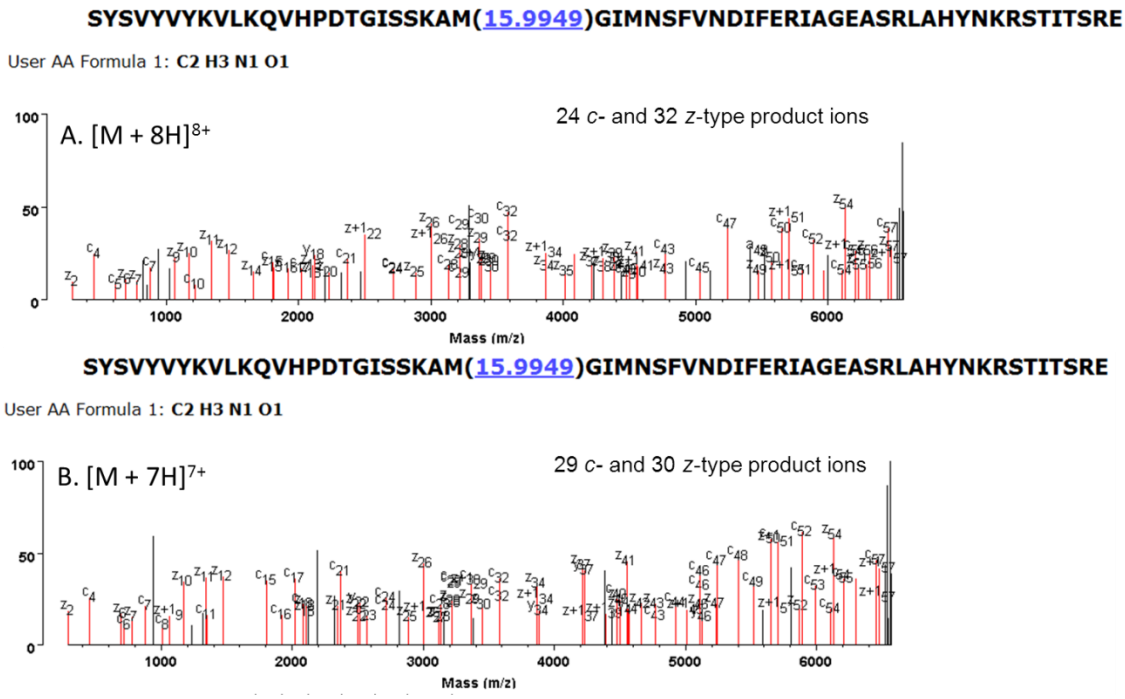

Figure S15. ECD spectra of the $[M + 8H]^{8+}$ (A) and $[M + 7H]^{7+}$ (B) precursor ions of the peptide 36-93 from histone H2B 1-C/E/F/G/I (and/or H2B 1-K, H2B 1-M, H2B 2-F, H2B 1-H). Overall, similar ECD fragmentation was observed. For the ECD experiments the electron energy was set at 0.75 eV and the irradiation time at 50 ms. The peptide was derived from a Glu-C digestion of histones from MCF-7 cells. Deconvoluted spectra are displayed using Protein Prospector (http://prospector.ucsf.edu/prospector/cgi-bin/msform.cgi?form=msproduct).

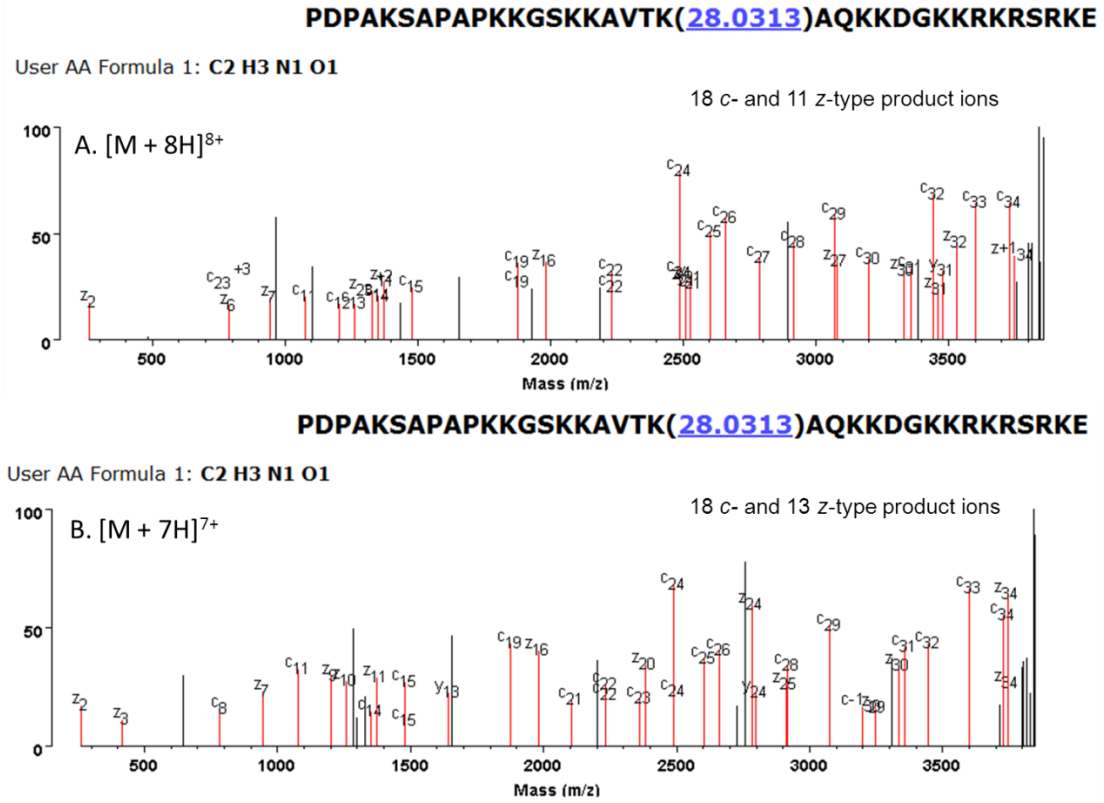

Figure S16. ECD spectra of the $[M + 8H]^{8+}$ (A) and $[M + 7H]^{7+}$ (B) precursor ions of the peptide 36-93 from histone H2B 2-F. Very similar ECD spectra were obtained resulting in the formation of 29 and 31 product ions for the $M + 8H]^{8+}$ and $[M + 7H]^{7+}$ precursor ions, respectively. For the ECD experiments the electron energy was set at 0.75 eV and the irradiation time at 50 ms. The peptide was derived from a Glu-C digestion of histones from MCF-7 cells. Deconvoluted spectra are displayed using Protein Prospector (http://prospector.ucsf.edu/prospector/cgi-bin/msform.cgi?form=msproduct).

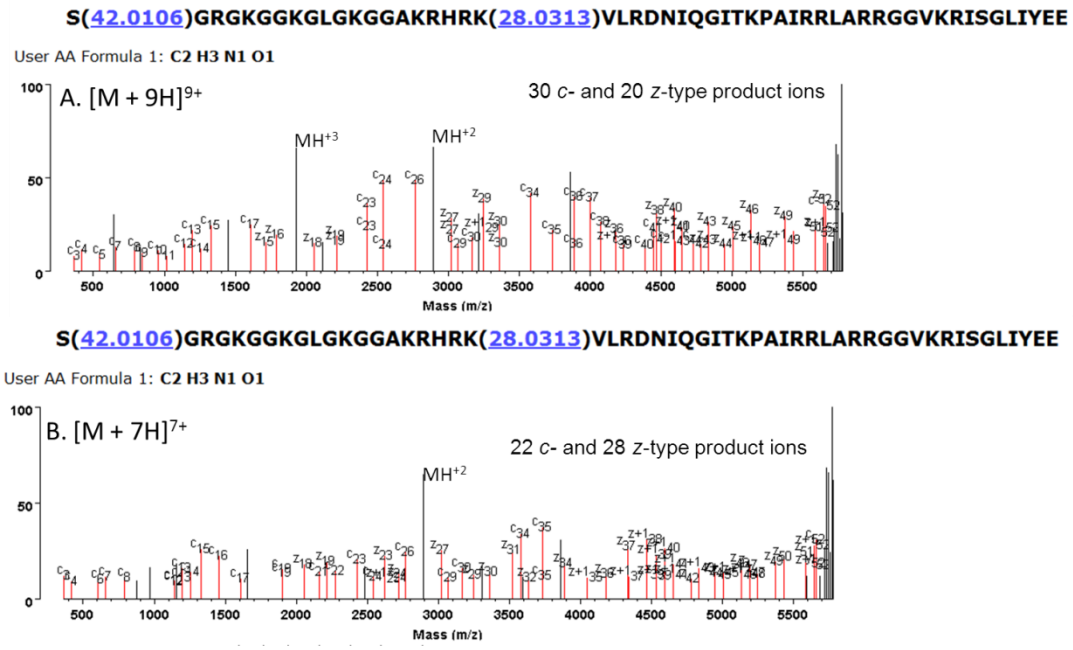

Figure S17. ECD spectra of the $[M + 9H]^{9+}$ (A) and $[M + 7H]^{7+}$ (B) precursor ions of the peptide 1-53 from histone H4. Very similar ECD spectra were obtained resulting in the formation of an identical number of *c*- and *z*- type product ions. For the ECD experiments the electron energy was set at 0.75 eV and the irradiation time at 50 ms. The peptide was derived from a Glu-C digestion of histones from MCF-7 cells. Deconvoluted spectra are displayed using Protein Prospector (http://prospector.ucsf.edu/prospector/cgi-bin/msform.cgi?form=msproduct).

(Q) TARKSTGGK(42.0106)APRKQLATK(42.0106)AARK(28.0313)SAPATGGVKKPHRYRPGTVALRE

User AA Formula 1: **C2 H3 N1 O1**

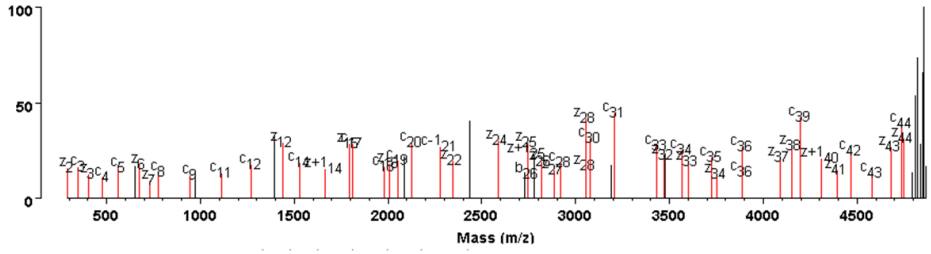

(G) GKAPRKQLATK(42.0106)AARK(28.0313)SAPATGGVKKPHRYRPGTVALRE

User AA Formula 1: **C2 H3 N1 O1**

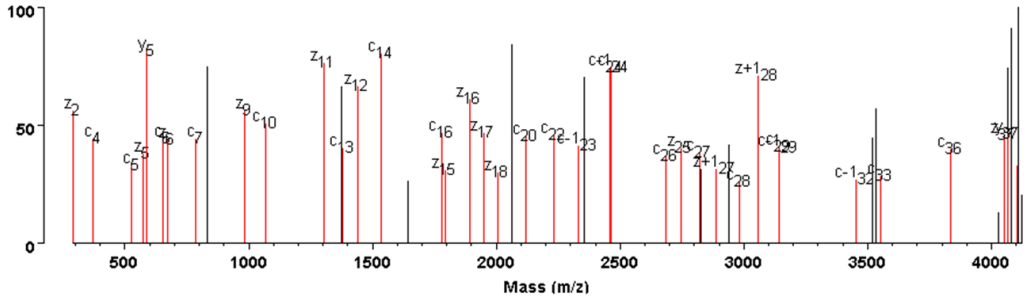

(K) AARK(28.0313)SAPATGGVKKPHRYRPGTVALRE

User AA Formula 1: **C2 H3 N1 O1**

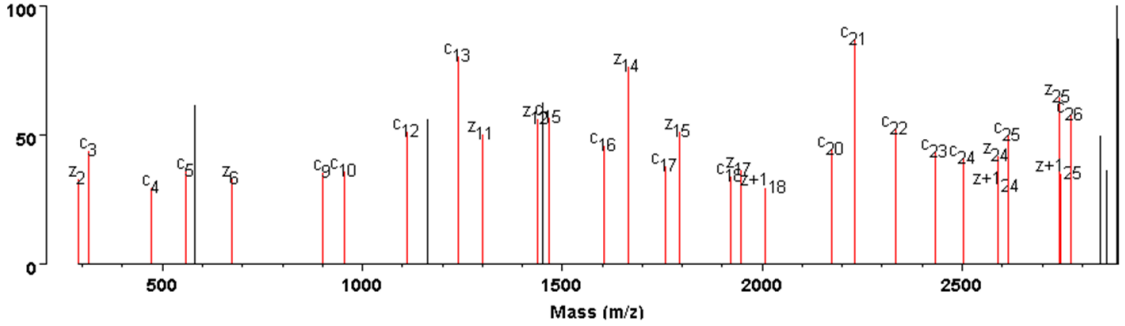

(Q) LATK(42.0106)AARK(28.0313)SAPATGGVKKPHRYRPGTVALRE

User AA Formula 1: **C2 H3 N1 O1**

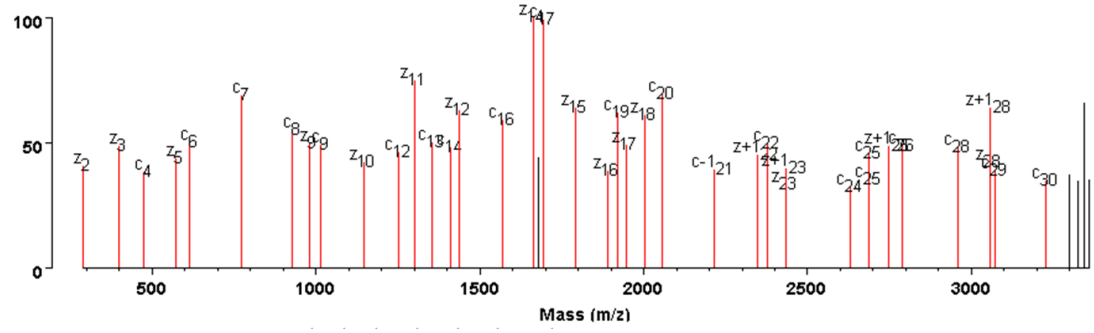

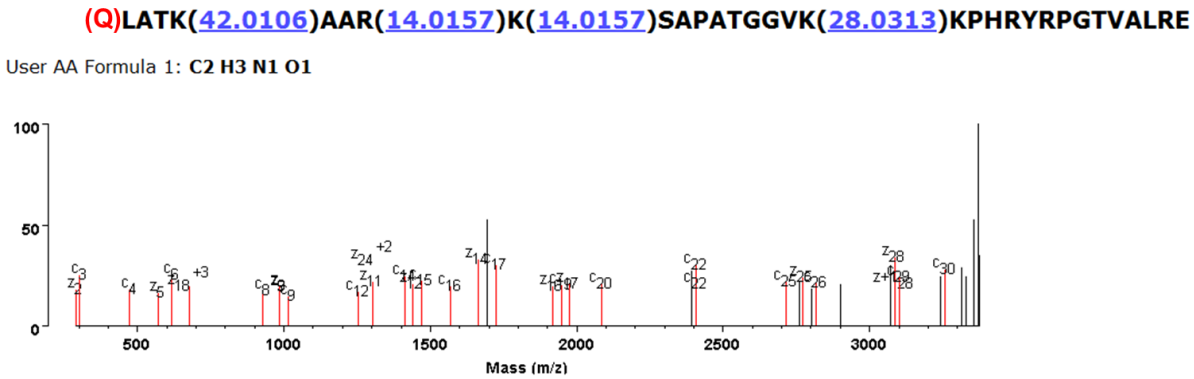

Figure S18. Peptides from H3.2 (Jurkat cells) corresponding to Glu-C unspecific cleavages. The unspecific cleavage sites are indicated in red in the peptide sequence.

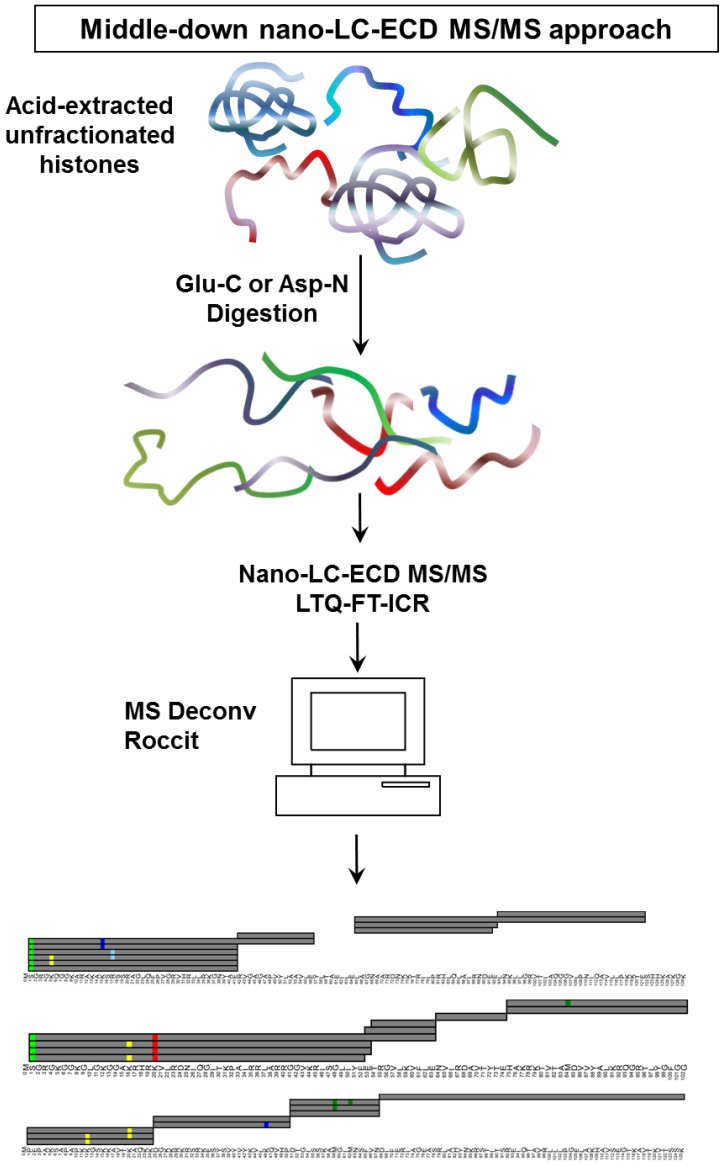

Figure S19. Experimental outline.

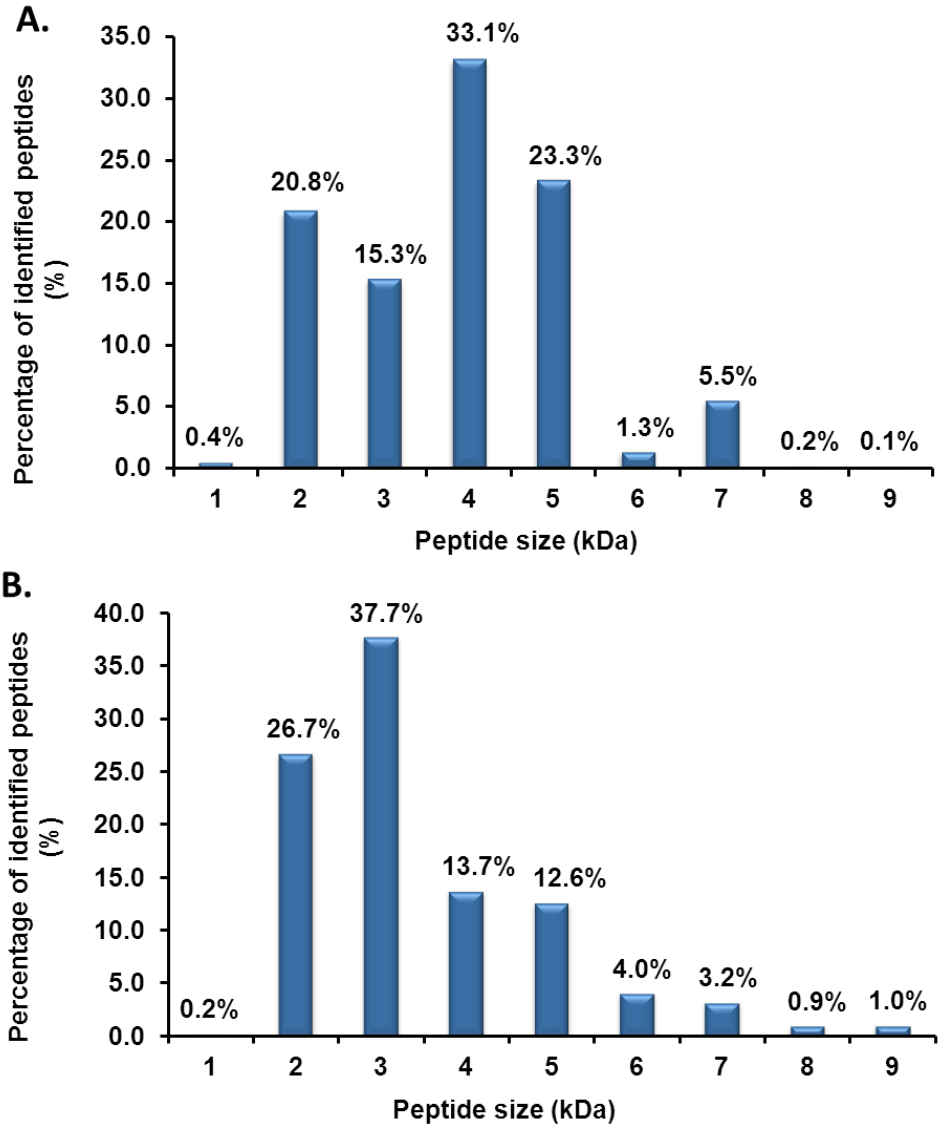

Figure S20. Percentage of identified peptides as a function of mass distribution for Glu-C (A) and Asp-N (B) derived peptides. Identified peptides from all samples examined (calf thymus, HeLa, Jurkat and MCF-7 cells) are summed and displayed together for each protease. As illustrated in the figure, the vast majority of the identified peptides had a mass greater than 3 kDa.

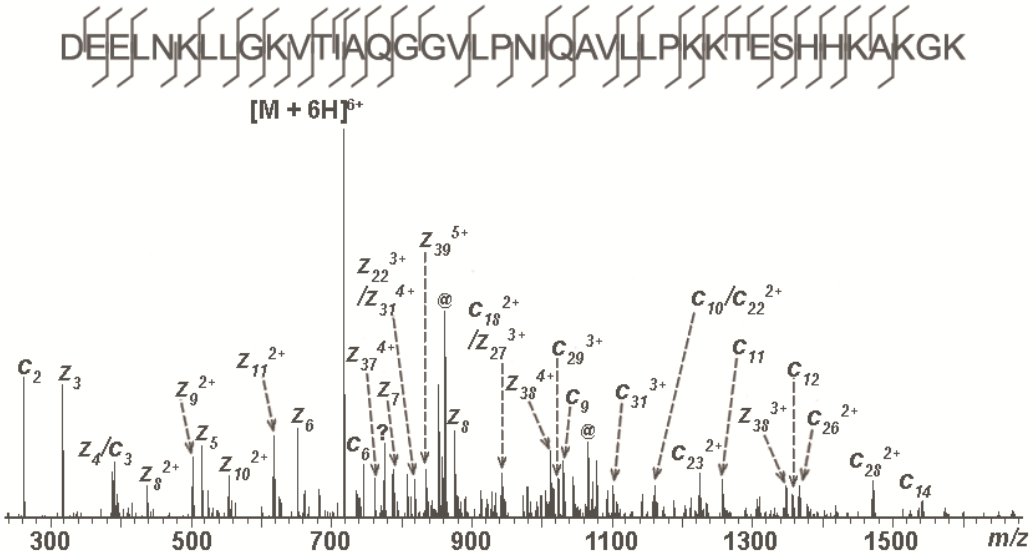

Figure S21. ECD spectrum of the peptide 90-130 (4.3 kDa) from histone H2A type 2-A (and/or H2A.1). Extensive ECD fragmentation was observed by data dependent middle-down LC-ECD MS/MS resulting in 77% peptide sequence coverage. The peptide was derived from Asp-N digestion of histones extracted from Jurkat cells. Only the major peaks are labeled in the figure. @ = charge-reduced species and neutral or side chain losses

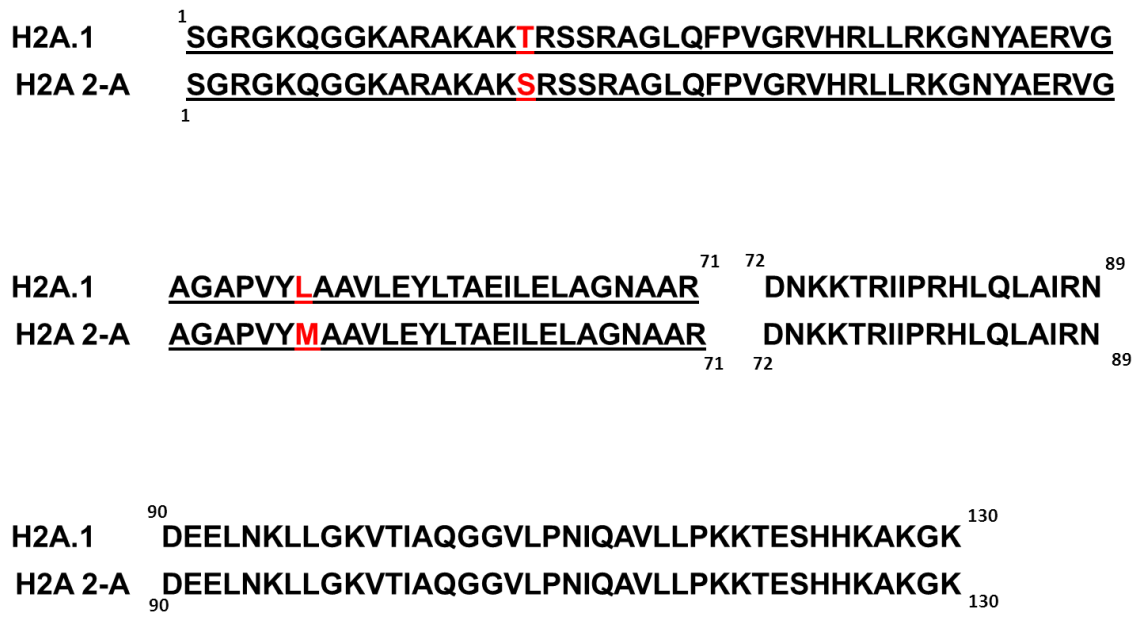

Figure S22. Sequence alignment for human histones H2A 2-A and H2A.1. Amino acid sequence differences are indicated in red. These two histones variants differ only at amino acids at positions 16 and 51. Peptides 1-71, 72-89 and 90-130 were all detected and fragmented by data-dependent ECD, resulting in complete protein sequence coverage for both variants. Peptides 72-89 and 90-130 are shared between H2A type 2-A and H2A type 1 and, therefore do not allow differentiation between these two variants. However, the detection and identification of peptide 1-71 (underlined in the figure) from H2A 2-A and H2A.1 enabled differentiation and assignment of both histone variants. The ECD spectrum of peptide 90-130 is shown in Figure S21.The ECD spectra of peptide 1-71 from H2A 2-A and H2A.1 are displayed in Figure S23.

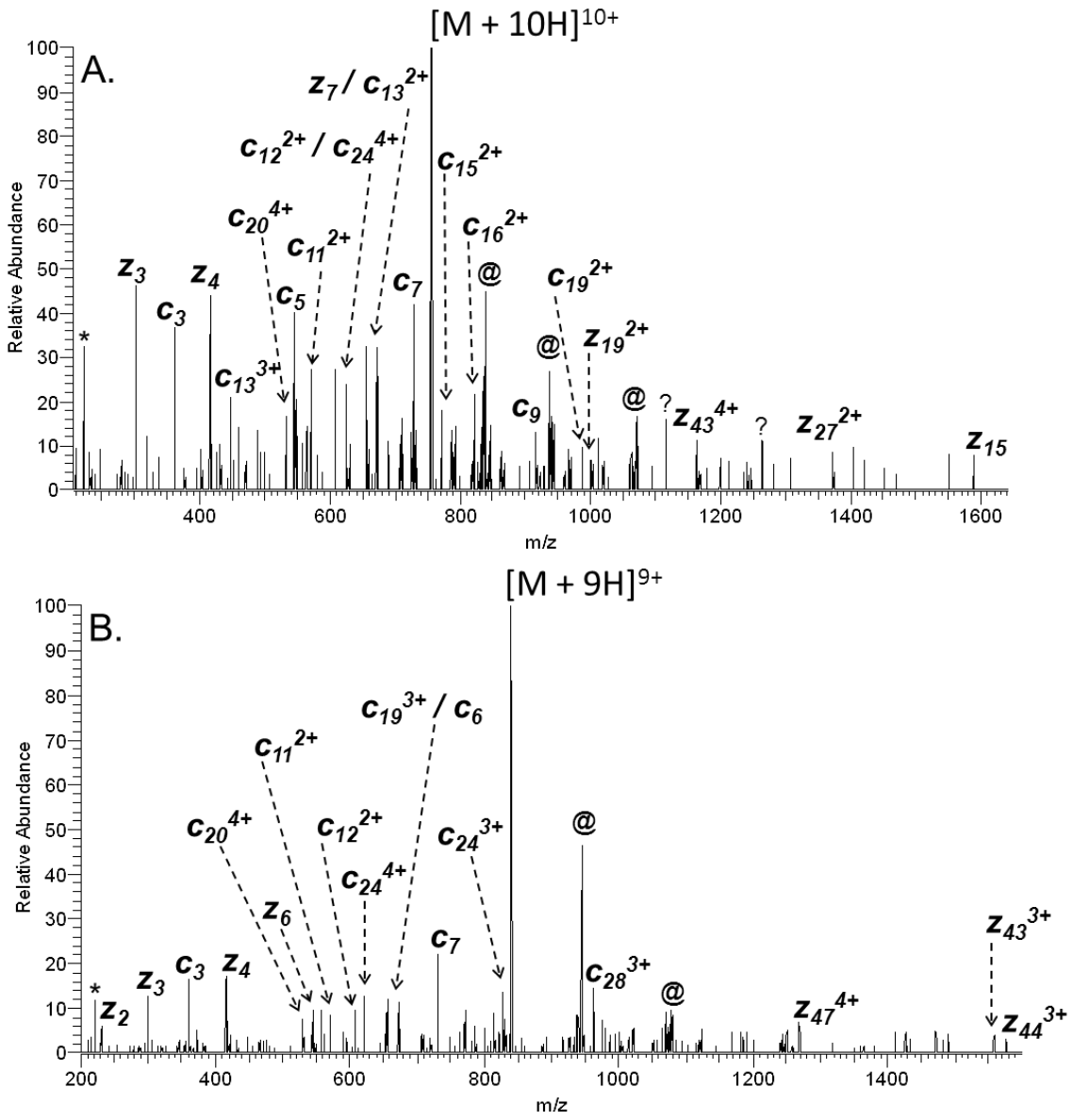

Figure S23. Data-dependent ECD of peptide 1-71 from H2A.1 (A) and H2A 2-A (B). The peptide sequences are shown in Figure S22. Only the major peaks are labeled in the figure.

@ = charge-reduced species and neutral or side chain losses.

Figure S24A. Peptides identified and PTM combinations observed for H2A 1-H (A), H2A 1-B (B), H2A 1-D (C), H2A 2-B (D), H2A 2-C (E), and H2A.3 (F) from Jurkat cells. Peptides were derived from Glu-C digestion.

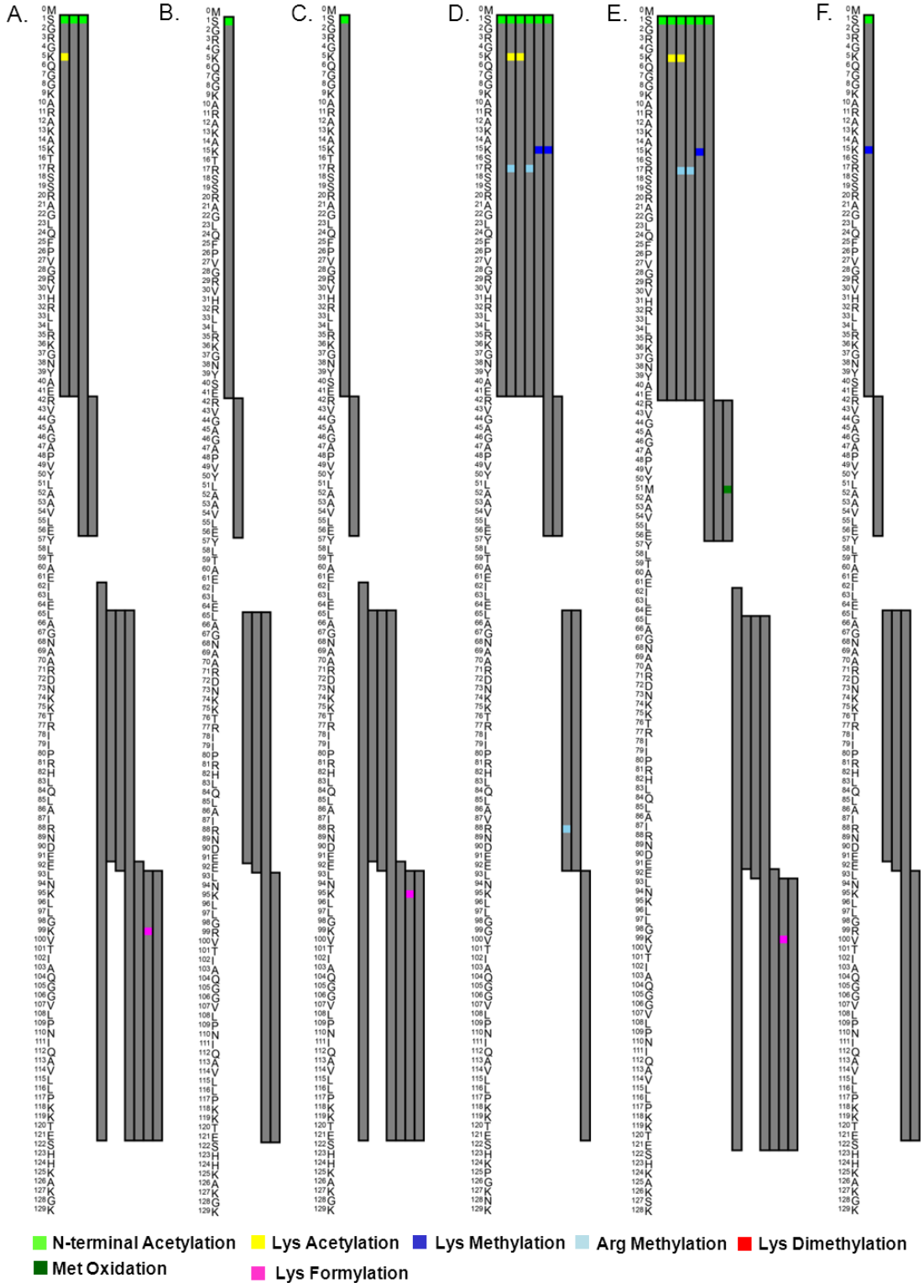

Figure S24B. Peptides identified and PTM combinations observed for H2A (A), H2A.x (B), H2A.Z (C) from Jurkat cells. Peptides were derived from Glu-C digestion.

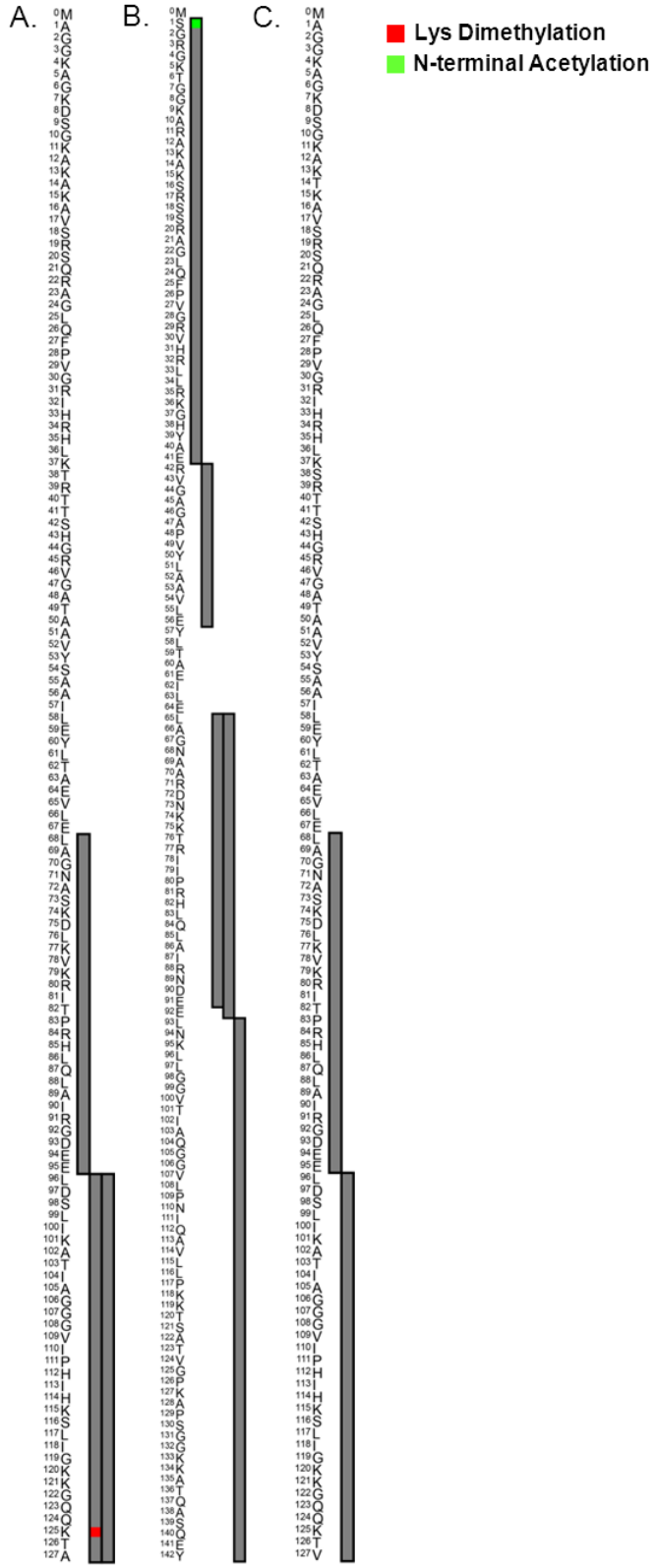

Figure S24C. Peptides identified and PTM combinations observed for H2B 1-C/E/F/G/I (A), H2B 1-J (B), H2AB 1-K (C) and H2B 2-E (D) from Jurkat cells. Peptides were derived from Glu-C digestion.

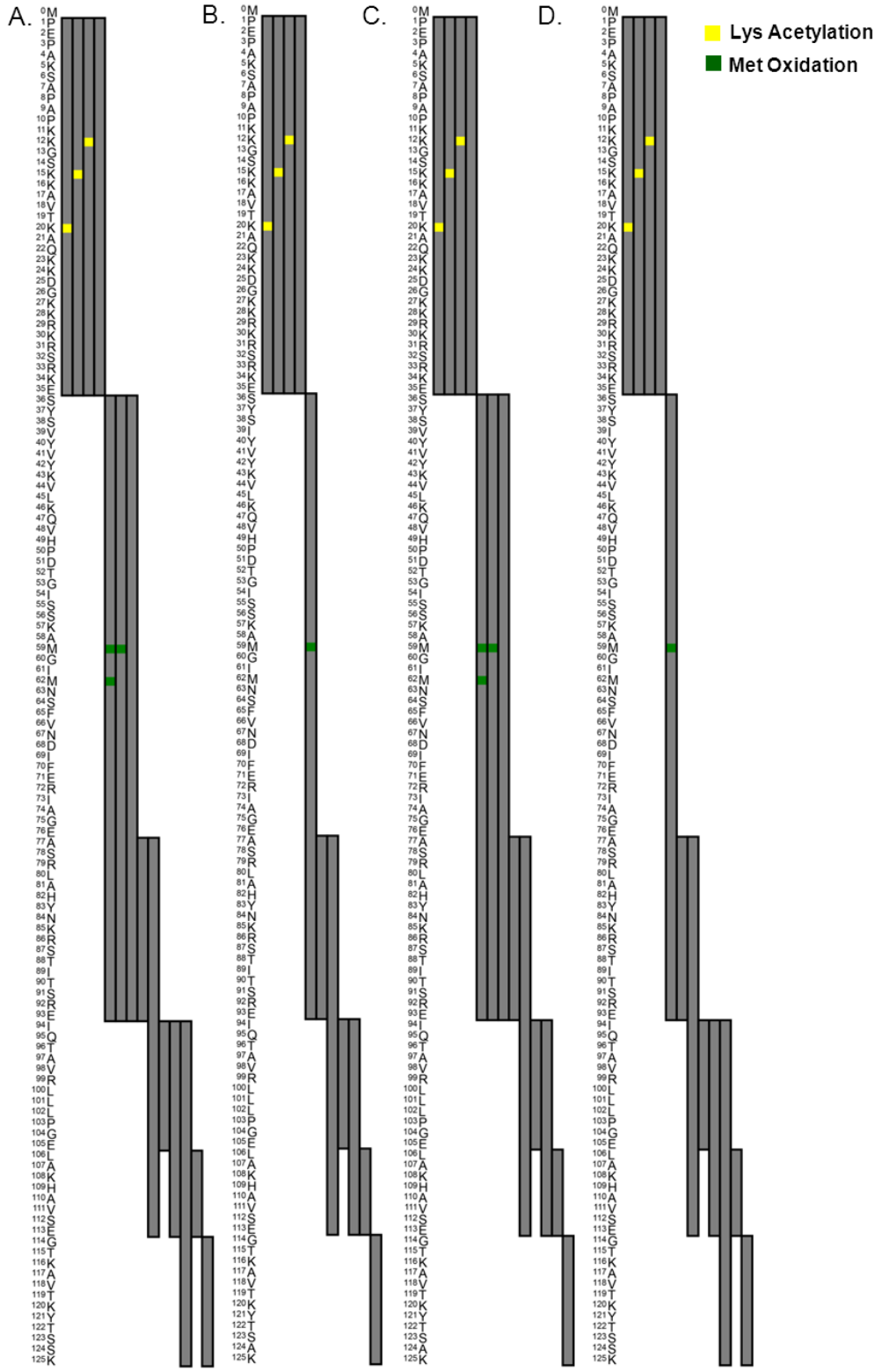

Figure S24D. Peptides identified and PTM combinations observed for H2B 1-H (A), H2B 1-O (B), H2B 2-F (C) and H2B 3-B (D) from Jurkat cells. Peptides were derived from Glu-C digestion.

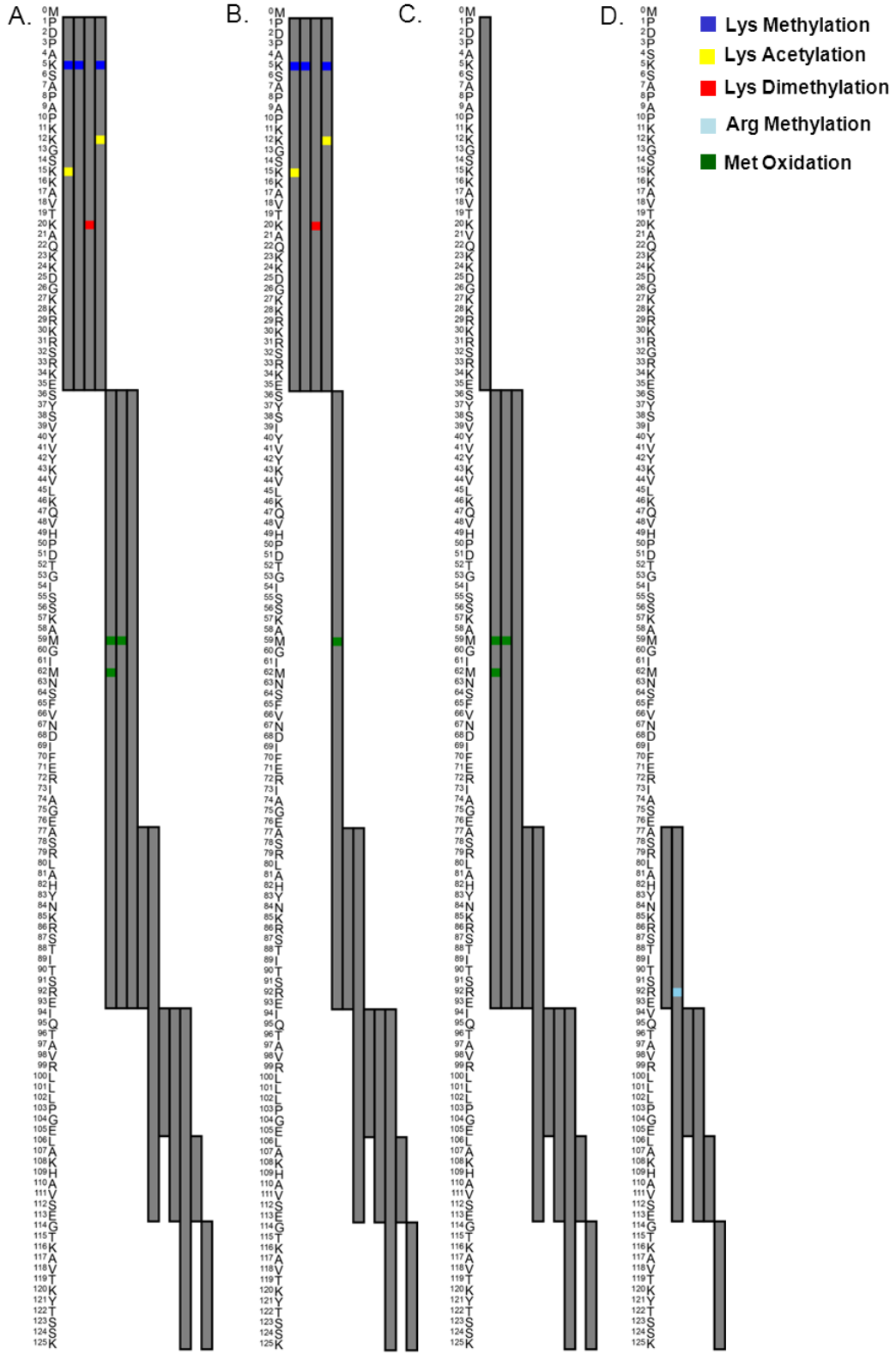

Figure S24E. Peptides identified and PTM combinations observed for H1.x (A), H1.2 (B), H1.3 (C), and H1.4 (D) and H1.5 (E) from Jurkat cells. Peptides were derived from Glu-C digestion.

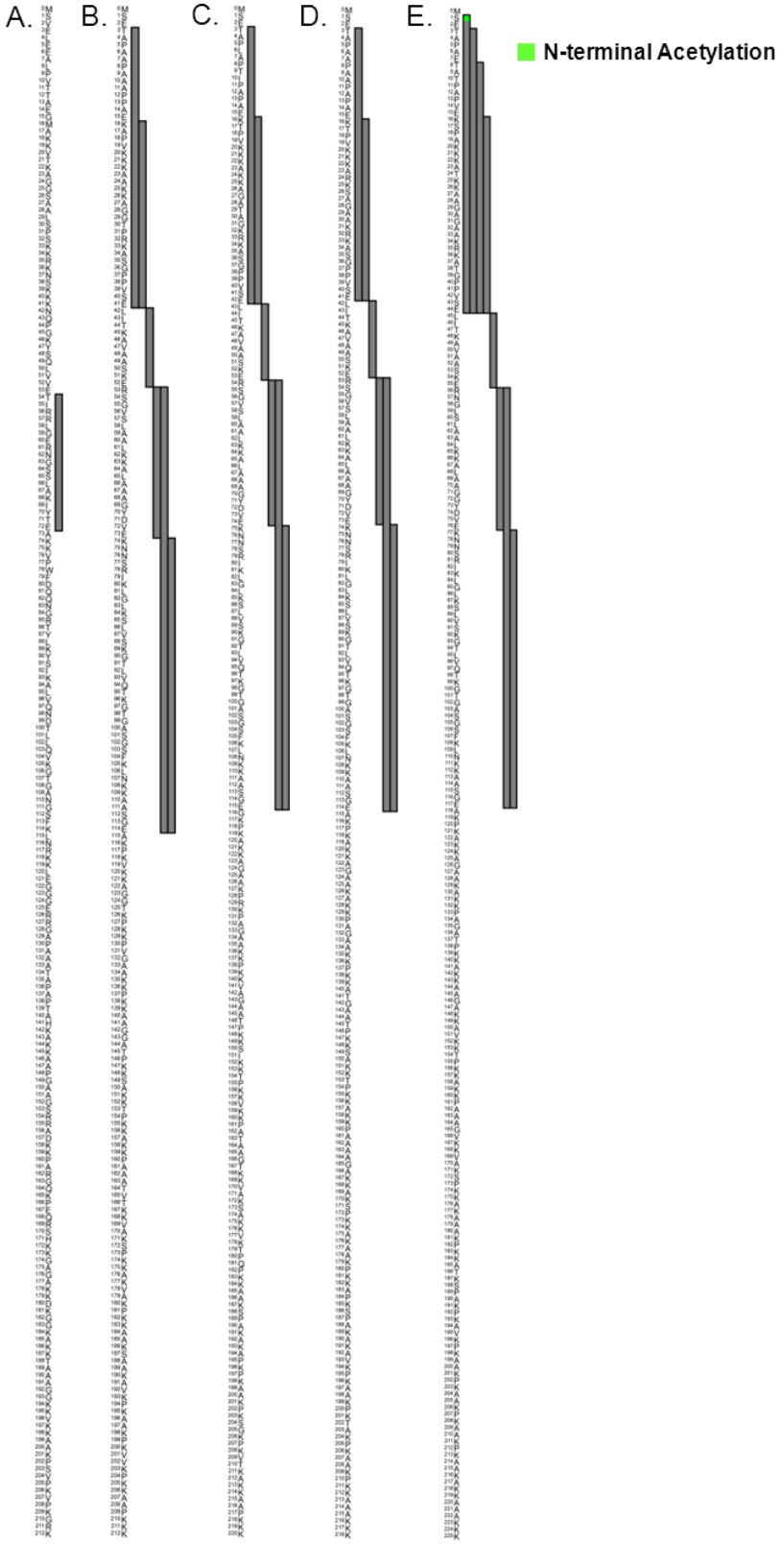

Figure S24F. Peptides identified and PTM combinations observed for H4 (A) and H3.2 (B) from Jurkat cells. Peptides were derived from Glu-C digestion.

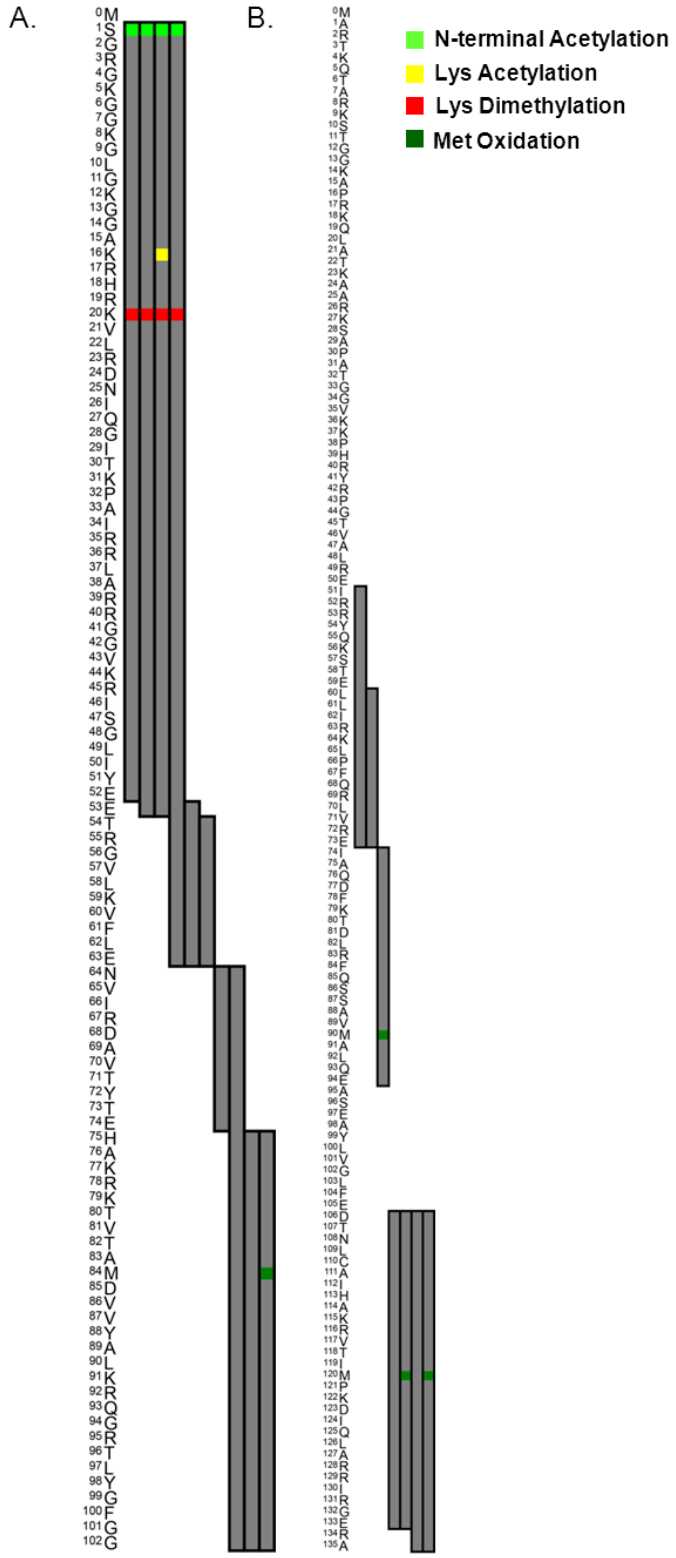

Figure S25A. Peptides identified and PTM combinations observed for H2A.1 (A), H2A 1-C (B), H2A 2-B (C), H2A 1-H (D), H2A 1-J (E) H2A 2-A (F) and H2A 2-C (G) from Jurkat cells. Peptides were derived from Asp-N digestion.

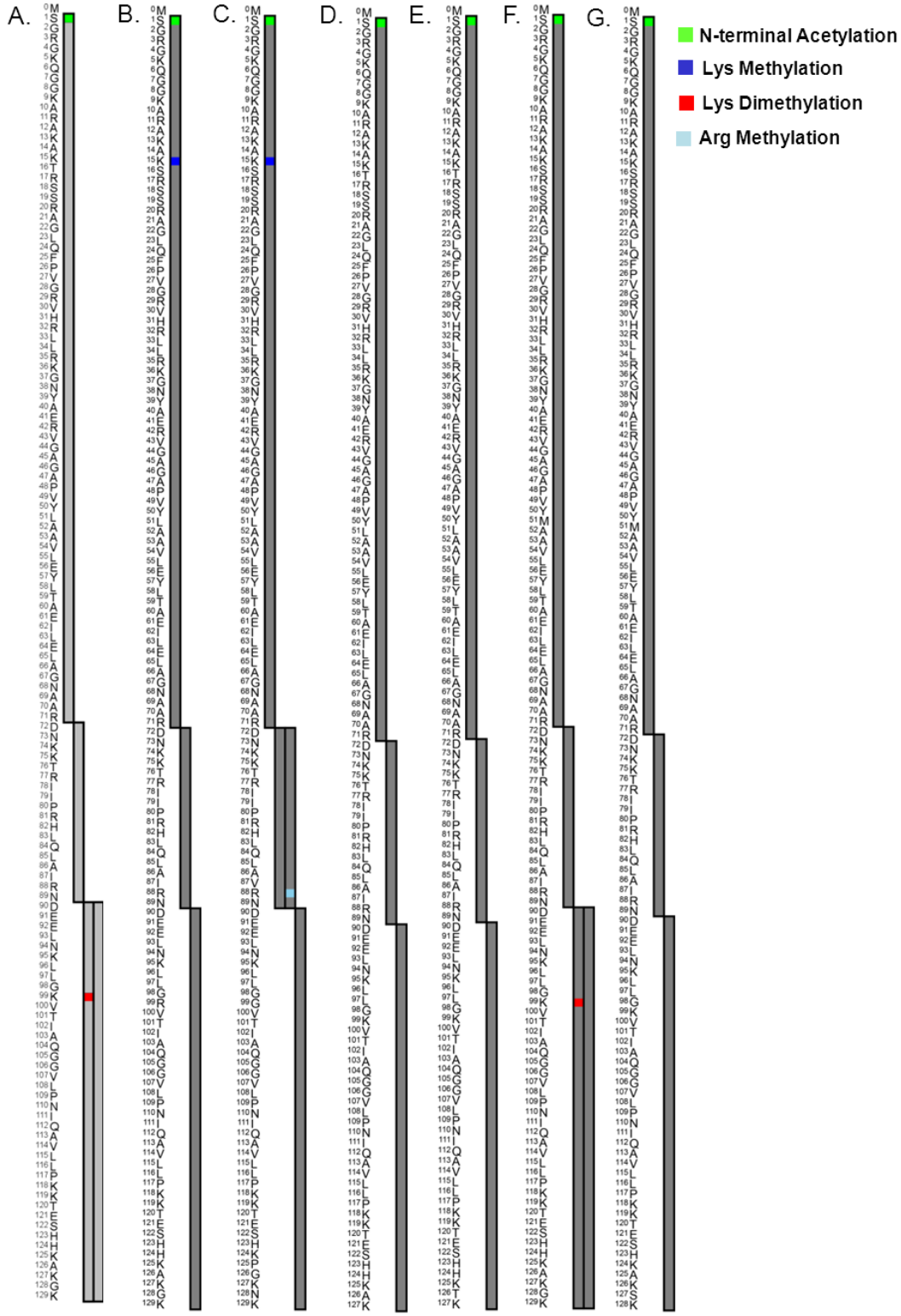

Figure S25B. Peptides identified and PTM combinations observed for H2A 1-B/E (A), H2A.3 (B), H2A (C), H2A.x (D) and H2A.Z 2-A (E) from Jurkat cells. Peptides were derived from Asp-N digestion.

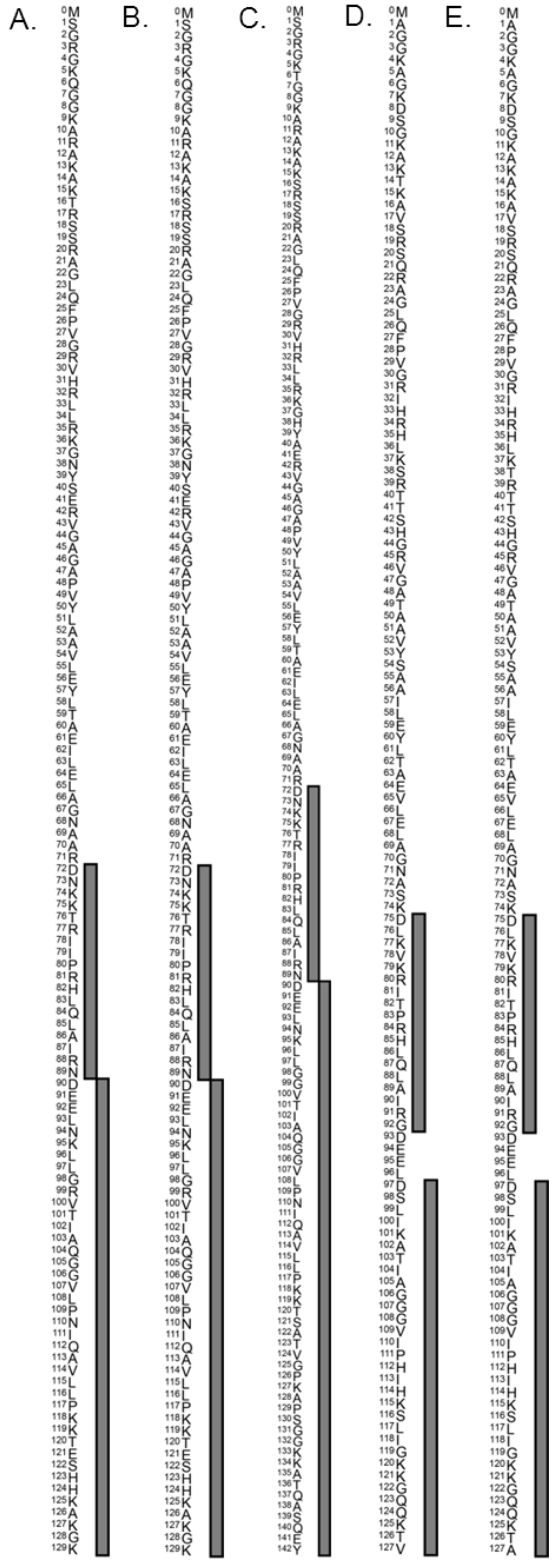

Figure S25C. Peptides identified and PTM combinations observed for H2B 1-C/E/F/G/I (A), H2B 1-J (B), H2B 1-K (C), H2B 2-E (D), H2B 1-H (E) and H2B 1-O (F) from Jurkat cells. Peptides were derived from Asp-N digestion.

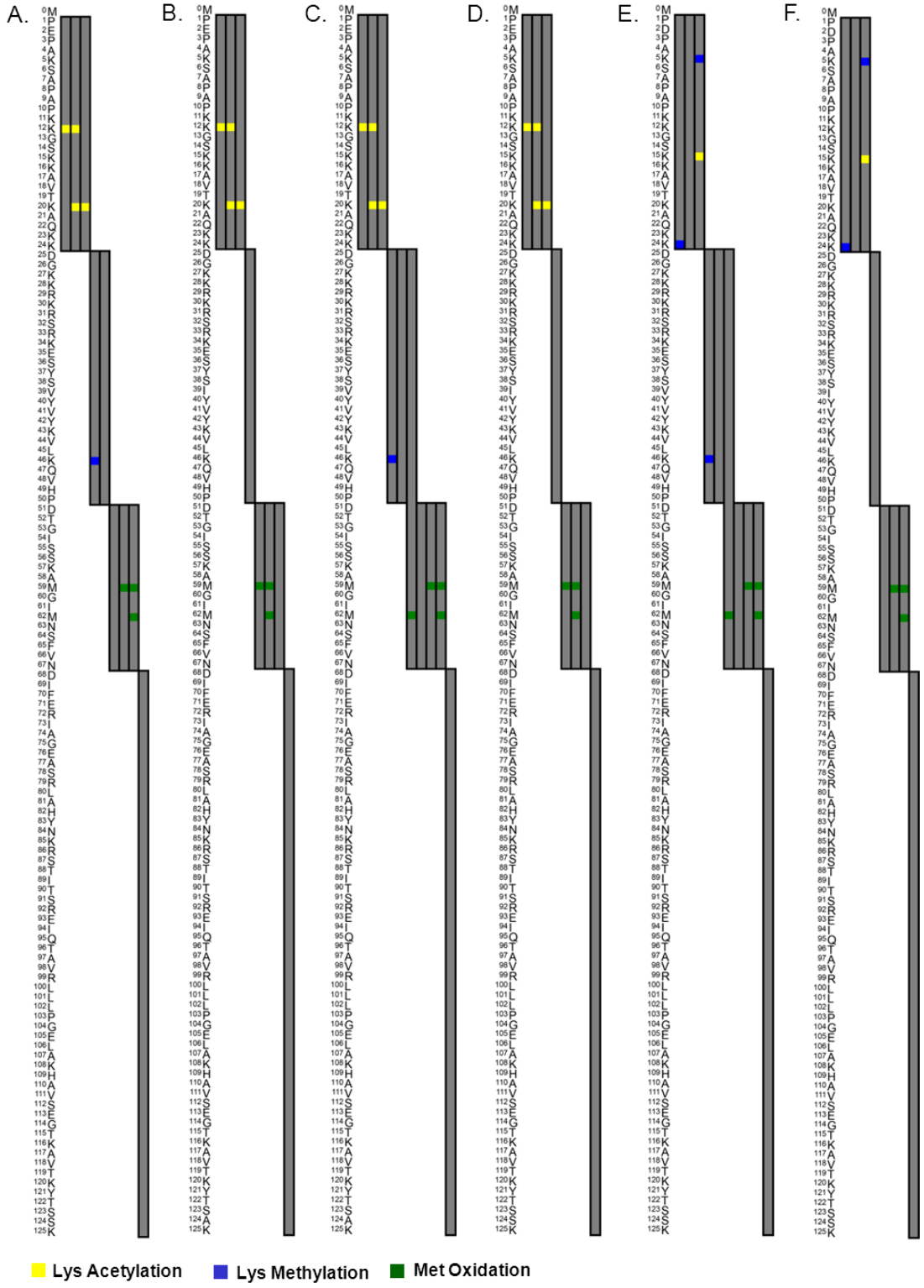

Figure S25D. Peptides identified and PTM combinations observed for H2B 1-B (A), H2B 1-N (B), H2B 1-L (C) and H2B 3-B from Jurkat cells. Peptides were derived from Asp-N digestion.

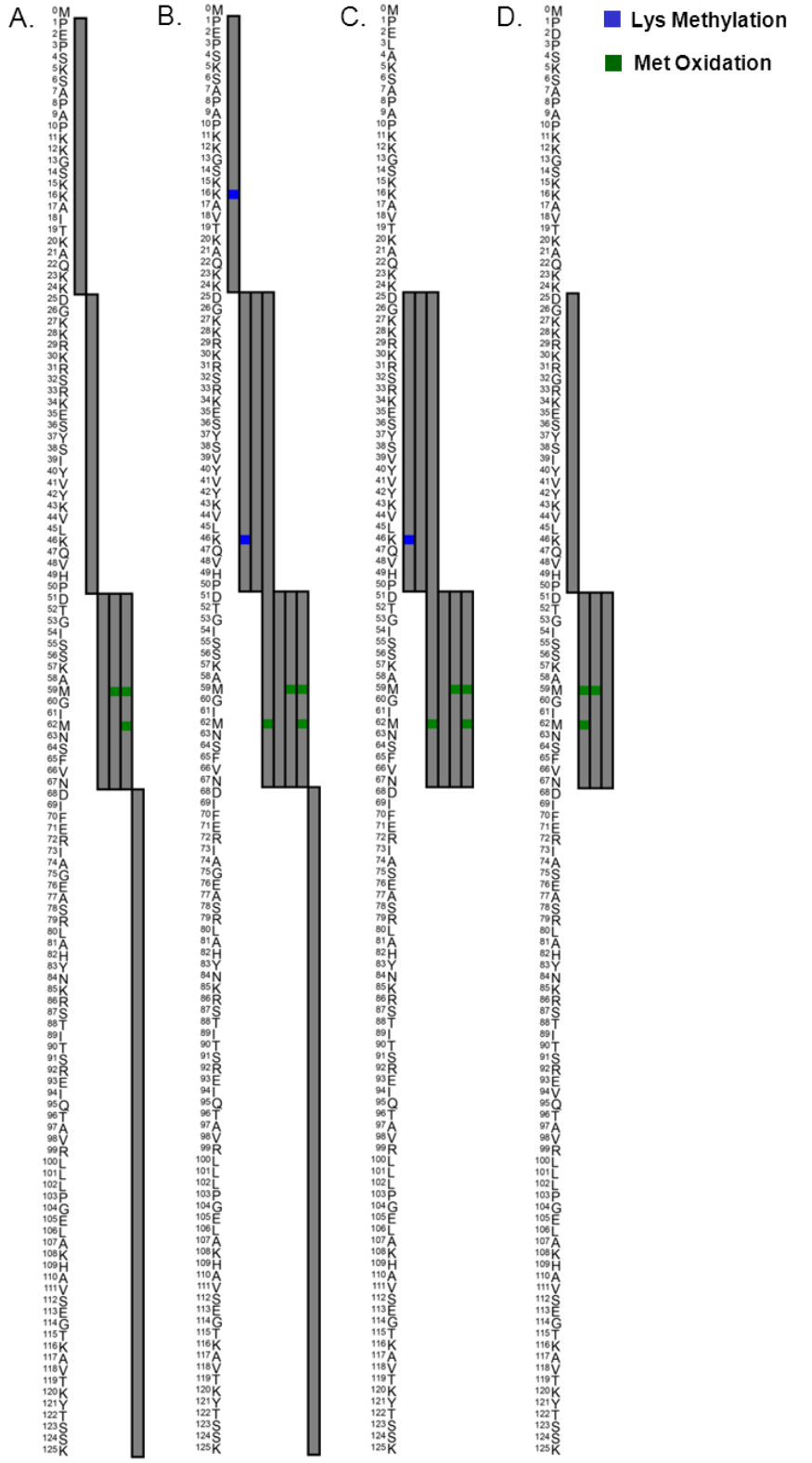

Figure S25E. Peptides identified and PTM combinations observed for H1.x (A), H1.0 (B), H1.2 (C), H1.3 (D) and H1.4 (E) from Jurkat cells. Peptides were derived from Asp-N digestion.

Figure S25F. Peptides identified and PTM combinations observed for H4 (A) and H3.2 (B) from Jurkat cells. Peptides were derived from Asp-N digestion.

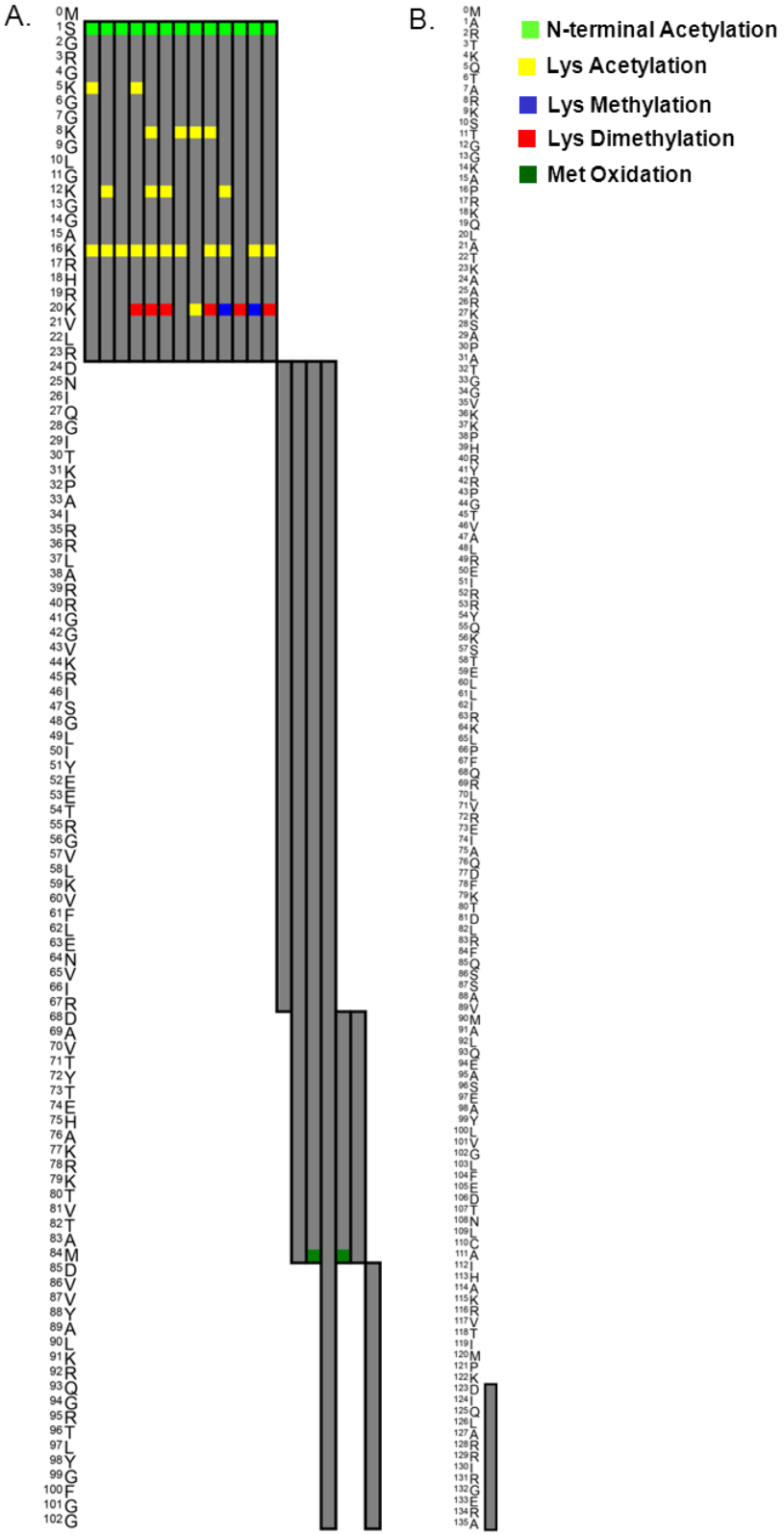

Figure S26A. Peptides identified and PTM combinations observed for H2A 2-C (A), H2A 1-C (B), H2A 2-B (C), H2A 1-D (D) and H2A 1-H (E) from HeLa cells. Peptides were derived from Glu-C digestion.

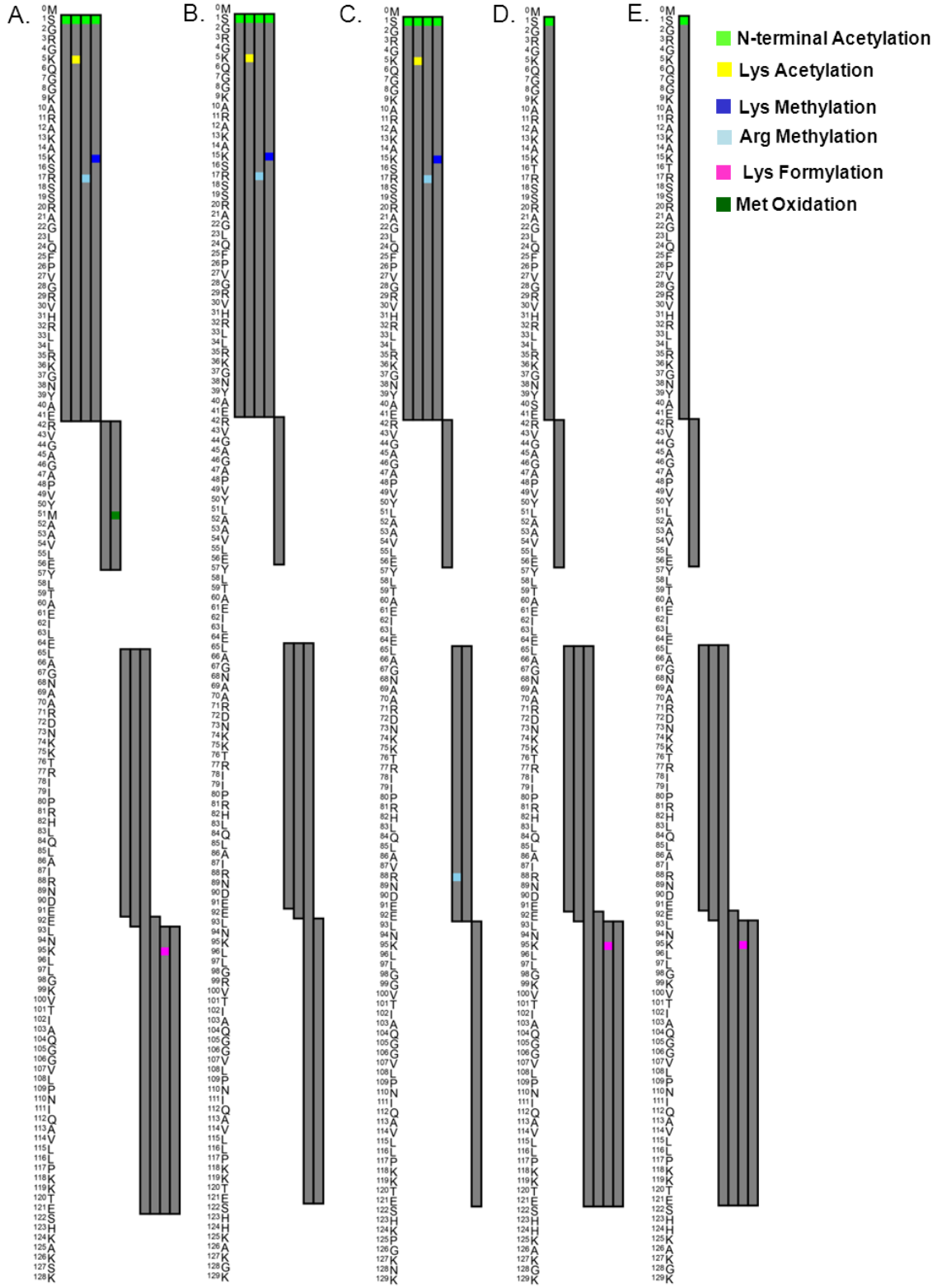

Figure S26B. Peptides identified and PTMs combinations observed for H2A 1-B/E (A), H2A.3 (B), H2A.x (C), H2A (D) and H2A.Z (E) from HeLa cells. Peptides were derived from Glu-C digestion.

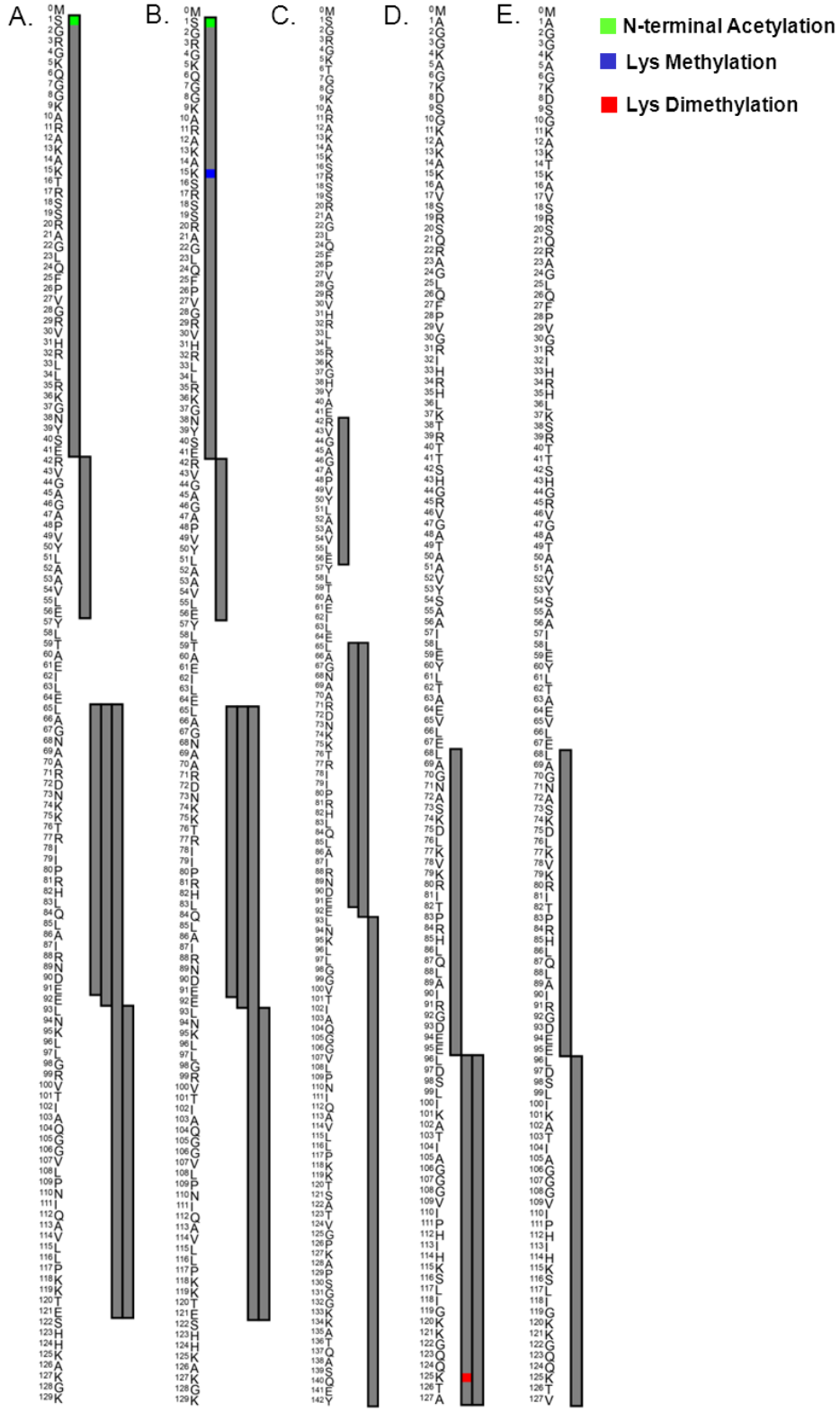

Figure S26C. Peptides identified and PTM combinations observed for H2B 1-C/E/F/G/I (A), H2B 1-J (B), H2B 1-K (C), H2B 2-E (D) and H2.B 1-H (E) from HeLa cells. Peptides were derived from Glu-C digestion.

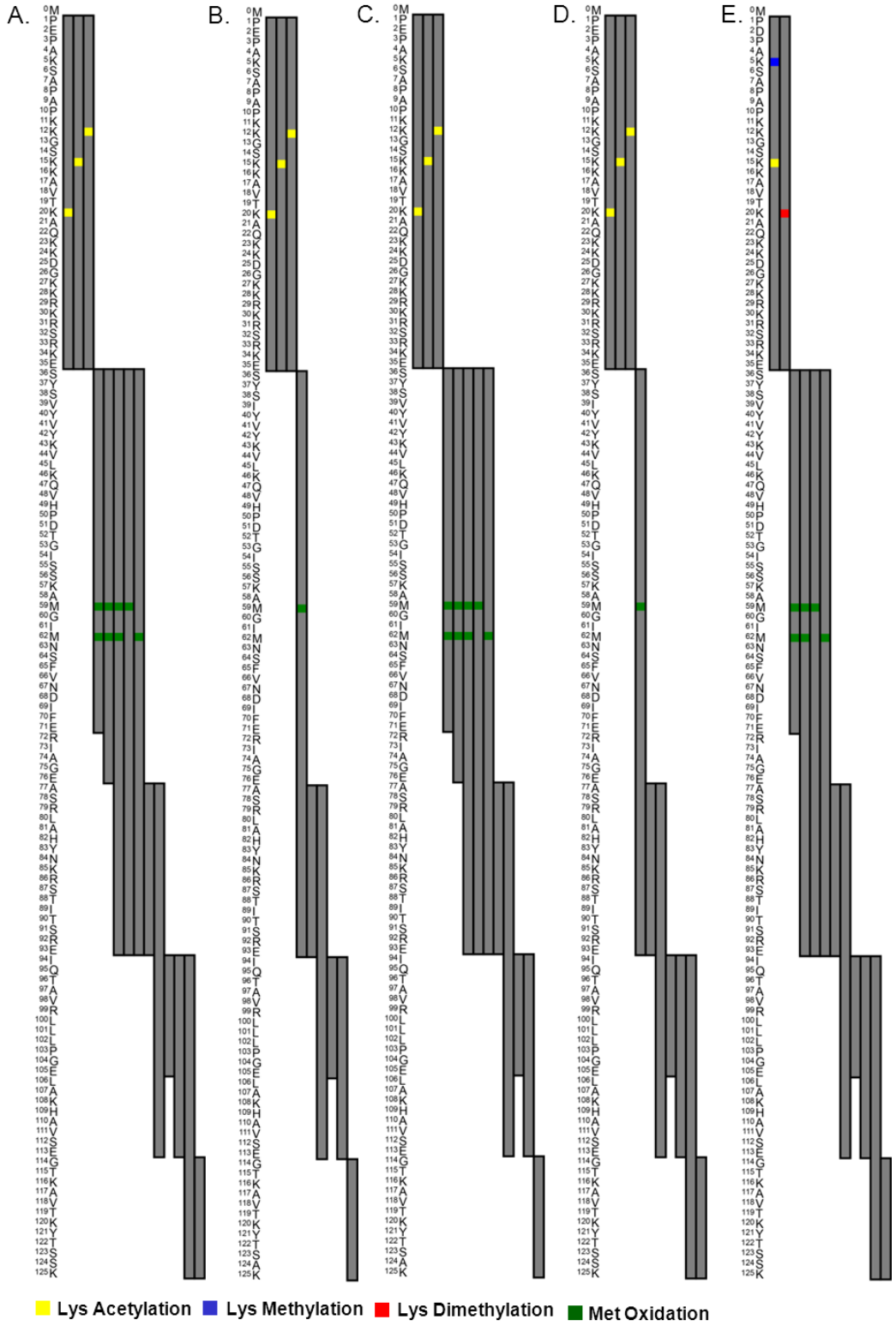

Figure S26D. Peptides identified and PTM combinations observed for H2B 2-F (A) and H2B 3-B (B) from HeLa cells. Peptides were derived from Glu-C digestion.

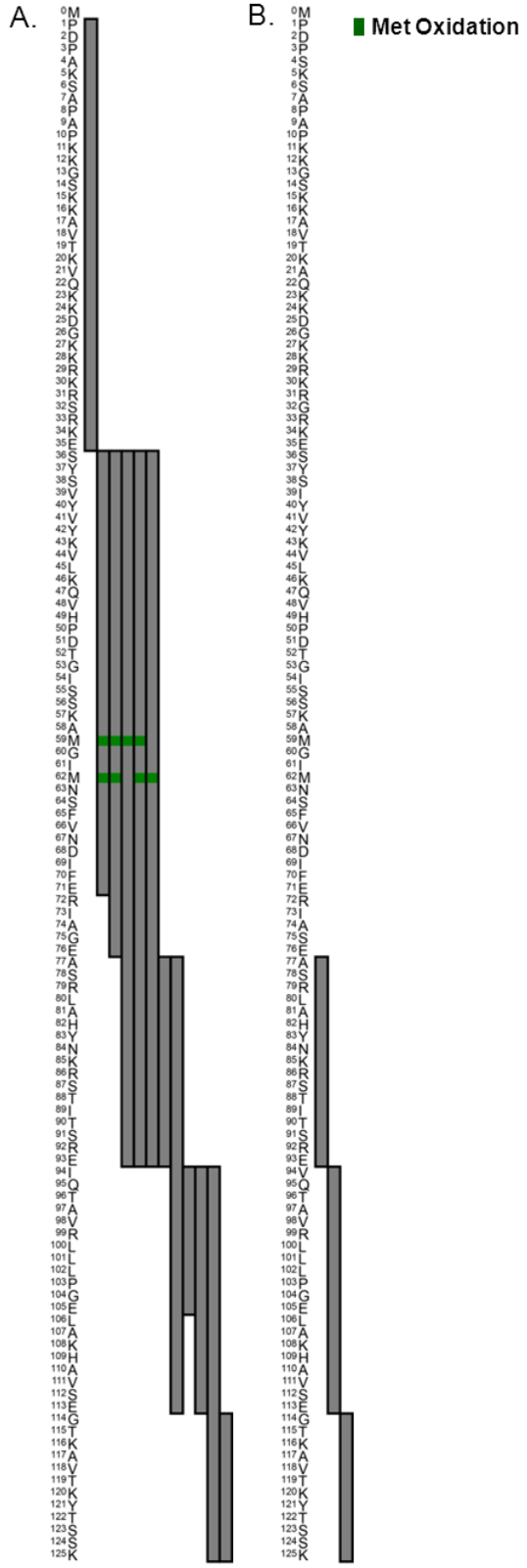

Figure S26E. Peptides identified and PTM combinations observed for H1.2 (A), H1.4 (B) and H1.5 (C) from HeLa cells. Peptides were derived from Glu-C digestion.

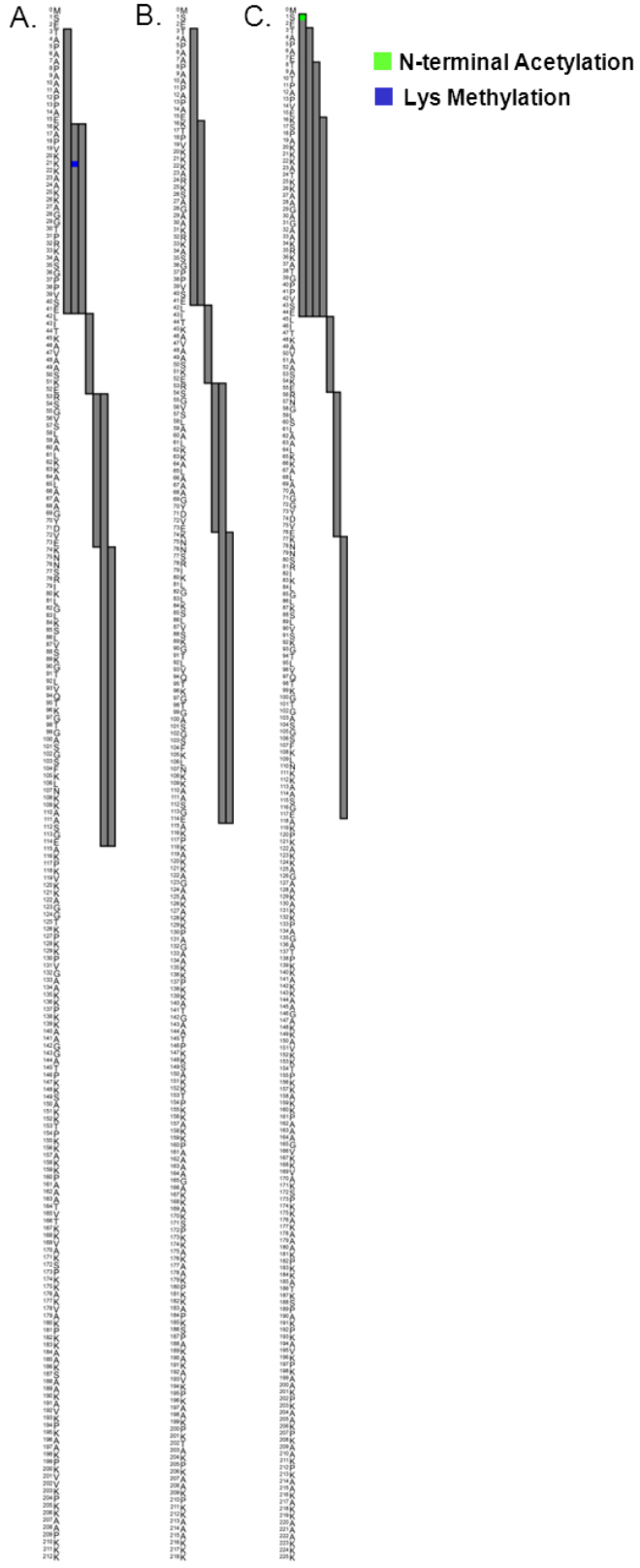

Figure S26F. Peptides identified and PTM combinations observed for H4 (A) and H3.2 (B) from HeLa cells. Peptides were derived from Glu-C digestion.

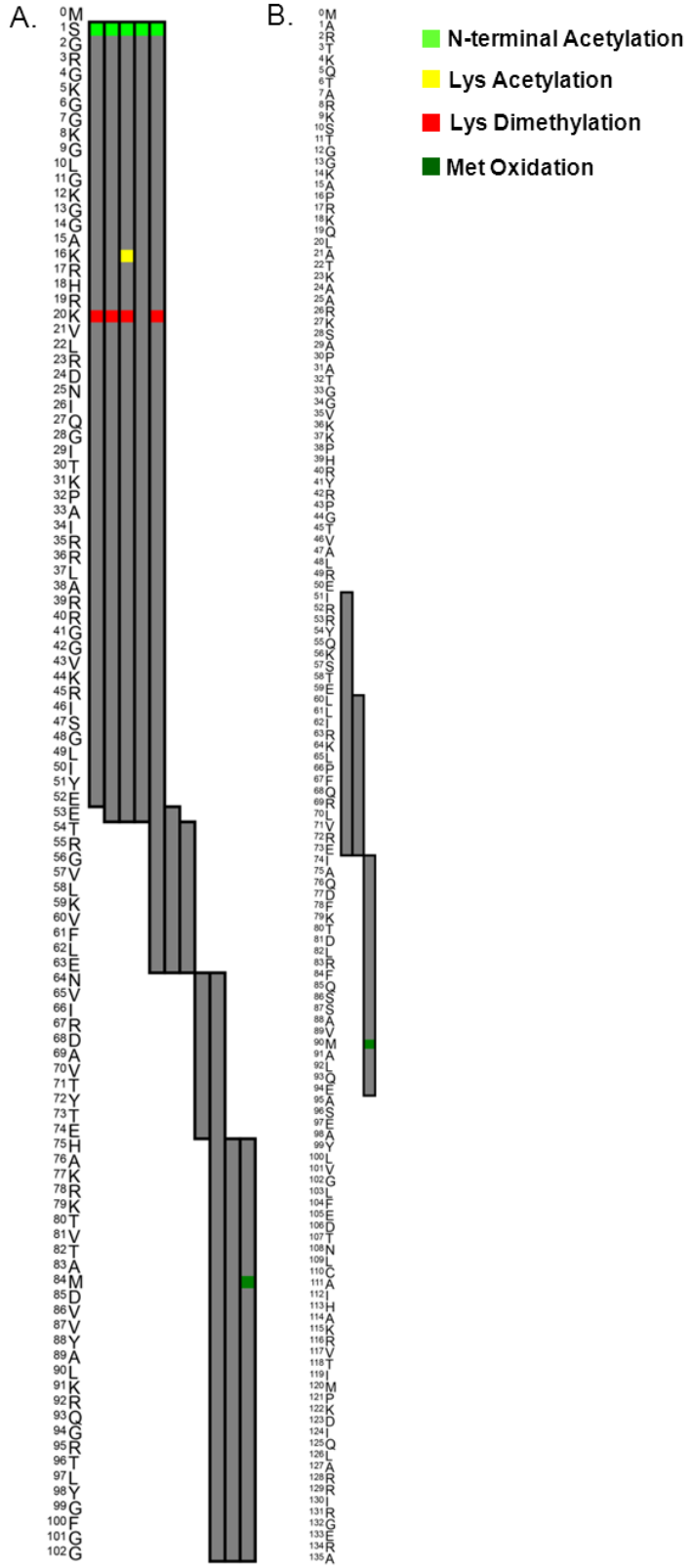

Figure S27A. Peptides identified and PTM combinations observed for H2A 2-C (A), H2A 2-A (B), H2A.1 (C), H2A 1-H (D), H2A 1-J (E), H2A 1-C (F) and H2A 2-B (G) from HeLa cells. Peptides were derived from Asp-N digestion.

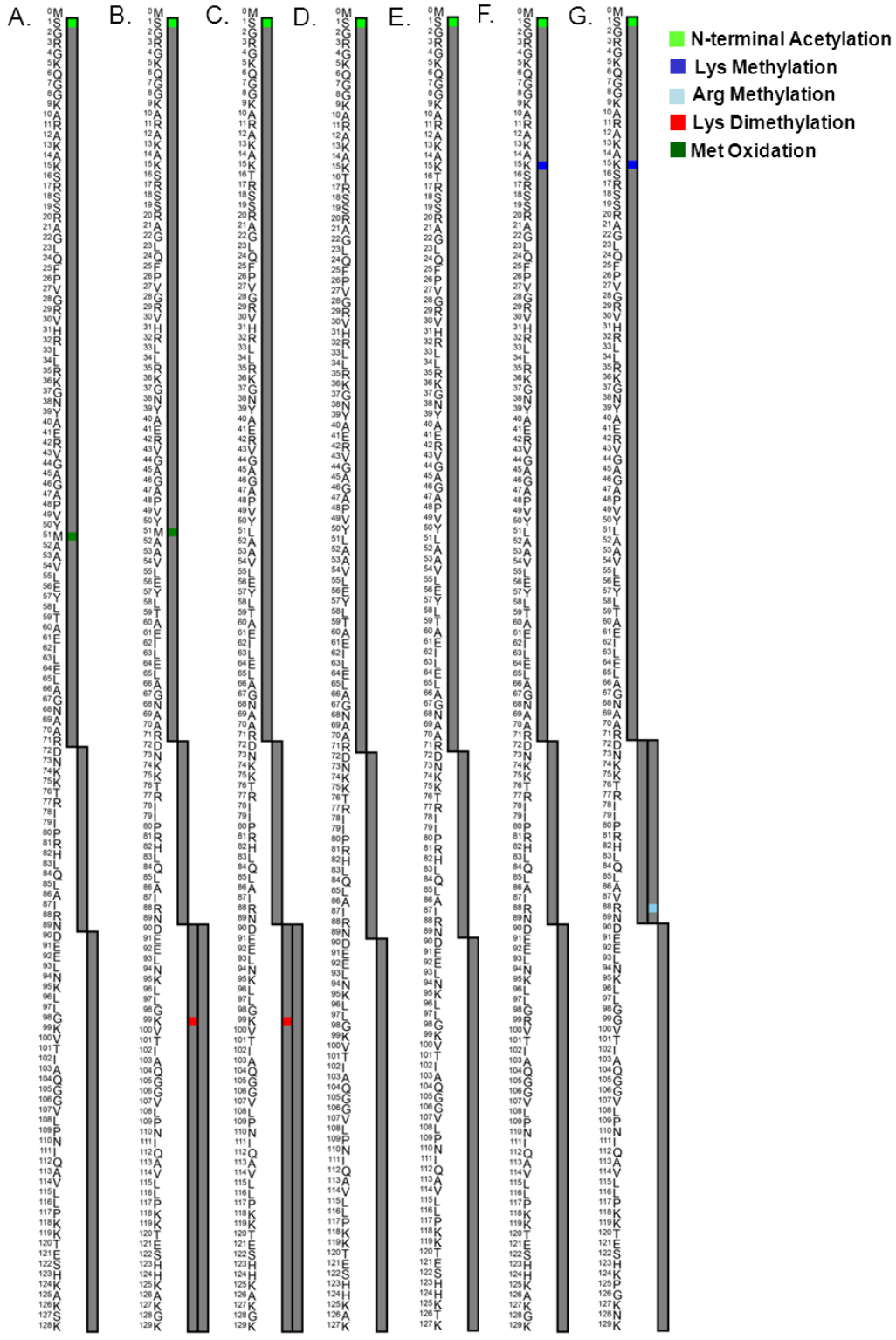

Figure S27B. Peptides identified and PTM combinations observed for H2A.x (A), H2A (B) and H2A.Z (C) from HeLa cells. Peptides were derived from Asp-N digestion.

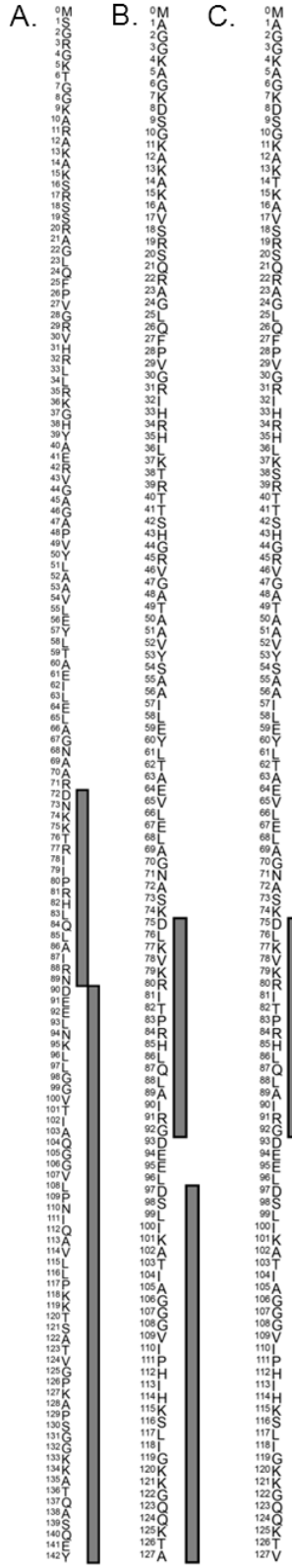

Figure S27C. Peptides identified and PTM combinations observed for H2B 1-C/E/F/G/I (A), H2B 2-E (B), H2B 1-J (C) and H2B 1-K (D) from HeLa cells. Peptides were derived from Asp-N digestion.

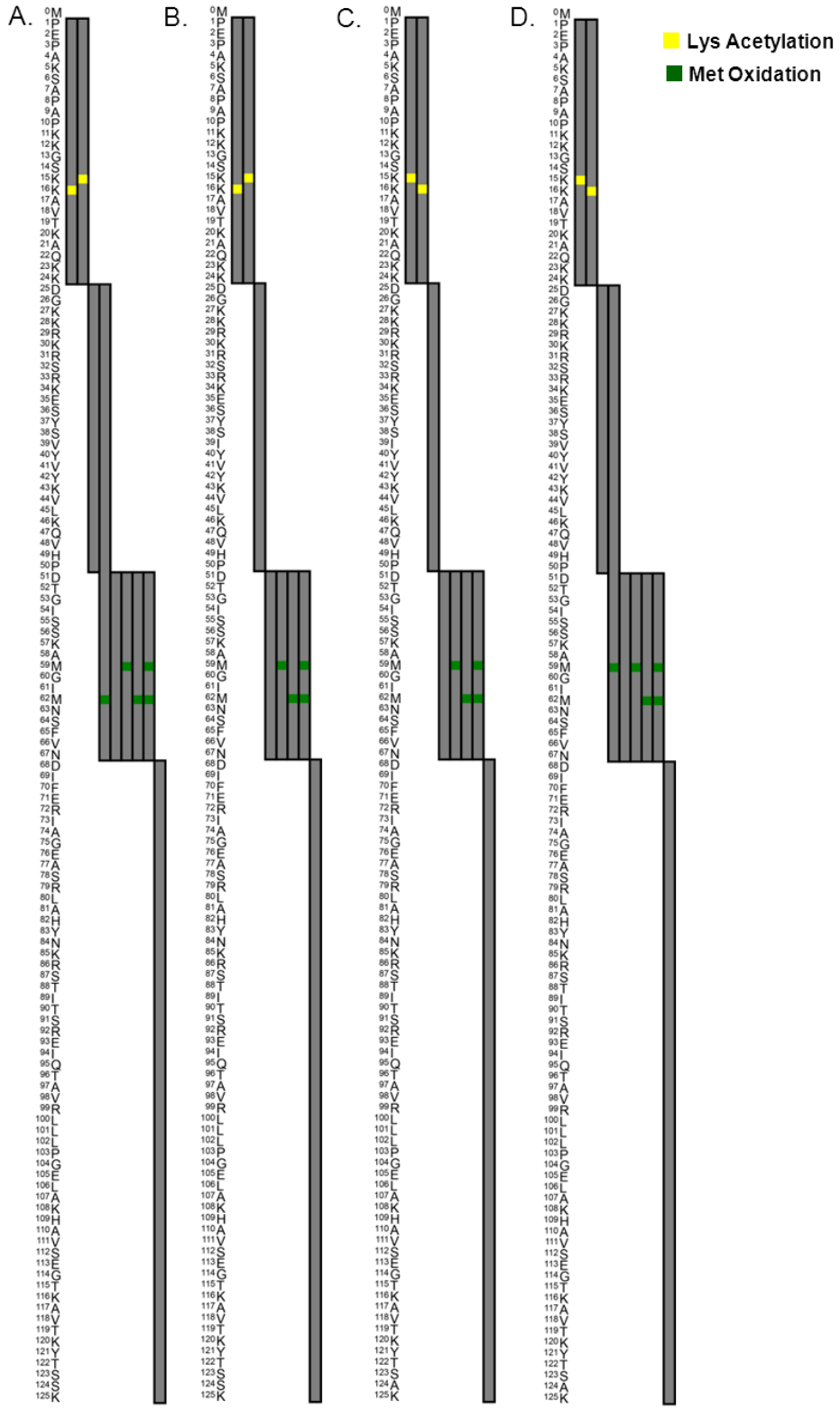

Figure S27D. Peptides identified and PTM combinations observed for H2B 1-O (A), H2B 1-H (B), H2B 2-F (C) and H2B 3-B (D) from HeLa cells. Peptides were derived from Asp-N digestion.

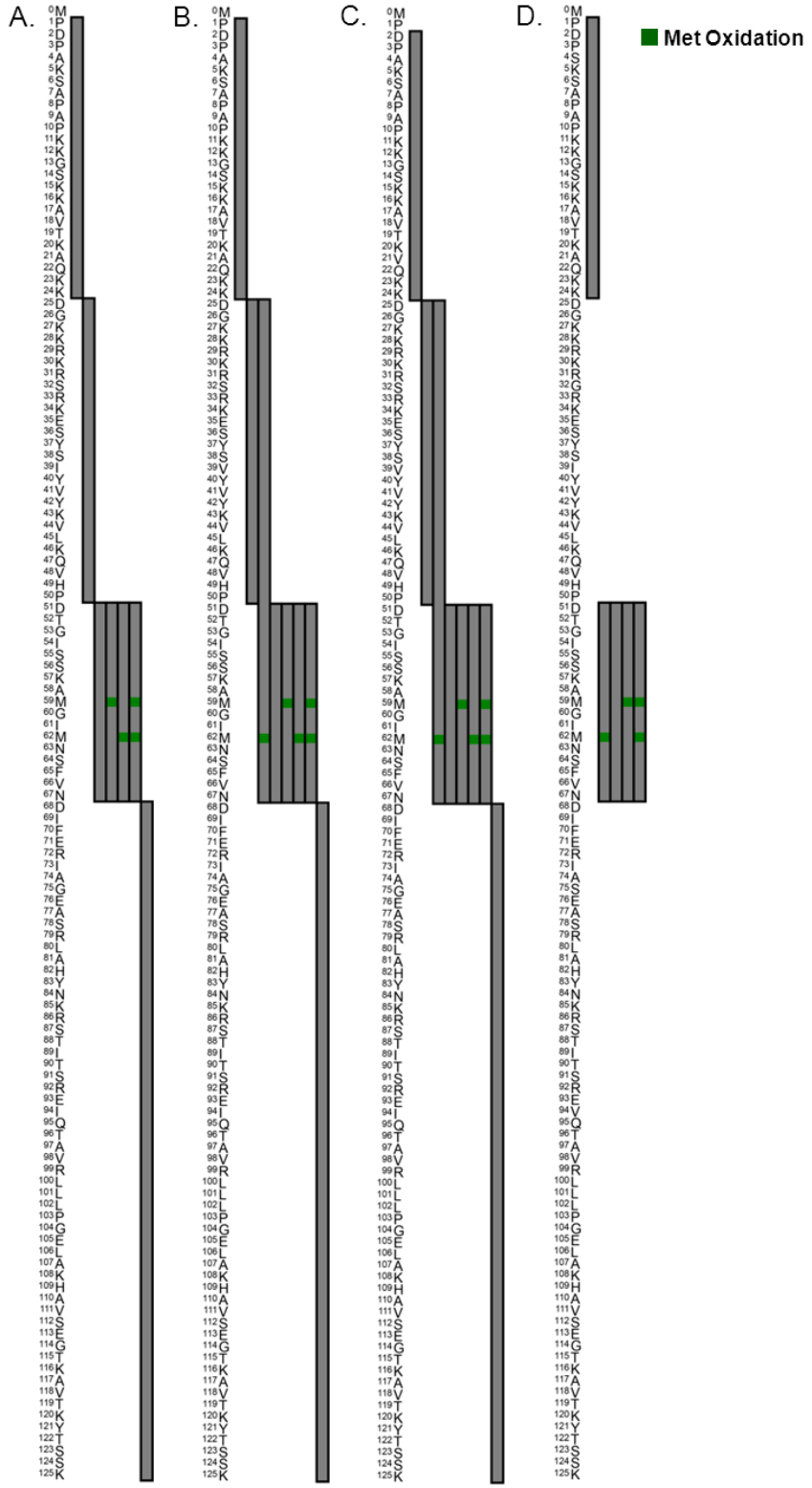

Figure S27E. Peptides identified and PTM combinations observed for H1.x (A), H1.2 (B) and H1.4 (C) from HeLa cells. Peptides were derived from Asp-N digestion.

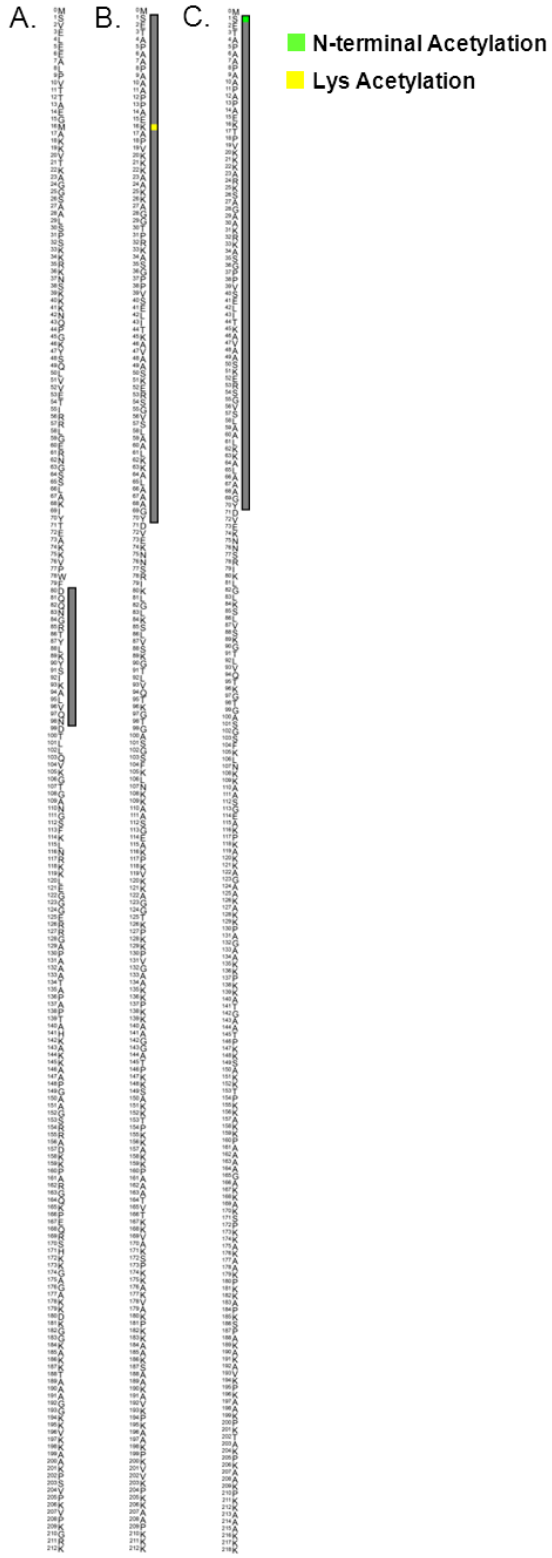

Figure S27F. Peptides identified and PTM combinations observed for H4 (A) and H3.3 (B) from HeLa cells. Peptides were derived from Asp-N digestion.

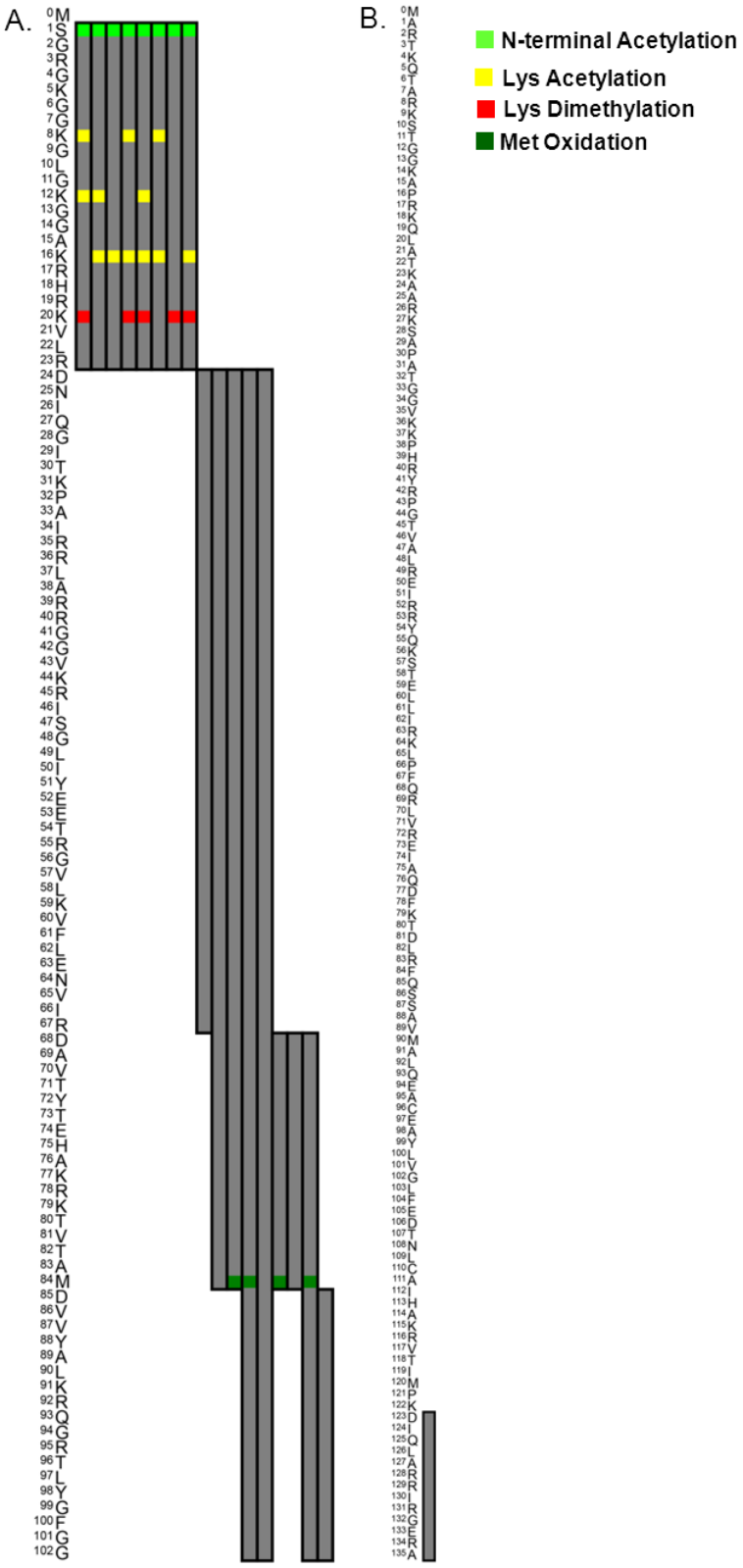

Figure S28A. Peptides identified and PTM combinations observed for H2A 1-H (A), H2A 1-D (B), H2A 1-B/E (C), H2A 2-C (D), H2A 1-C (E), H2A 2-B (F) and H2A.3 (G) from MCF-7 cells. Peptides were derived from Glu-C digestion.

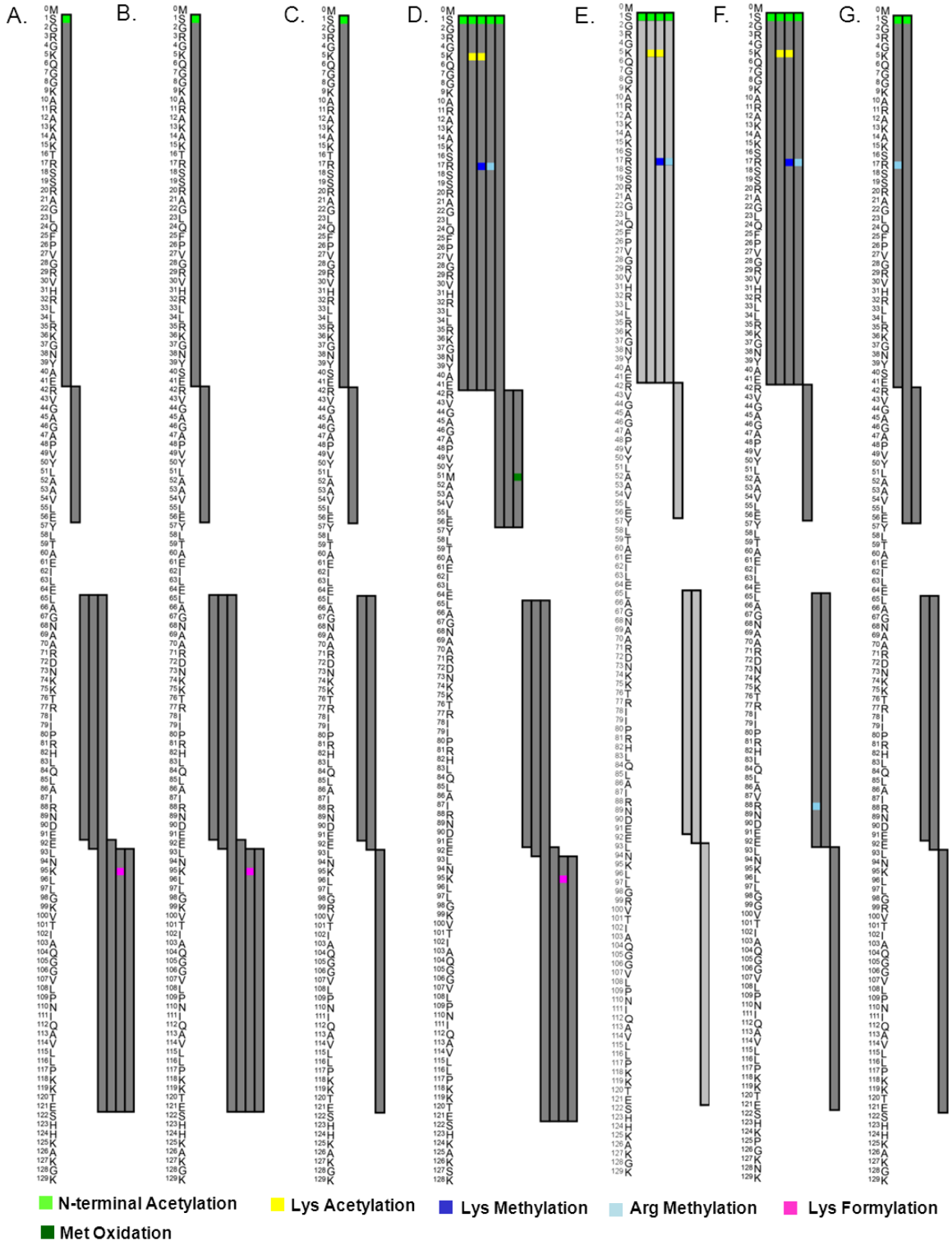

Figure S28B. Peptides identified and PTM combinations observed for H2A.x (A), H2A (B) and H2A.Z (C) from MCF-7 cells. Peptides were derived from Glu-C digestion.

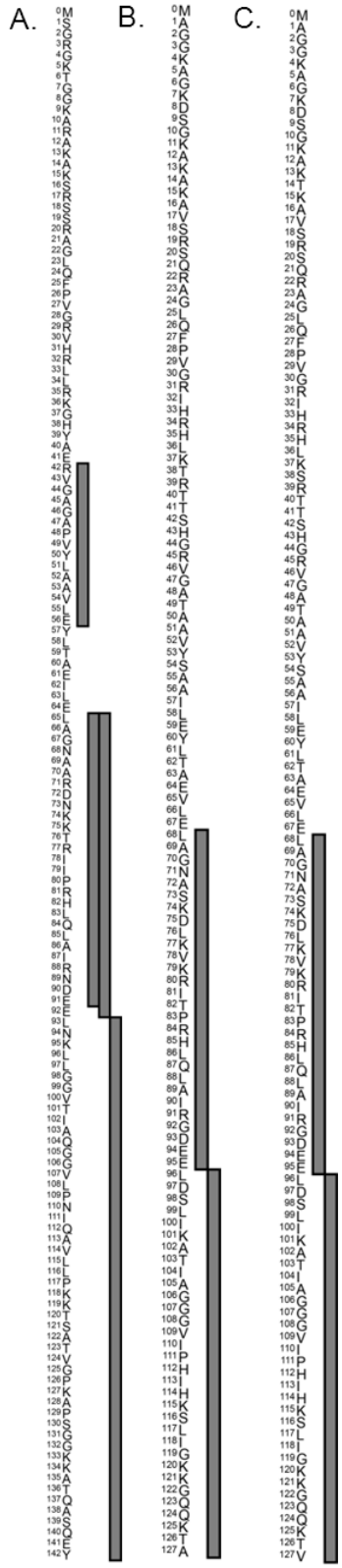

Figure S28C. Peptides identified and PTM combinations observed for H2B 1-M (A), H2B 1-K (B), H2B 1-C/E/F/G/I (C), H2B 2-F (D), H2B 1-H (E) and H2B 1-O (F) from MCF-7 cells. Peptides were derived from Glu-C digestion.

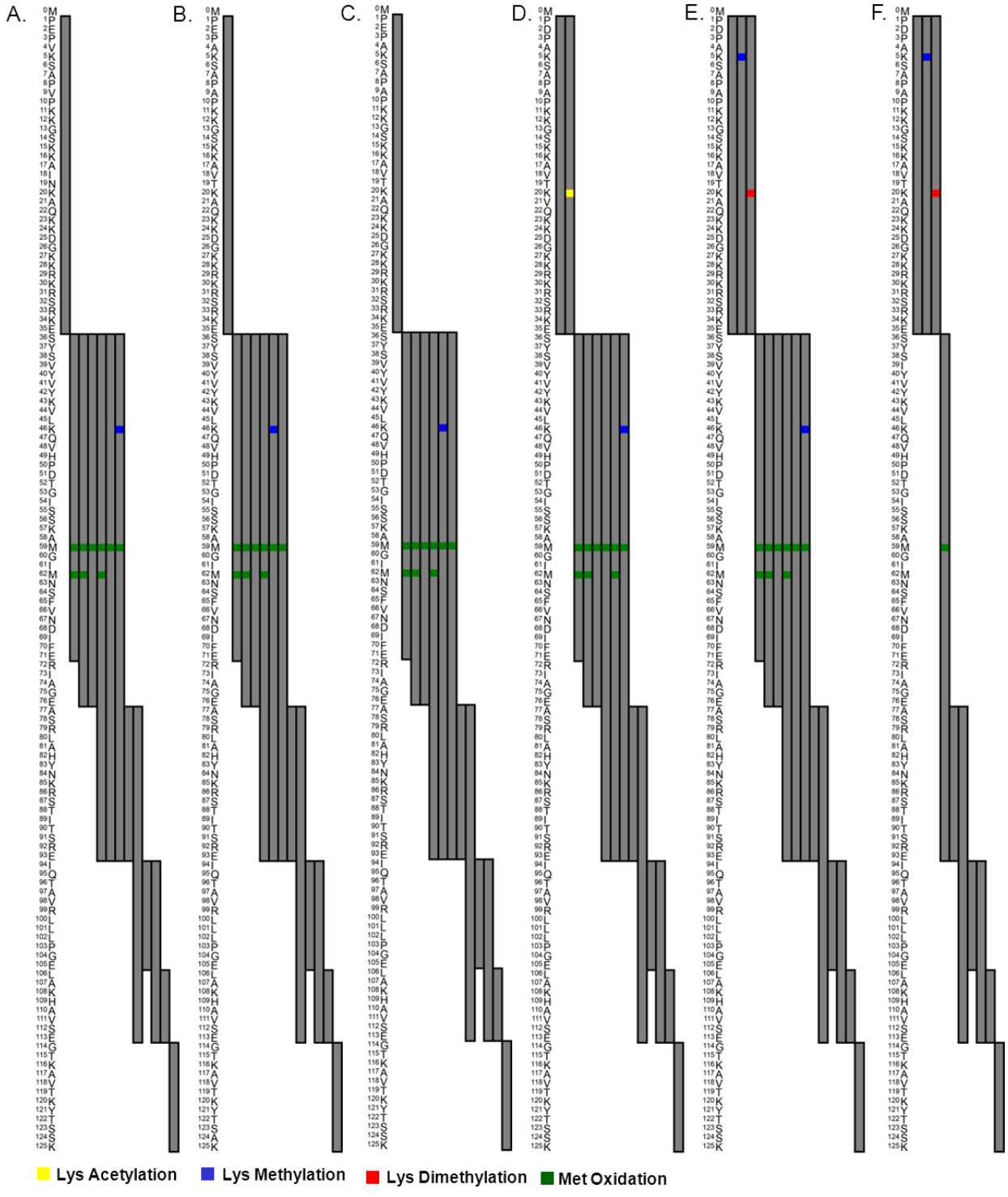

Figure S28D. Peptides identified and PTM combinations observed for H2B 1-J (A), H2B 2-E (B) and H2B 3-E (C) from MCF-7 cells. Peptides were derived from Glu-C digestion.

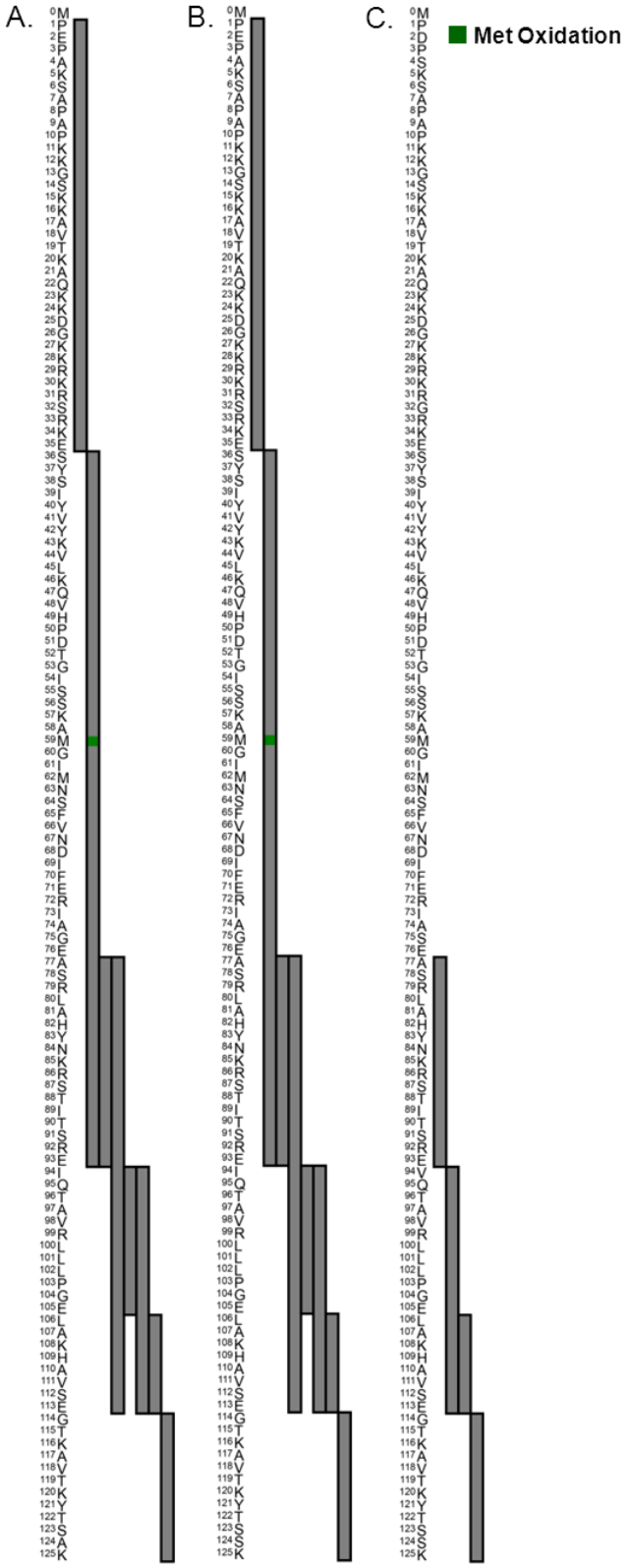

Figure S28E. Peptides identified and PTM combinations observed for H1.x (A), H1.0 (B), H1.2 (C), H1.3 (D), H1.4 (E) and H1.5 (F) from MCF-7 cells. Peptides were derived from Glu-C digestion.

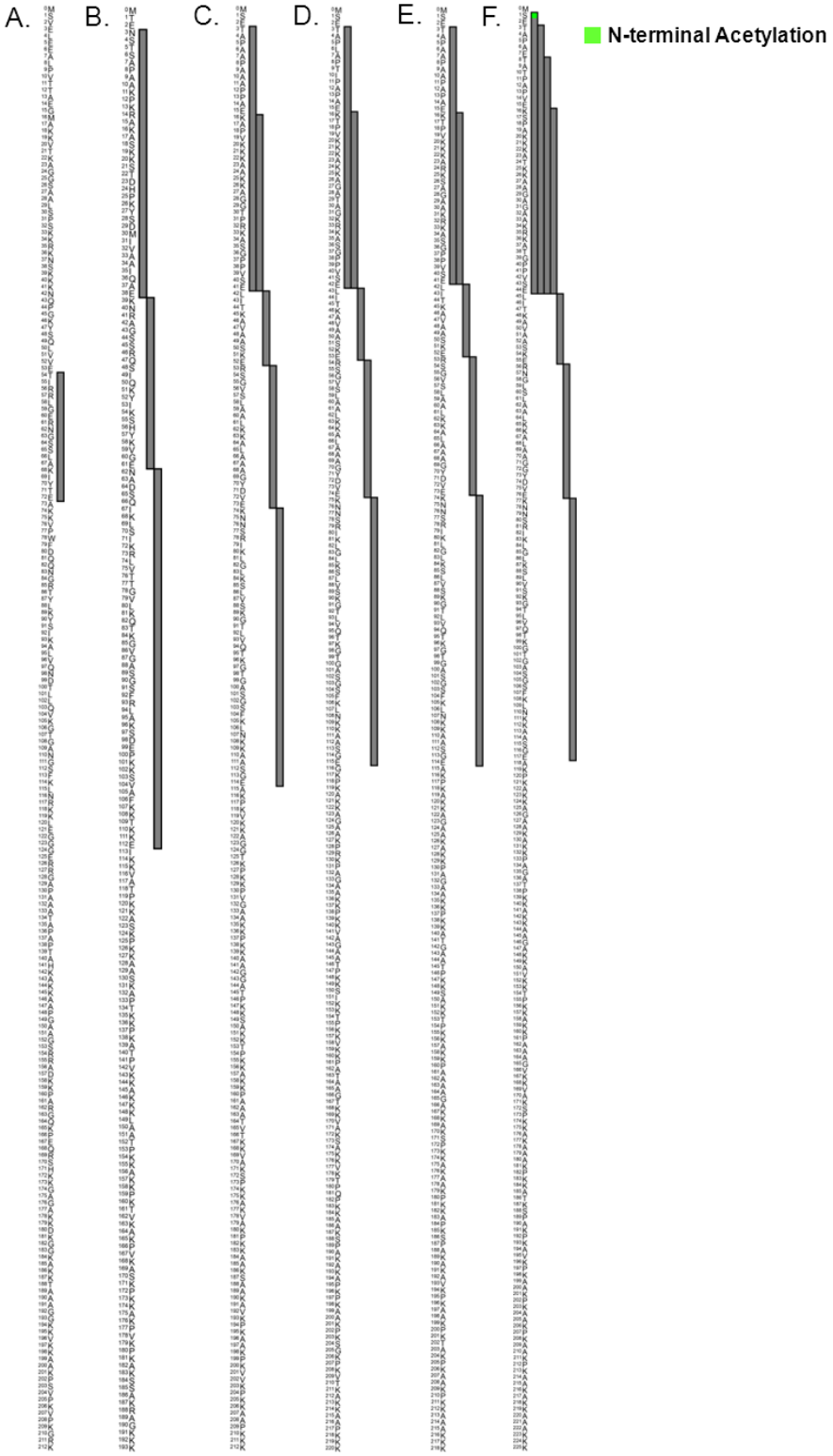

Figure S28F. Peptides identified and PTM combinations observed for H3.2 (A) and H3.3 (B) from MCF-7 cells. Peptides were derived from Glu-C digestion.

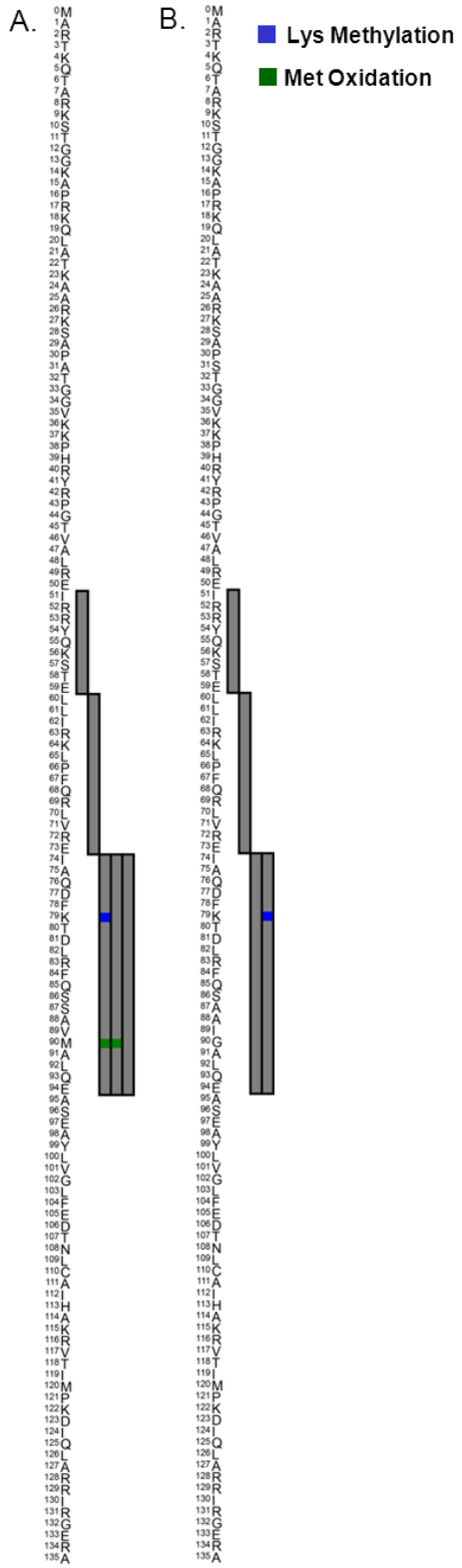

Figure S29A. Peptides identified and PTM combinations observed for H2A 2-A (A), H2A 2-C (B), H2A (C), H2A 2-B (D), H2A 1-J (E), H2A 1-H (F) and H2A 1-C (G) from MCF-7 cells. Peptides were derived from Asp-N digestion.

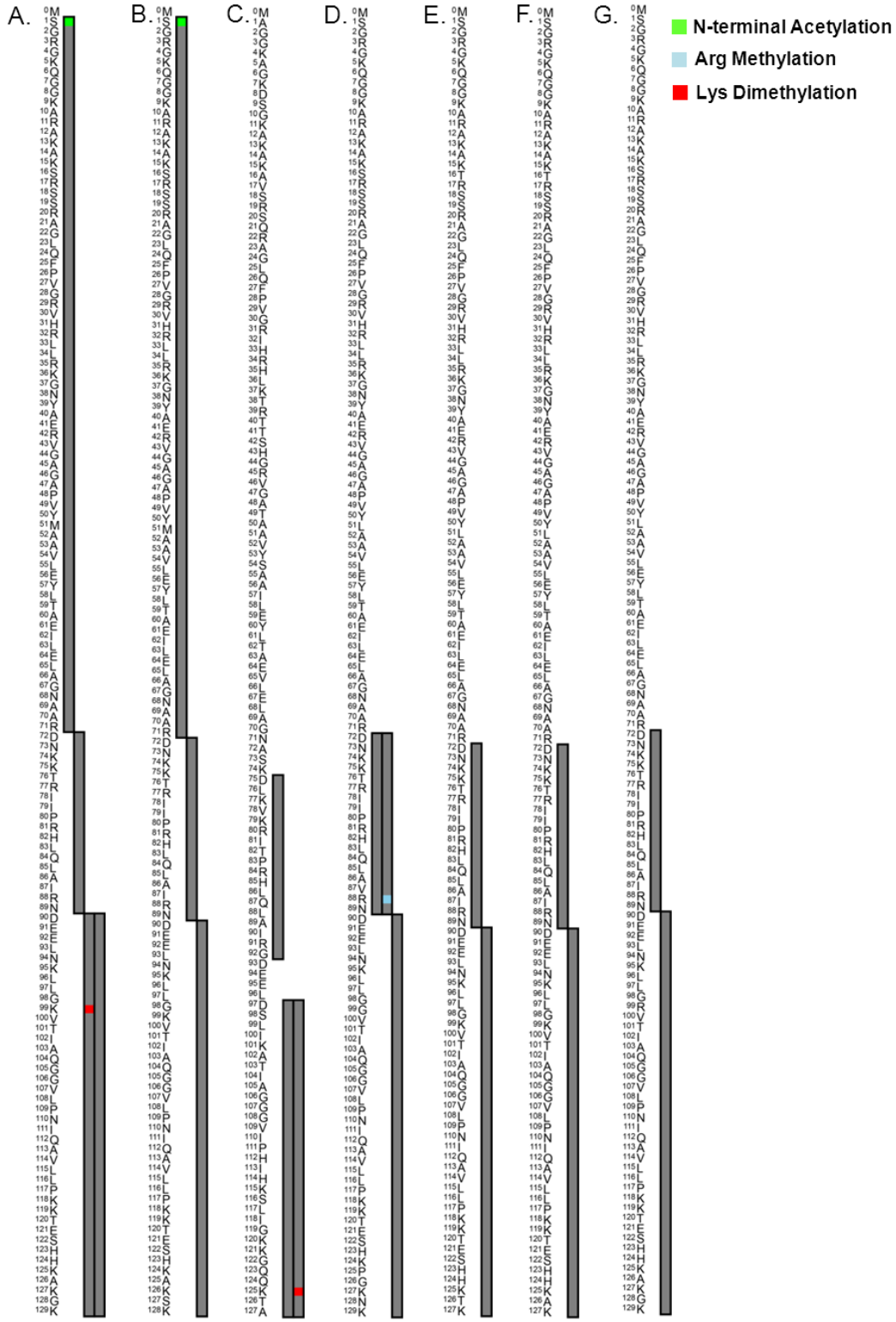

Figure S29B. Peptides identified and PTM combinations observed for H2A.x (A) and H2A.Z (B) from MCF-7 cells. Peptides were derived from Asp-N digestion

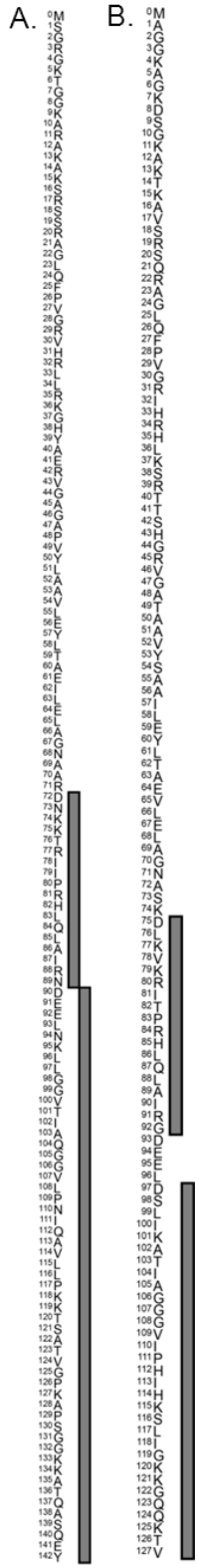

Figure S29C. Peptides identified and PTM combinations observed for H2B 2-F (A), H2B 1-C/E/F/G/I (B), H2B 2-E (C) H2B 1-H (D), H2B 1-N (E) and H2B 1-O (F) from MCF-7 cells. Peptides were derived from Asp-N digestion.

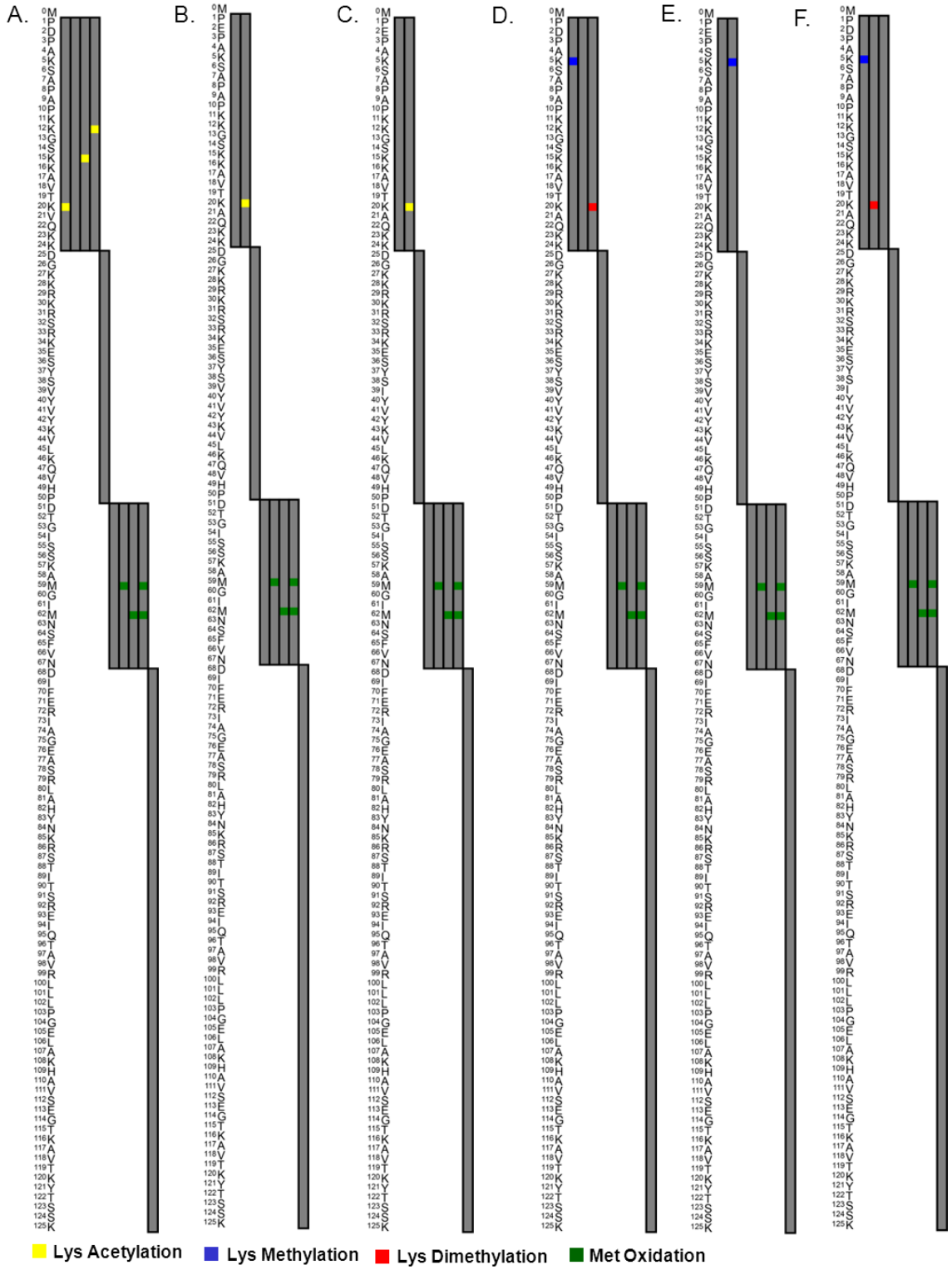

Figure S29D. Peptides identified and PTM combinations observed for H2B 1-D (A), H2B 1-M (B) and H2B 3-B (C) from MCF-7 cells. Peptides were derived from Asp-N digestion.

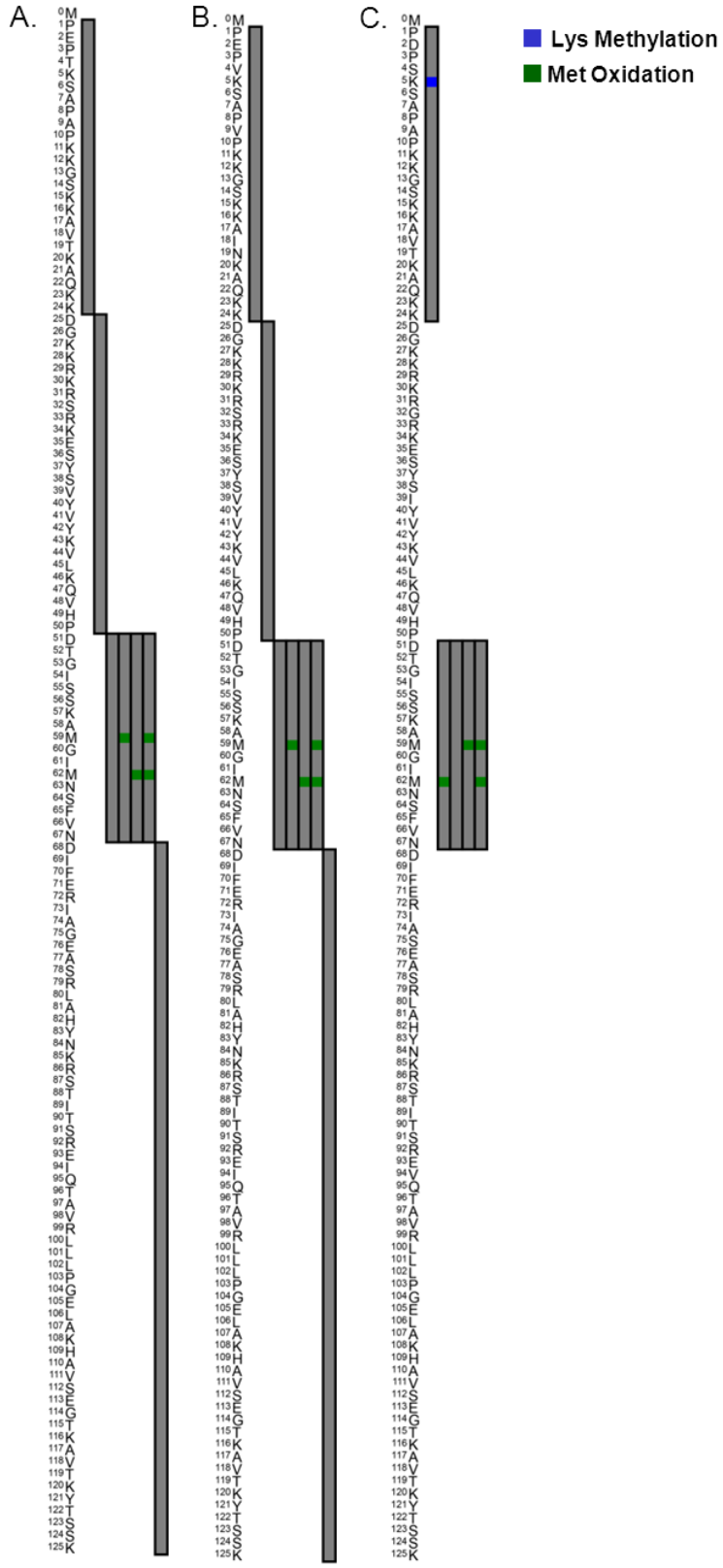

Figure S29E. Peptides identified and PTM combinations observed for H1x (A), H1.0 (B), H1.3(C) and H1.4 (D) from MCF-7 cells. Peptides were derived from Asp-N digestion.

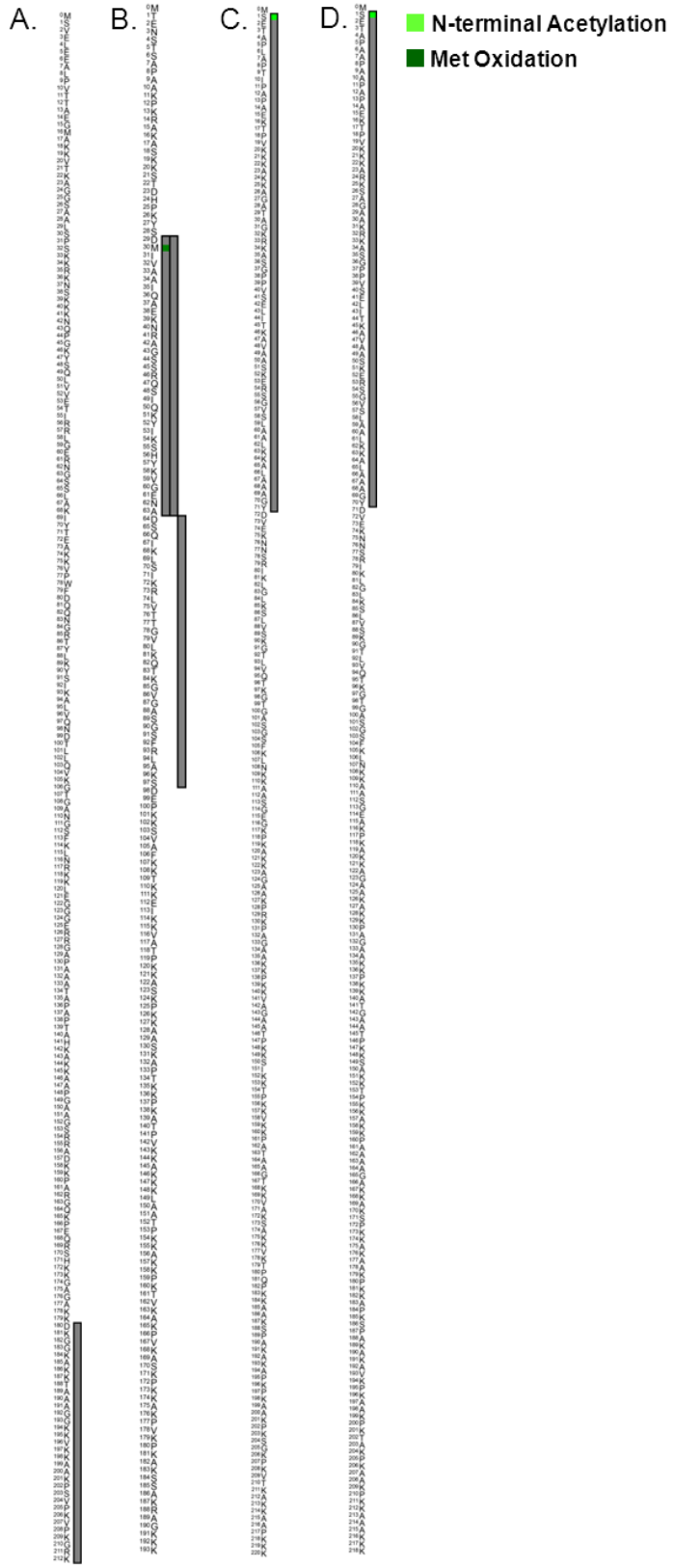

Figure S29F. Peptides identified and PTM combinations observed for H4 (A) and H3.3 (B) from MCF-7 cells. Peptides were derived from Asp-N digestion.

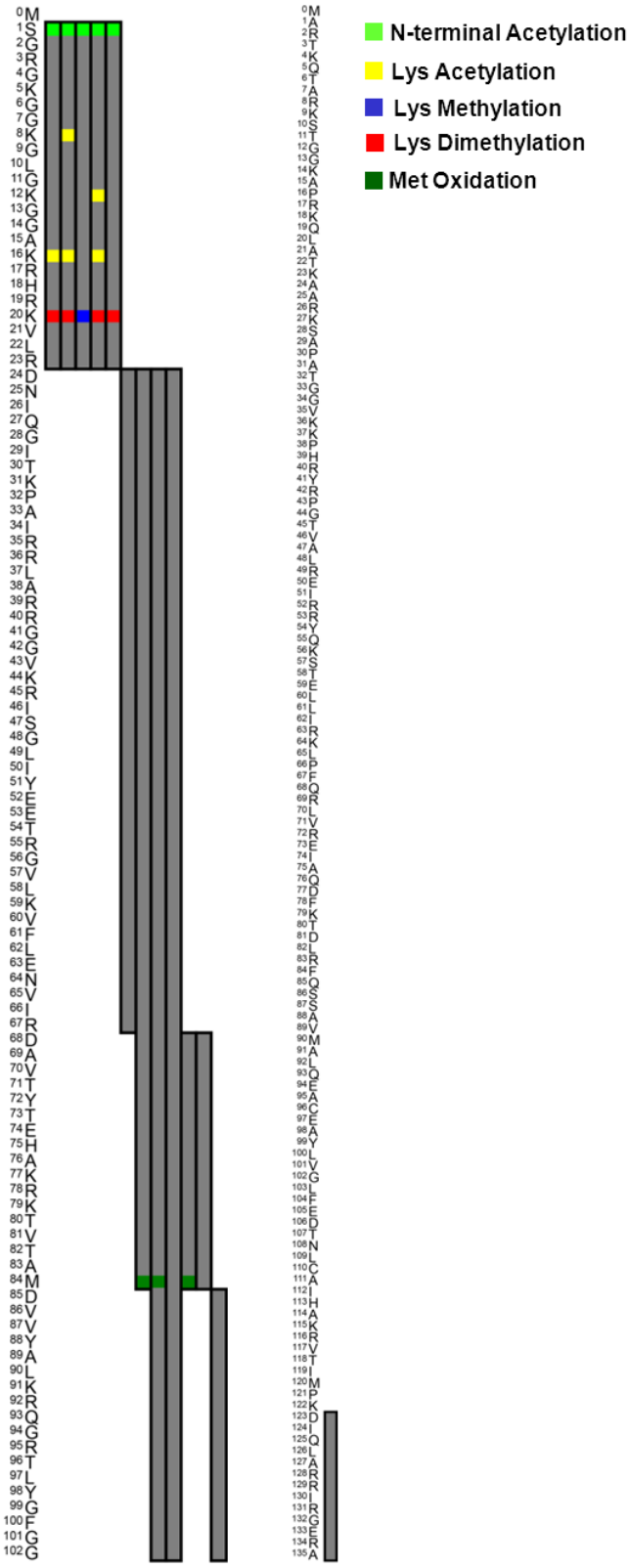

Figure S30A. Peptides identified and PTMs combinations observed for H2A 2-C (A), H2A.1 (B), H2A/A4IFU5 (C), H2A/Q17QG8 (D) and H2A/E1BH22 (E) from calf thymus. Peptides were derived from Glu-C digestion.

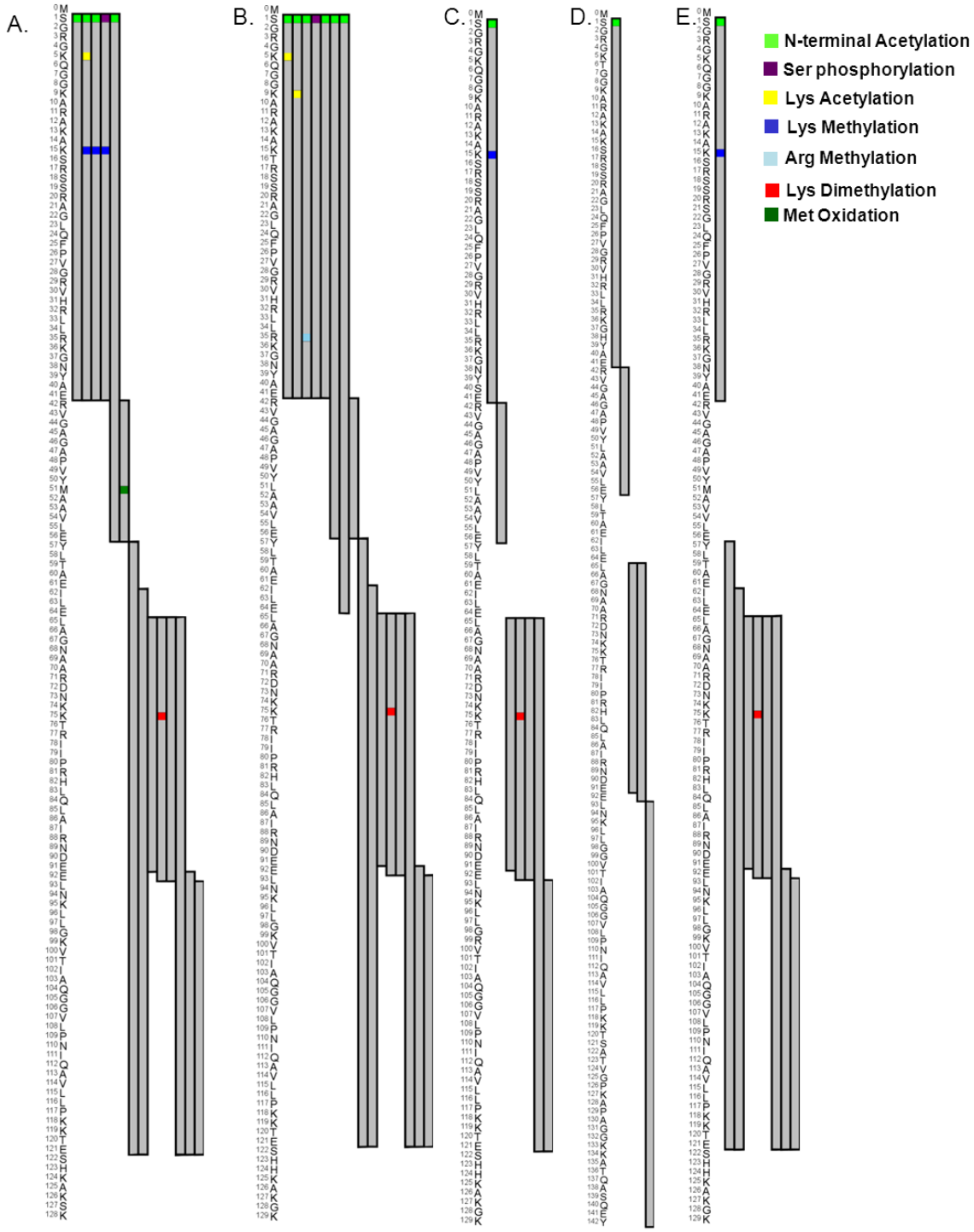

Figure S30B. Peptides identified and PTM combinations observed for H2A/A7E366 (A), H2A.Z (B) and H2A.V (C) from calf thymus. Peptides were derived from Glu-C digestion.

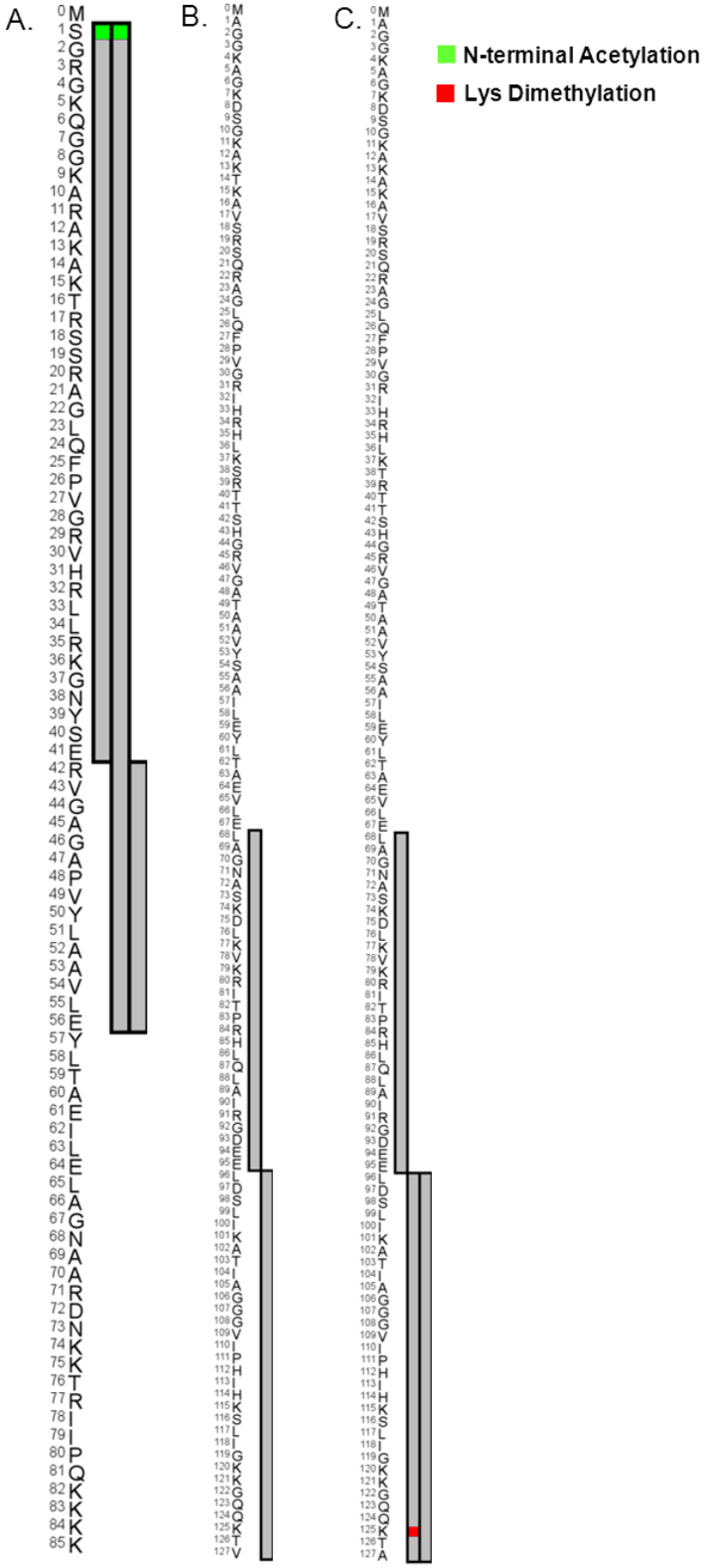

Figure S30C. Peptides identified and PTM combinations observed for H2B 1-K (A), H2B.1 (B) and H2B (C) from calf thymus. Peptides were derived from Glu-C digestion.

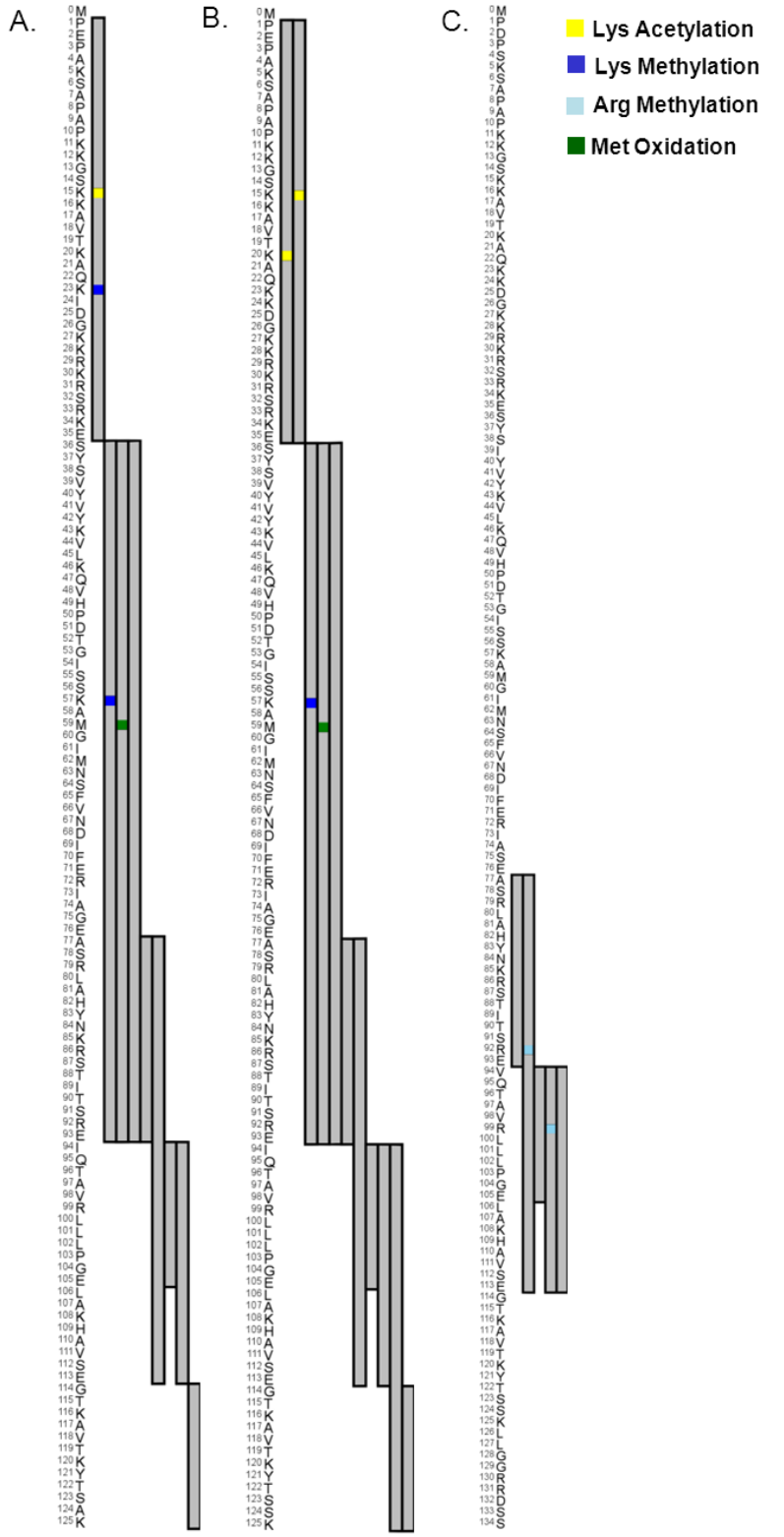

Figure S30D. Peptides identified and PTM combinations observed for H4 (A), H3.1 (B) and H1.3 (C) from calf thymus. Peptides were derived from Glu-C digestion.

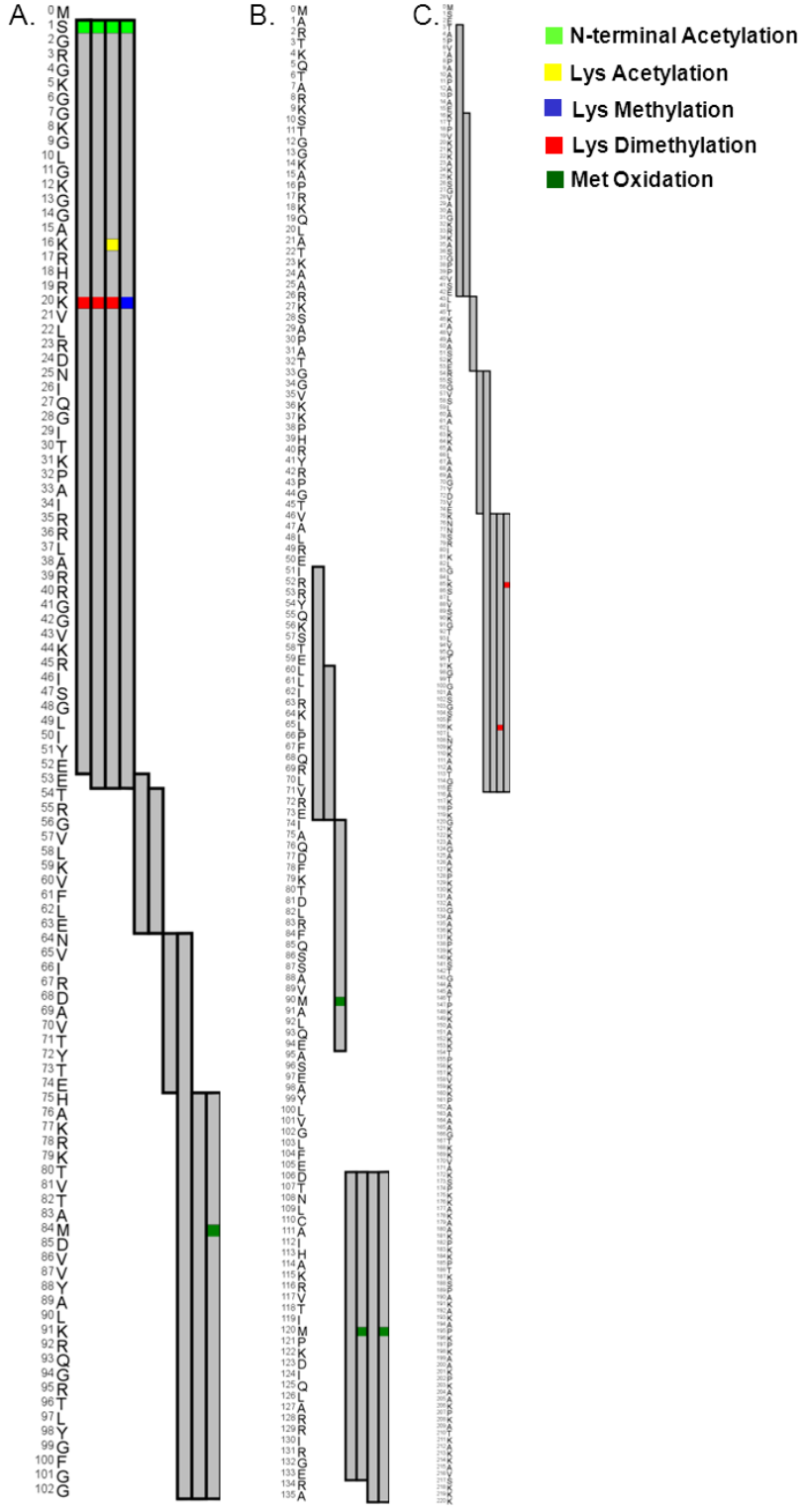

Figure S31A. Peptides identified and PTM combinations observed for H2A/A4IFU5 (A), H2A.1 (B), and H2A/E1BDT6 from calf thymus. Peptides were derived from Asp-N digestion.

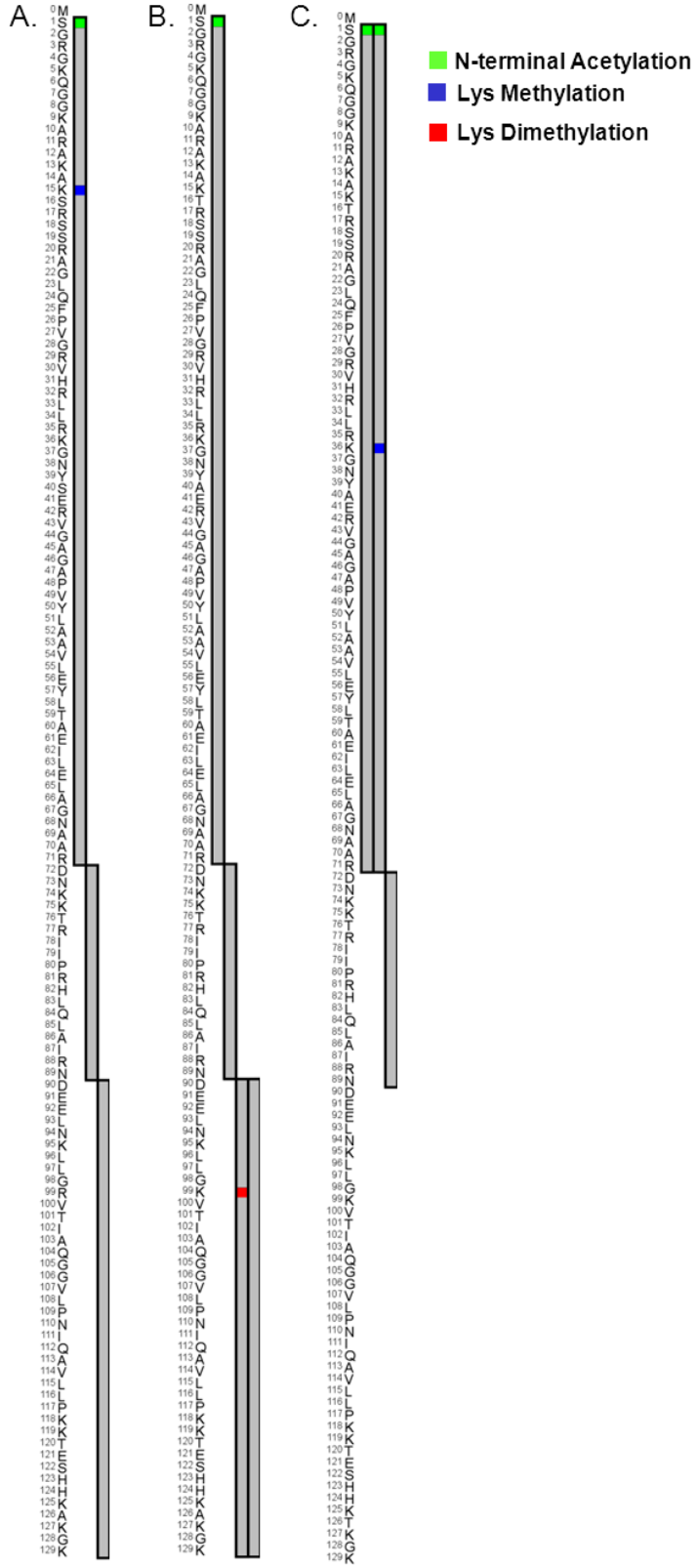

Figure S31B. Peptides identified and PTM combinations observed for H2A/Q17QG8 (A), H2A 2-C (B), H2A.V (C) and H2A.Z (D) from calf thymus. Peptides were derived from Asp-N digestion.

Figure S31C. Peptides identified and PTM combinations observed for H2B 1-K (A), H2B.1 (B), H2B/A5D7N2 (C) and H2B/E1BGW2 (D) from calf thymus. Peptides were derived from Asp-N digestion.

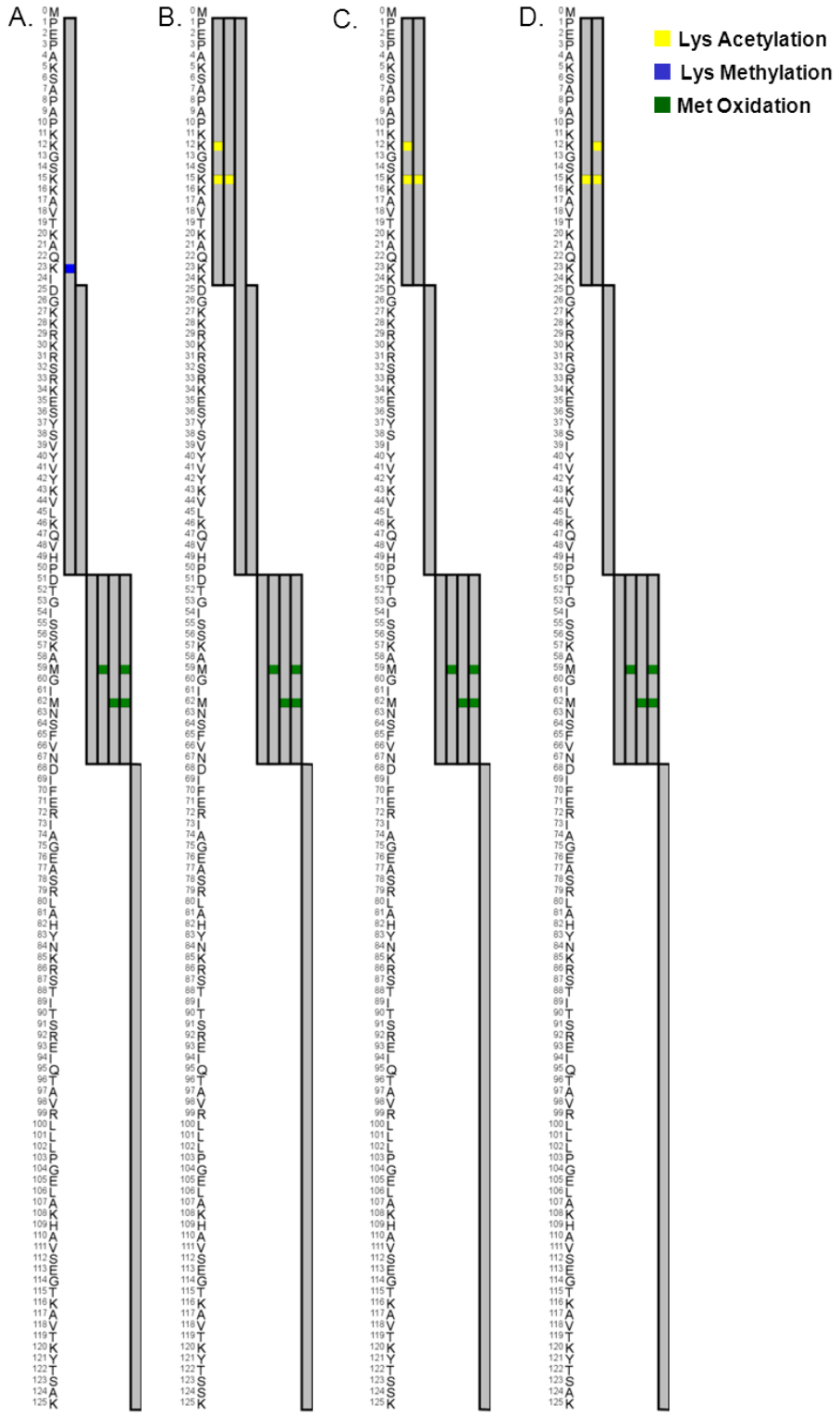

Figure S31D. Peptides identified and PTM combinations observed for H4 (A), H3.3 (B), H1.1 (C), H1.0 (D) and H1.3 (E) from calf thymus. Peptides were derived from Asp-N digestion.

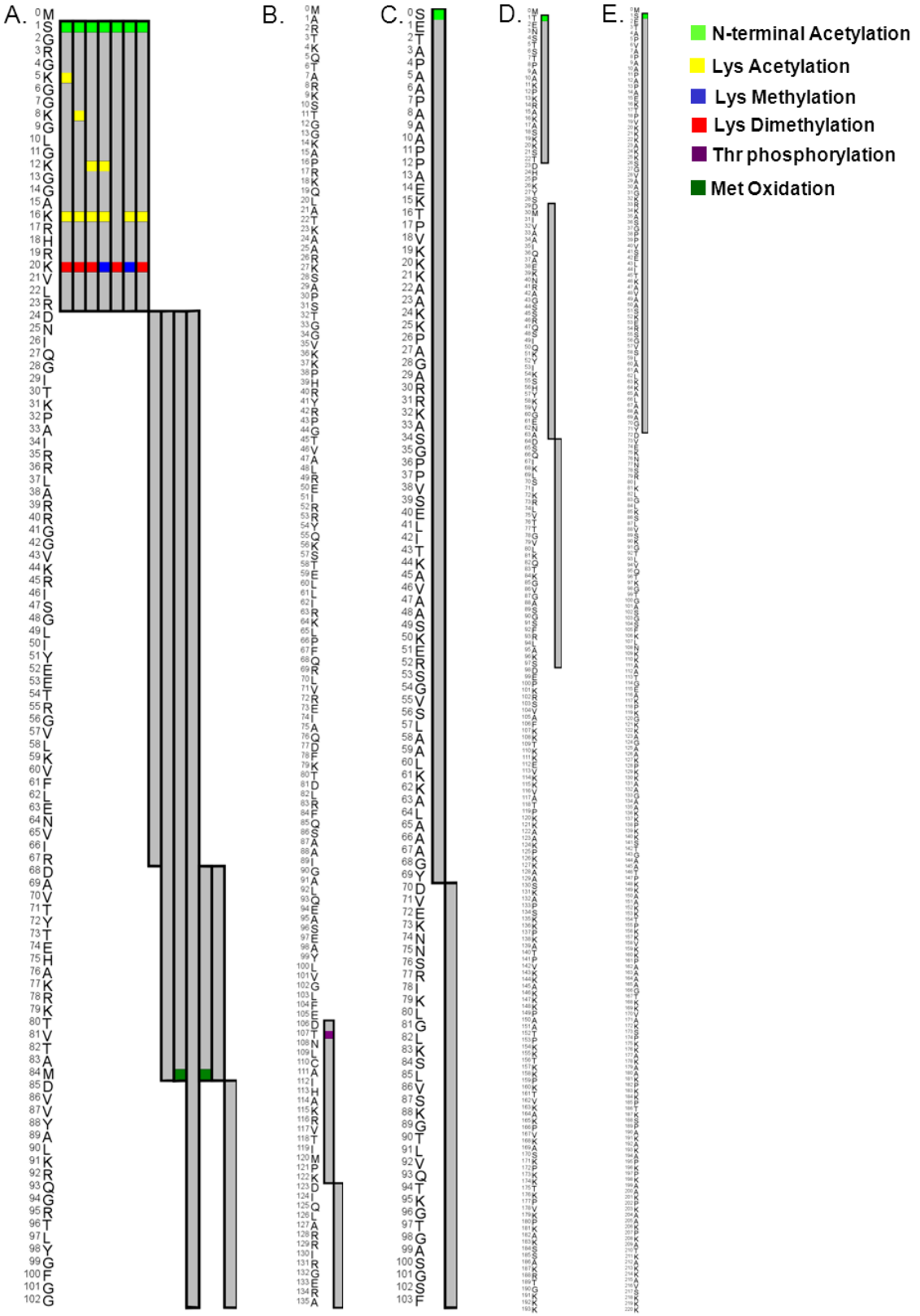

Table S1. Electron energies, irradiation times and MS/MS resolution (at m/z 400) employed for each sample during nano-LC-ECD-MS/MS.

Calf Thymus	Glu-C	Asp-N
LC-MS/MS ECD 1	0.21 eV / 50 ms MS/MS Resolution 25000	0.21 eV / 50 ms MS/MS Resolution 50000
LC-MS/MS ECD 2	0.71 eV / 50 ms MS/MS Resolution 25000	0.71 eV / 50 ms MS/MS Resolution 50000
LC-MS/MS ECD 3	0.71 eV / 50 ms MS/MS Resolution 50000	1.21 eV / 50 ms MS/MS Resolution 25000
LC-MS/MS ECD 4	1.21 eV / 50 ms MS/MS Resolution 25000	2.21 eV / 50 ms MS/MS Resolution 25000
LC-MS/MS ECD 5	2.21 eV / 70 ms MS/MS Resolution 25000	2.21 eV / 70 ms MS/MS Resolution 25000

MCF-7	Glu-C	Asp-N
LC-MS/MS ECD 1	0.75 eV / 50 ms MS/MS Resolution 50000	0.75 eV / 50 ms MS/MS Resolution 25000
LC-MS/MS ECD 2	0.75 eV / 50 ms MS/MS Resolution 50000	1.25 eV / 50 ms MS/MS Resolution 50000
LC-MS/MS ECD 3	1.25 eV / 50 ms MS/MS Resolution 50000	1.55 eV / 60 ms MS/MS Resolution 25000
LC-MS/MS ECD 4	1.55 eV / 60 ms MS/MS Resolution 25000	1.75 eV / 60 ms MS/MS Resolution 25000
LC-MS/MS ECD 5	1.75 eV / 60 ms MS/MS Resolution 25000	1.75 eV / 60 ms MS/MS Resolution 50000

HeLa	Glu-C	Asp-N
LC-MS/MS ECD 1	0.71 eV / 50 ms MS/MS Resolution 50000	0.21 eV / 50 ms MS/MS Resolution 50000
LC-MS/MS ECD 2	1.21 eV / 50 ms MS/MS Resolution 25000	0.71 eV / 50 ms MS/MS Resolution 50000
LC-MS/MS ECD 3	1.21 eV / 50 ms MS/MS Resolution 50000	1.21 eV / 50 ms MS/MS Resolution 25000
LC-MS/MS ECD 4	1.25 eV / 50 ms MS/MS Resolution 50000	2.21 eV / 50 ms MS/MS Resolution 25000
LC-MS/MS ECD 5	1.75 eV / 60 ms MS/MS Resolution 25000	2.21 eV / 70 ms MS/MS Resolution 25000

Jurkat	Glu-C	Asp-N
LC-MS/MS ECD 1	0.21 eV / 50 ms MS/MS Resolution 50000	0.21 eV / 50 ms MS/MS Resolution 50000
LC-MS/MS ECD 2	0.71 eV / 50 ms MS/MS Resolution 25000	0.71 eV / 50 ms MS/MS Resolution 50000
LC-MS/MS ECD 3	1.21 eV / 50 ms MS/MS Resolution 25000	1.21 eV / 50 ms MS/MS Resolution 25000
LC-MS/MS ECD 4	1.21 eV / 50 ms MS/MS Resolution 50000	2.21 eV / 50 ms MS/MS Resolution 25000
LC-MS/MS ECD 5	2.21 eV / 50 ms MS/MS Resolution 25000	2.21 eV / 70 ms MS/MS Resolution 25000

Table S2. Summary of identified histone variants, protein sequence coverage obtained, and observed PTMs from an Asp-N digested sample of histones extracted from Jurkat cells.

Histone Variant	Accession Number	Protein Sequence Coverage	Observed PTMs
H2A 2-B	Q8IUE6	100%	N-terminal Ac, Lys-15 Me, Arg-88 Me
H2A.1	P0C0S8	100%	N-terminal Ac, Lys-99 2Me
H2A 1-C	Q93077	100%	N-terminal Ac, Lys-15 Me
H2A 2-A	Q6FI13	100 %	N-terminal Ac, Lys-99 2Me
H2A 2-C	Q16777	100 %	N-terminal Ac
H2A 1-H	Q96KK5	100 %	N-terminal Ac
H2A 1-J	Q99878	100 %	N-terminal Ac
H2B 1-N	Q99877	100 %	Lys-16 Me, Lys-46 Me
H2B 1-H	Q93079	100 %	Lys-5Me, Lys-15 Ac, Lys-24 Me, Lys-46 Me
H2B 1-C/E/F/G/I	P62807	100 %	Lys-12 Ac, Lys-20 Ac, Lys-46 Me
H2B 1-J	P06899	100 %	Lys-12 Ac, Lys-20 Ac
H2B 2-E	Q16778	100 %	Lys-12 Ac, Lys-20 Ac
H2B 1-K	O60814	100 %	Lys-12 Ac, Lys-20 Ac, Lys-46 Me
H2B 1-B	P33778	100 %	None
H2B 1-O	P23527	100 %	Lys-5Me, Lys-15 Ac, Lys-24 Me
H4	P62805	100 %	N-terminal Ac, Lys-5 Ac, Lys-8 Ac, Lys-12 Ac, Lys-16 Ac, Lys-20 Me, Lys-20 2Me
H2A.x	P16104	50 %	None
H2A 1-B/E	P04908	45 %	None
H2A	A6NKY0	48 %	None
H2A.3	Q7L7L0	45 %	None
H2A.Z	P0C0S5	38 %	None
H1.0	P07305	36 %	None
H2B 1-L	Q99880	34 %	Lys-46 Me
H2B 3-B	Q8N257	34 %	None
H1.2	P16403	33 %	N-terminal Ac
H1.3	P16402	32 %	N-terminal Ac
H1.4	P10412	32 %	N-terminal Ac
H1.x	Q92522	24 %	None
H3.2	Q71DI3	10 %	None

Ac= acetylation, Me= methylation, 2Me=dimethylation, For= formylation

Table S3. Summary of identified histone variants, protein sequence coverage obtained, and observed PTMs from a Glu-C digested sample of histones extracted from HeLa cells.

Histone Variant	Accession Number	Protein Sequence Coverage	Observed PTMs
H2B 1-H	Q93079	100 %	Lys-20 2Me, Lys-5 Me, Lys-15 Ac
H2B 2-F	Q5QNW6	100 %	None
H2B 1-C/E/F/G/I	P62807	100 %	Lys-12 Ac, Lys-15 Ac, Lys-20 Ac
H2B 1-J	P06899	100 %	Lys-12 Ac, Lys-15 Ac, Lys-20 Ac
H2B 1-O	P23527	100 %	Lys-20 2Me, , Lys-5 Me, Lys-15 Ac
H2B 2-E	Q16778	100 %	Lys-12 Ac, Lys-15 Ac, Lys-20 Ac
H2B 1-K	O60814	100 %	Lys-12 Ac, Lys-15 Ac, Lys-20 Ac
H4	P62805	100%	N-terminal Ac, Lys-16 Ac, Lys-20 2Me
H2A 1-H	Q96KK5	88 %	N-terminal Ac, Lys-95 For
H2A 2-C	Q16777	88%	N-terminal Ac, Lys-5 Ac, Lys-15 Me, Arg-17 Me, Lys-95 For
H2A 1-D	P20671	87 %	N-terminal Ac, Lys-95 For
H2A 1-B/E	P04908	87 %	N-terminal Ac
H2A 1-C	Q93077	87 %	N-terminal Ac, Lys-5 Ac, Lys-15 Me, Arg-17 Me
H2A 2-B	Q8IUE6	87 %	N-terminal Ac, Lys-5 Ac, Lys-15 Me, Arg-17 Me, Arg-88 Me
H2A.3	Q7L7L0	87 %	N-terminal Ac, Lys-15 Me
H2A.x	P16104	65%	None
H2A	A6NKY0	59 %	Lys-99 2Me
H1.2	P16403	53 %	Lys-21 Me
H1.5	P16401	52 %	N-terminal Ac
H1.4	P10412	51 %	None
H2A.Z	P0C0S5	47 %	None
H2B 3-B	Q8N257	39 %	None
H3.2	Q71DI3	33 %	None

Ac= acetylation, Me= methylation, 2Me=dimethylation, For= formylation

Table S4. Summary of identified histone variants, protein sequence coverage obtained, and observed PTMs from Asp-N digested sample of histones extracted from HeLa cells.

Histone Variant	Accession Number	Protein Sequence Coverage	Observed PTMs
H2A 1-C	Q93077	100 %	N-terminal Ac, Lys-15 Me
H2A 2-A	Q6FI13	100 %	N-terminal Ac, Lys-99 2Me
H2A 2-B	Q8IUE6	100 %	N-terminal Ac, Lys-15 Me, Arg-88 Me
H2A.1	P0C0S8	100 %	N-terminal Ac, Lys-99 2Me
H2A 2-C	Q16777	100 %	N-terminal Ac
H2A 1-J	Q99878	100 %	N-terminal Ac
H2A 1-H	Q96KK5	100 %	N-terminal Ac
H2B 2-E	Q16778	100 %	Lys-15 Ac, Lys-16 Ac
H2B 1-K	O60814	100 %	Lys-15 Ac, Lys-16 Ac
H2B 1-J	P06899	100 %	Lys-15 Ac, Lys-16 Ac
H2B 1-O	P23527	100 %	None
H2B 1-C/E/F/G/I	P62807	100 %	Lys-15 Ac, Lys-16 Ac
H2B 1-H	Q93079	100 %	None
H4	P62805	100%	N-terminal Ac, Lys-8 Ac, Lys-12 Ac, Lys-16 Ac, Lys-20 2Me
H2B 2-F	Q5QNW6	98 %	None
H2A.x	P16104	50%	None
H2A	A6NKY0	48 %	None
H2A.Z	P0C0S5	38 %	None
H1.2	P16403	33 %	N-terminal Ac
H2B 3-B	Q8N257	33 %	None
H1.4	P10412	32 %	N-terminal Ac
H3.3	P84243	10 %	None
H1.x	Q92522	9 %	None

Ac= acetylation, Me= methylation, 2Me=dimethylation, For= formylation

Table S5. Summary of identified histone variants, protein sequence coverage obtained, and observed PTMs from a Glu-C digested sample of histones extracted from MCF-7cells.

Histone Variant	Accession Number	Protein Sequence Coverage	Observed PTMs
H2B 1-M	Q99879	100 %	Lys-46 Me
H2B 1-K	O60814	100 %	Lys-46 Me
H2B 1-J	P06899	100 %	None
H2B 1-C/E/F/G/I	P62807	100 %	Lys-46 Me
H2B 2-F	Q5QNW6	100 %	Lys-20 Ac, Lys-46 Me
H2B 1-H	Q93079	100 %	Lys-5 Me, Lys-20 2Me, Lys-46 Me
H2B 2-E	Q16778	100 %	None
H2B 1-O	P23527	100 %	Lys-5 Me, Lys-20 2Me
H4	P62805	100%	N-terminal Ac, Lys-16 Ac, Lys-20 2Me
H2A 2-C	Q16777	88 %	N-terminal Ac, Lys-5 Ac, Arg-17 Me, Lys-95 For
H2A 1-H	Q96KK5	88%	N-terminal Ac, Lys-95 2Me
H2A 1-C	Q93077	87%	N-terminal Ac, Lys-5 Ac, Arg-17 Me
H2A 2-B	Q8IUE6	87 %	N-terminal Ac, Lys-5 Ac, Arg-17 Me, Arg-88 Me
H2A 1-B/E	P04908	87 %	N-terminal Ac
H2A.3	Q7L7L0	87 %	N-terminal Ac, Arg-17 Me
H2A 1-D	P20671	87 %	N-terminal Ac, Lys-95 2Me
H2A.x	P16104	65 %	None
H2A	A6NKY0	59 %	None
H1.0	P20671	57 %	None
H1.2	P16403	53 %	None
H1.5	P16401	52 %	N-terminal Ac
H1.4	P10412	51 %	None
H1.3	P16402	52 %	None
H2A.Z	P0C0S5	47 %	None
H2B 3-B	Q8N257	39 %	None
H3.3	P84243	33 %	Lys-79 Me
H3.2	Q71DI3	33 %	Lys-79 Me
H1.x	Q92522	9 %	None

Ac= acetylation, Me= methylation, 2Me=dimethylation, For= formylation

Table S6. Summary of identified histone variants, protein sequence coverage obtained, and observed PTMs from Asp-N digestion of histones extracted from MCF-7cells.

Histone Variant	Accession Number	Protein Sequence Coverage	Observed PTMs
H2A 2-A	Q6FI13	100 %	N-terminal Ac, Lys-99 2Me
H2A 2-C	Q16777	100 %	N-terminal Ac
H2B 2-F	Q5QNW6	100 %	Lys-12 Ac, Lys-15 Ac, Lys-20 Ac
H2B 1-H	Q93079	100 %	Lys-5 Me, Lys-20 2Me
H2B 1-O	P23527	100 %	Lys-5 Me, Lys-20 2Me
H2B 1-D	P58876	100 %	None
H2B 1-N	Q99877	100 %	Lys-5 Me
H2B 1-C/E/F/G/I	P62807	100 %	Lys-20 Ac
H2B 1-M	Q99879	100 %	None
H2B 2-E	Q16778	100 %	Lys-20 Ac
H4	P62805	100%	N-terminal Ac, Lys-8 Ac, Lys-12 Ac, Lys-16 Ac, Lys-20 2Me, Lys-20 Me
H2A.x	P16104	50 %	None
H2A	A6NKY0	48 %	Lys-99 2Me
H2A 2-B	Q8IUE6	45 %	Arg-88 Me
H2A 1-C	Q93077	45 %	None
H2A 1-J	Q99878	44%	None
H2A 1-H	Q96KK5	44 %	None
H2A.Z	P0C0S5	38 %	None
H1.0	P20671	36 %	None
H2B 3-B	Q8N257	33 %	Lys-5 Me
H1.3	P16402	32 %	N-terminal Ac
H1.4	P10412	32 %	N-terminal Ac
H1.x	Q92522	16 %	None
H3.3	P84243	10 %	None

Ac= acetylation, Me= methylation, 2Me=dimethylation, For= formylation

Table S7. Summary of identified histone variants, protein sequence coverage obtained, and observed PTMs from Glu-C digestion of histones extracted from calf thymus.

Histone Variant	Accession Number	Protein Sequence Coverage	Observed PTMs
H2B 1-K	Q2M2T1	100 %	Lys-15 Ac , Lys-23 Me, Lys-57 Me
H2B.1	P62808	100 %	Lys-15 Ac, Lys-20 Ac, Lys-57 Me
H4	P62803	100 %	N-terminal Ac, Lys-16 Ac, Lys-20 Me, Lys-20 2Me
H2A 2-C	A1A4R1	95 %	N-terminal Ac, Ser-1 Ph, Lys-5 Ac, Lys-15 Me, Lys-75 2Me
H2A	Q17QG8	94 %	N-terminal Ac
H2A.1	P0C0S9	93 %	N-terminal Ac, Ser-1 Ph, Lys-5 Ac, Lys-9 Ac, Arg-35 Me, Lys-75 2Me
H2A	A4IFU5	87 %	N-terminal Ac, Lys-15 Me, Lys-75 2Me
H2A	E1BH22	82 %	N-terminal Ac, Lys-15 Me
H2A	A7E366	65 %	N-terminal Ac
H3.1	P68432	54 %	None
H1.3	A7MAZ5	51 %	Lys-84 2Me, Lys-106 2Me
H2A.Z	P0C0S4	47 %	None
H2A.V	Q32LA7	47 %	Lys-125 2Me
H2B	E1B7L1	27 %	Arg-92 Me, Arg-99 Me

Ac= acetylation, Me= methylation, 2Me=dimethylation, Ph= phosphorylation

Table S8. Summary of identified histone variants, protein sequence coverage obtained, and observed PTMs from Asp-N digestion of histones extracted from calf thymus.

Histone Variant	Accession Number	Protein Sequence Coverage	Observed PTMs
H1.1	P02253	100 %	N-terminal Ac
H2A	A4IFU5	100 %	N-terminal Ac, Lys-15 Me
H2A.1	P0C0S9	100 %	N-terminal Ac, Lys-99 2Me
H2B 1-K	Q2M2T1	100 %	Lys-23 Me
H2B.1	P62808	100 %	Lys-12 Ac, Lys-15 Ac
H2B	A5D7N2	100 %	Lys-12 Ac, Lys-15 Ac
H2B	E1BGW2	100 %	Lys-12 Ac, Lys-15 Ac
H4	P62803	100 %	N-terminal Ac, Lys-8 Ac, Lys-5 Ac, Lys-12 Ac, Lys-16 Ac, Lys-20 Me, Lys-20 2Me
H2A	E1BDT6	69 %	N-terminal Ac
H2A	Q17QG8	50 %	None
H2A 2-C	A1A4R1	44 %	None
H2A.V	Q32LA7	38 %	Lys-125 2Me
H2A.Z	P0C0S4	38 %	None
H1.0	Q0IIJ2	36 %	Thr-1 Ac
H1.3	A7MAZ5	32 %	N-terminal Ac
H3.3	Q5E9F8	22 %	Thr-107 Ph

Ac= acetylation, Me= methylation, 2Me=dimethylation, Ph= phosphorylation

Table S9. Comparison of the middle-down nano-LC ECD MS/MS method presented in this manuscript with previously employed methods for histone analysis.[4-10]

	Intact protein analysis / CID	Intact protein analysis / ETD	Trypsin, Glu-C, Asp-N, chymotrypsin digestion / CID	Trypsin, Asp-N digestion / CID, ETD	Trypsin digestion / CID, ETD	Trypsin digestion/ CID	Glu-C, Asp-N, digestion / ETD	Glu-C, Asp-N, digestion / ECD
Sample preparation	Unfractionated histones	Unfractionated histones	Prefractionation of individual histones by HPLC followed by digestion with each enzyme	Separation of each core histone by HPLC/ H3 digestion with trypsin, H4 digestion with Asp-N	Unfractionated histones/ trypsin digestion	Purification of each histone by SDS-page / trypsin digestion	Separation of each histone family by HPLC/ H3 digestion with Glu-C, H4 digestion with Asp-N/ Further HPLC purification of the N-terminal peptide of H3.2 and H4	Unfractionated histones / Glu-C and Asp-N digestion
LC-MS/MS analysis time	19 min	55 min	60 min per digested sample	67 min per digested sample	110 min	40 or 90 min per histone gel band	90 or 260 min (H3.2) (H4)	90 min per LC-MS/MS analysis
Amount loaded	10 µg	45 pmol	0.2 µg per digested sample	10 -15 pmol per digested sample	N/A	N/A	0.5 - 1.0 µg	1 ug per LC-MS/MS analysis
Precursor ion mass tolerance/ Product ions mass tolerance	N/A	30 ppm / 30 ppm	N/A	5 ppm / N/A	0.1 Da / 0.5 Da	5 ppm / 2 Da (LTQ-FT-ICR) 50 ppm / 0.8 Da (Q-TOF)	N/A	15 ppm / 15 ppm
Throughput	+++	+++	+	+	+++	+	-	++
Differentiation of histone variants	++	++	N/A	N/A	++	++	N/A	++
Combinatorial PTMs information	+	+	++	- (H3) +++ (H4)	+	+	+++	++
PTMs localization	_	++	++	+++	++	++	+++	+++
Reference	4	5	6	7	8	9	10	This manuscript

Legend: +++ = very good, ++ = good, + = acceptable, - = average

REFERENCES

(1) Shechter, D.; Dormann, H. L.; Allis, C. D.; Hake, S. B. *Nature Protoc.* **2007**, *2*, 1445-1457.
(2) Kalli, A.; Hakansson, K. *Mol. Biosyst.* **2010**, *6*, 1668-1681.
(3) Gupta, N.; Hixson, K. K.; Culley, D. E.; Smith, R. D.; Pevzner, P. A. *Proteomics* **2010**, *10*, 2833-2844.
(4) Contrepois, K.; Ezan, E.; Mann, C.; Fenaille, F. *J. Proteome Res.* **2010**, *9*, 5501-5509.
(5) Eliuk, S. M.; Maltby, D.; Panning, B.; Burlingame, A. L. *Mol. Cell. Proteomics* **2010**, *9*, 824-837.
(6) Xiong, L.; Wang, Y. S. *Int. J. Mass Spectrom.* **2011**, *301*, 159-165.
(7) Nicklay, J. J.; Shechter, D.; Chitta, R. K.; Garcia, B. A.; Shabanowitz, J.; Allis, C. D.; Hunt, D. F. *J. Biol. Chem.* **2009**, *284*, 1075-1085.
(8) Plazas-Mayorca, M. D.; Zee, B. M.; Young, N. L.; Fingerman, I. M.; LeRoy, G.; Briggs, S. D.; Garcia, B. A. *J. Proteome Res.* **2009**, *8*, 5367-5374.
(9) Trelle, M. B.; Salcedo-Amaya, A. M.; Cohen, A. M.; Stunnenberg, H. G.; Jensen, O. N. *J. Proteome Res.* **2009**, *8*, 3439-3450.
(10) Young, N. L.; DiMaggio, P. A.; Plazas-Mayorca, M. D.; Baliban, R. C.; Floudas, C. A.; Garcia, B. A. *Mol. Cell. Proteomics* **2009**, *8*, 2266-2284.